Flexible thin-glass IGU

Design and testing for increasing curvature for cold bent insulated glass units

PILKINGTON

NSG GROUP

KÖMMERLING

Edgetech
A SUBSIDIARY OF Quanex

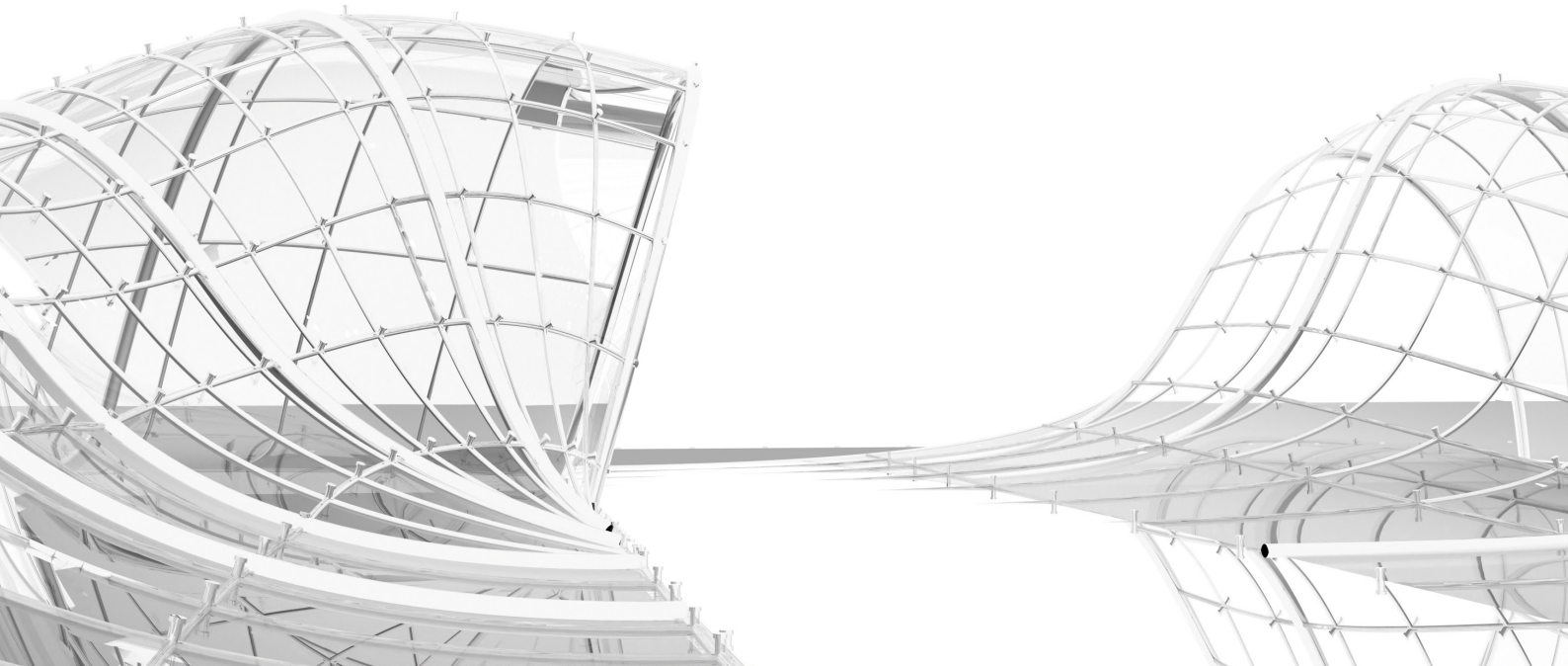

Flexible thin-glass IGU

Designing and testing a thin-glass IGU with chemically strengthened thin-glass and a flexible spacer to increase curvature for cold bending

Msc Graduation Thesis Report

Koen van Deurzen
4884469

Mentors
Prof. Dr. Mauro Overend
AE+T | Structural Design
Dr. Marcel bilow
AE+T | Façade & Product Design

Delegate of the board of examiners
Ir. Wouter Willers

3rd of July 2025

TU Delft Faculty of Architecture and the Built Environment
Msc Architecture, Urbanism and Building Sciences - Building Technology

Abstract

This thesis explores the feasibility of constructing a flexible insulated glazing unit (IGU) using chemically strengthened thin-glass to enable higher cold bending curvatures. The research focuses on identifying optimal material combinations and structural configurations to accommodate significant deformation without compromising integrity. Both numerical modelling and physical testing were employed. In the absence of sufficient data, material properties were experimentally derived to enhance model accuracy. Strain gauges were used to validate simulations against real-world tests. Findings demonstrate that a thin-glass IGU can endure corner deformations of up to 16.3 cm, offering a performance enhancement of 4.2 times over traditional fully tempered glass units. These panels have a curvature constant of 0.112. A case study is performed to investigate how well the panels would perform in a real situation.

Acknowledgement

This graduation project concludes my master's degree in building technology and ends my time at the TU-Delft. This master and especially this thesis has broadened my knowledge about the technical side of architecture including structure, materials, computational design and façades. If i was told 5 years ago that I would perform research to material science I would have found that hard to believe. Therefore I want to thank everyone who contributed to the realization of this thesis.

First of all, thanks to my two mentors Mauro Overend and Marcel Bilow. Mauro for his endless knowledge about everything I could think of to ask during the sessions, and willingness to think alongside my ideas for this graduation. These sessions always ended with enthousiasm and provided me extra drive for finishing this thesis. I also want to thank Marcel for providing me insightful knowledge about the practical aspect of my project and thereby keeping my feet to the ground. I also thank him for the tips he gave me on how to build a prototype and a testing rig.

I want to thank Rory Back, Arai Daichi and the rest of the team at Pilkington/NSG who believed in this project and were willing to provide chemically strengthened thin-glass sheets. I also want to thank Roger Kahlen from Edgetech/Superspacer for providing their Triseal flexible spacer, which was crucial to this research project.

I want to thank Fred Veer for assisting me with material testing in the mechanical engineering lab. And I thank Cornelis van Beek, Giorgos Stamoulis and the rest of the crew at civil engineering for helping me setup my experiments and trusting me with my tests.

I also want to thank my graduating companion Sanguk Ryu for helping with the delivery of the thin-glass, and being a good brainstorm partner during our meetings.

I thank my family for always showing unconditional support and being there for me. Furthermore I want to thank my friends Roelof, Raymen, Pim and Tijmen who I have become very close with during my studies. Our after-study sessions at the bouwpub will remain one of my fondest memories here at the TU. Lastly my girlfriend Jisca for always showing interest in my project and helping me assemble my IGU's, which I could not have done alone.

List of symbols and abbreviations

Symbol	Description
E	Young's modulus (Elasticity modulus), unit: Pa
v (ν)	Poisson's ratio – ratio of lateral contraction to longitudinal extension
D	Flexural rigidity, unit: Nm
h	Thickness of the glass panel, unit: m
R	Radius of curvature, unit: m
K	Curvature = 1 / R
δAC,z	Vertical displacement from corner A to C in z-direction
α	General heat transfer coefficient, unit: $W/(m^2 \cdot K)$
αcd	Heat transfer through conduction
αcv	Heat transfer through convection
αR	Heat transfer through radiation
Rc	Total thermal resistance of the construction, unit: $m^2 \cdot K/W$
t	Thickness of the glass pane, unit: mm
μ (mu)	Friction coefficient
σ	(Maximum) stress, unit: Pa or MPa
ε	Strain (dimensionless)
K-factor	Calibration factor for strain gauge
Kmod	Load duration strength modification factor for glass

Abbreviation	Full Form / Meaning
IGU	Insulated Glass Unit
PMMA	Polymethylmethacrylate (Plexiglass)
FEM	Finite Element Method
PVB	Polyvinyl Butyral (interlayer for laminated glass)
TPS	Thermoplastic Spacer
GFRP	Glass Fiber Reinforced Polymer
DOWSIL	Brand name for a series of silicone-based adhesives/sealants by Dow
EPDM	Ethylene Propylene Diene Monomer (rubber used in seals – context inferred)

Contents

01

Research framework

1.1 Problem statement

Glass is becoming increasingly popular in architecture. It's transparent optical quality provides daylight aswel as increasing the observable area in from within buildings. The most common glass used in architectural applications, float glass, was developed in the 1950's by the Pilkington brothers. Since then, production methods have been developed and altered to make glass safer and stronger. This has lead to new developments and design being possible for architectural applications.

Furthermore, the rise of computational design methods in architecture have moved the boundary's of what can be achieved in terms of shapes of buildings and façades. Fluid glass façades have become popular for landmark architecture. Currently there are two main methods of fabricating glass for curved applications; hot bending, and cold bending.

Hot bending glass uses molds for shaping the glass in the right shape. With this process, high curvatures of glass panes can be achieved. However, this process often requires a lot of time and money. For example, the glass façade for the Emporia shopping mall in Mälmo used hot bending to build the curved façade, whereby 567 individual molds where created to anneal the glass in its desired shape. 815 glass panes where heated up to 540 degrees and softened into shape. *(Vanceva, n.d.)*

Overall this process is cost ineffective and time consuming, therefore adding constraints to the possibility of design.

Cold bending is a technique whereby flat glass units are brought onto the building site, where after it is cold bent into its desired shape. This process allows for easier manufacturing and requires less unique fabrication processes, therefore being a more sustainable option. The disadvantage of using cold bending is the limited flexibility of the glass unit. The stiff glass panes dictate the maximum allowable curve of the panel, and for highly fluid façades this constrains the design.
In the 1960's demand for thinner glass grew out of the watch industry which started development of new production methods. Glass sheet thickness had then been reduced to 1.4-1.2 millimetres. Since recent times, another industry has taken interest in glass. The technology sector is advancing in a rapid tempo, and with the request for thinner electronic devices, innovations in glass production have been made. Ultra-thin, flexible glass has been developed for high-tech applications.

The building sector is as of yet still reliant on traditional thick float glass sheets. With thickness's of 4-8 millimetres often used in insulated glass units. Using thin glass sheets could provide a real improvement in the design flexibility of curved glass façades by combining the convenience of the cold bending method, and the high achievable curvature of the hot bending method.

Figure 1. (Emporia Shopping Mall, 2023)

1.2 Research objective

The objective of this research is to find out if the use of cold bent thin glass insulated glass units can reduce the need for hot bend glass units. Reducing the need for hot bending during the façade construction process and thus reducing the CO2 footprint of curved glass façades. Cold bending insulated glass units with regular glass thickness' only allows for relatively small cold bent curvatures. Using thinner glass panes could increase the maximum curve radius possibly achievable with insulated glass units.

For this research question it is required to research how thin-glass behaves during cold bending and how cold bending affects its mechanical properties. It is also important to research how different materials in the insulated glass unit (from now IGU) behave during its bending. For this specific research, single corner cold bending of an IGU is numerically modelled and physically validated with prototyping.

1.3 Research questions

Can a higher degree of curvature be achieved in cold bent insulated glass units by applying thin glass?

1. What dictates the maximum bending capacity of a cold bent insulated glazing unit.

2. How can an IGU be designed to accommodate bending behaviour of thin glass?

3. How can a setup be constructed for cold bending a thing glass IGU, and how can strain/stress data be accurately measured during the bending process?

4. How accurate can a finite elements model be made to simulate cold bending of a thin glass IGU?

5. How does a thin glass IGU perform under a single corner deflection?

6. How does extreme cold bending affect the optical reflective quality of thin glass?

1.4 Methodology

This research consists of multiple phases and approaches.

Literature study
The first method is literature study. Thin-glass is a relevant field with papers on its application in architecture being released very recently. These papers are important to obtain a good understanding of the state of the art of thin glass. First of all the mechanical properties and the behaviour of glass needs to be studied. These papers contain knowledge on how glass and thin glass behaves during bending conditions. The literature study includes reading literature on correct finite element modelling.

The finite element method
The second phase is the modelling phase. To asses the strength and structural properties of thin glass under bending stress and to predict stresses in the glass surface during deformation, a finite elements model is made. Finite elements software can accurately calculate stresses and deformations, and with this model, changes can be made in the material composition of the panel. Allowing for finding an ideal panel composition. With numerical modelling, the maximum allowable bend angles can also be predicted, making the process safer and easier. For a finite elements model that closely simulates reality, exact material properties have to be known and chosen in advance. The results of the finite element model will have to be validated using physical testing.

Physical model
The third phase of this research is constructing and testing a physical model. After numerical modelling, with knowledge of material properties, a physical model is assembled. A physical model will determine if the numerical model outcomes are in alignment with real life situations. If modelled correctly, the physical model should correspond with the numerical model. As glass is still a relatively unpredictable material due to its brittle nature and its strength being dependant on surface flaws. Strain gauges are applied to the glass' surface to accurately measure strain at certain locations. The location of these strain gauges can be corresponded to in the numerical model.

During this research, ordering chemically strengthened thin-glass proved to be a challenge as previous partners were unable to provide chemically strengthened thin glass panes in the sizes required for this research. The process of finding a new partner took longer than expected, and while delivery of the glass samples was successful, there was not enough time to wait on validating the numerical model with thin-glass prototypes. Therefore, in this research, a plexiglass prototype is constructed beforehand. A corresponding plexiglass model is made and with application of strain gauges on the thin-glass surface, this model is verified first.

This model is refitted to the thin-glass model by simply swapping the plexiglass panes to thin-glass panes.
At this point, the maximum principal stress in the glass' surface can be predicted and will determine the maximum bending capability of the panel. This hypothesis is then validated by bending the thin glass IGU samples. Strain gauges are still applied to the surface to gain accurate strain data of the glass' surface.

1.5 Single corner cold bending

This research will be performed by using the single corner cold bending method. The reason for choosing this particular method is its practicality. This method of cold bending could be performed by using regular materials for building a testing rig. Alternatively, double corner cold bending is a topic with valuable research performed. This method of cold bending is more difficult to perform accurately, and therefore single corner cold bending is used. Single corner cold bending is an established method for rigid frame façade panels. This research will conduct experiments with flexible edge spacers and chemically strengthened thin glass. The difference in material usage therefore makes this research valuable.

Step 1: Research conducted on cold bending methods.

Step 2: Research the best combination of materials to construct an flexible insulated glass unit.

Step 3: Order materials from suppliers.

Step 4: FEM modelling of an IGU during cold bending using said materials.

Step 5: Construct the insulated glass units with the ordered materials and constructing the cold bending setup.

Step 6: Perform cold bending tests and registering data using strain gauges on the surface of the glass.

Step 7: Compare the results and verify the model.

Step 8: Conclude on the usability of the design and provide recommendations on further research.

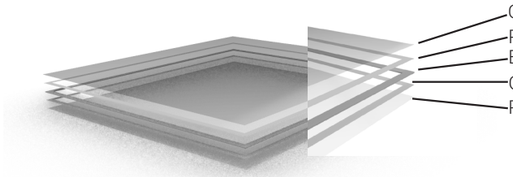

1: Assembly of thin glass IGU

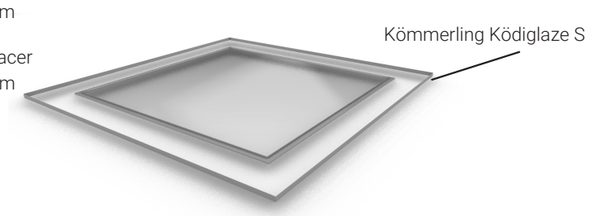

2: Sealing of the edges

3. Place IGU in cold bending setup and tighten the clamps

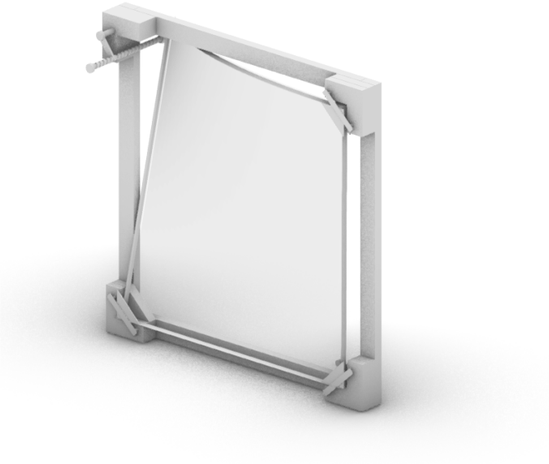

4. Cold bend IGU and record data

Figure 2. Cold bending process used during research (Own work)

1.6 Planning

Months	november				December				January				Februari				March					April				May				June				July
Presentations																																	
P1			18-nov																														
P2											23-jan																						
P3																			18-mar														
P4																									22-May								
P5																																	3-jul
Weeks	1.10		2.1	2.2	2.3	2.4	2.5	2.6	2.7	2.8	2.9	2.10	3.1	3.2	3.3	3.4	3.5	3.6	3.7	3.8	3.9	3.10	4.1	4.2	4.3	4.4	4.5	4.6	4.7	4.8	4.9	4.10	5.1
Context																																	
General Research																																	
Partners																																	
Draft grad. Plan																																	
Literature research																																	
Problem statement																																	
thin glass production																																	
Glass structural properties																																	
Glass bending capabilities																																	
Structural sealant																																	
Spacer behaviour																																	
Additional research																																	
Nummerical Research																																	
Material composition																																	
Nummerical modelling 1 (bending)																																	
Nummerical modelling 2 (optimization)																																	
Plexiglass IGU testing																																	
Construction of the setup																																	
Assembly of materials																																	
Cold bending experiment																																	
Thin glass IGU testing																																	
Assembly of materials																																	
Cold bending IGU																																	
Reflection test																																	
Finalizing																																	
Wind loads																																	
Panel assembly																																	
Panel optimization																																	
Conclusion & reflection																																	
Conclusion																																	
Reflection																																	
Presentation																																	

Figure 3. Planning during thesis period (Own work)

02
Glass

2.1 History of glass

Glass has a long and interesting history that dates back to at least 4000 years ago. The first discovery of glass was in the forms of naturally formed glass, mostly obsidian. Which was in its place used for making weapons, jewellery and money. Archaeological evidence found that the first man made glass was in Eastern Mesopotamia and Egypt at around 3500 BC and the first glass vessels were made at around 1500 BC. In the beginning of glass manufacturing, it was very hard and slow to manufacture glass. Glass melting furnaces were small and the heat they produced was hardly enough to melt glass. (Historyofglass.com, 2024).

In the first century before Christ, the glass blow pipe was invented, making production easier, faster and cheaper. Glass flourished in the Roman empire and spread through all countries under its rule. Stained glass became popular throughout Europa in churches and cathedrals. Partly because of its architectural appearance, and because glass panes couldn't yet produced at larger scales, so windows had to be divided into smaller panes separated by lead.

Since then many inventions were made improving the production process and glass composition.

Figure 4. Stained glass at chartres Rosette Nord (2015)

2.2 Float glass

In the 1950s the Pilkington brothers developed the float glass production method. Still the most important glass production method today. Before this, flat glass was either cast and rolled or drawn into sheets, both of which leaving imperfections on the surface.
The float glass production method ensures the production of perfectly flat glass sheets with uniform thickness, exceptional flatness and perfect optical quality.

In this method, a precise mixture of silica sand (SiO2), Soda ash (NA2CO3), Limestone (CaCo3) and cullet are blended and molten in a furnace at around 1500 degrees Celsius. *(Meechowas, 2013)* These components together form soda-lime-silicate glass, the most common type of commercial glass.

The molten glass is poured continuously onto a bath of molten tin. The glass is lighter than the tin and therefore it floats on top of the bath, while spreading out evenly.

The glass is then annealed, meaning its slowly cooled in a controlled environment. This controlled cooling ensures that internal stresses are relieved and the glass does not break because of temperature changes or minor impacts.

Once the glass is gradually cooled, the glass can be cut into its desired dimensions.

Nowadays there are many processes of manufacturing glass, including casting, rolling, spinning, blowing, floating and drawing. Whereby the float production takes up to 90% of the glass production. This glass consists of soda lime and silicate. There are multiple processes of manufacturing glass, including casting, rolling, spinning, blowing, floating and drawing. In architectural applications most glass consist of sand, soda lime silicate *(glasstips.blogspot.com, 2008)*

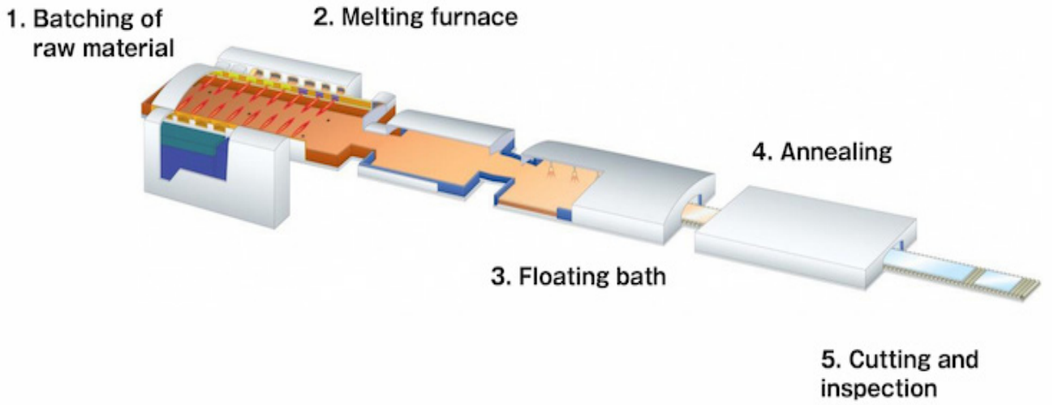

Figure 5. Float glass process (AGC, 2025)

2.3 Thin glass

Outside of the built environment, glass has also become extremely important. With the rise of electronics glass is used in screens. Reducing the thickness of glass in these products can greatly reduce the total weight and thickness of the product, being of great importance in hand-held products like phones, tablets and tv's. There are many types of glass which all have specific properties according to their applications. Advancements in the flexibility of glass have made advancements in technology with flexible or roll-able screens. This shows that innovations of the mechanical properties of glass can drive innovations of a sector as a whole. Other sectors where thin glass is becoming valuable include

- The automotive industry
- The solar energy industry
- Medical devices.

Thin glass has another production method than regular float glass. Regular float glass can typically be produced down to 2 mm, and with specialized production techniques down to 1.5 mm. Thin glass has multiple possible production processes.

In the overflown drawing fusion process, a sheet of glass is formed when molten glass overflows from a supply through, flows down both sides, and rejoins at the tapered bottom. There it is drawn away in a sheet form.

The drawn up process produces glass by drawing the molten glass upwards. This manufacturing method is suitable for somewhat thicker archtectural glasses, between 1 and 10 mm (glassonweb.com, 2018). But can be produced with thickness down to 25 µm.

To obtain extremely thin glasses between 250 and 210 µm, manufacturers use the down-drawn process. The glass is drawn downwards from the melting tank.

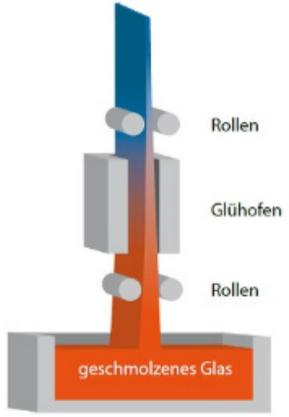

Figure 6. Drawn up process (Schott AG, NB)

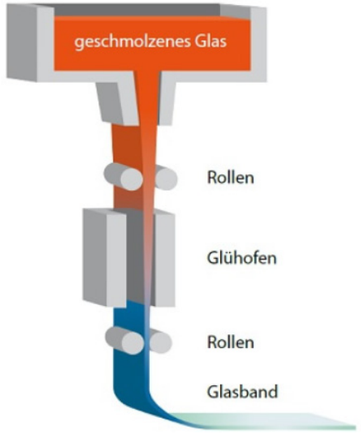

Figure 7. down-drawn process (Schott AG, NB)

2.4 The insulated glass unit (IGU)

In the building sector, insulation of a construction is defined in the Rc-value. The Rc value is the sum of multiple Rd-values of separate materials. The R-value can be obtained by dividing the thickness of the material with thermal conductivity coefficient of said material.

$$R_d = \frac{d}{\lambda}$$

Glass has a very high thermal conductivity coefficient, and combined with the low thickness of glass planes, glass has a very low insulating quality with an R-value of around 1 (m²K)/W. Because of this weak insulating capacity fitting a second pane of glass was began in the 1870s throughout Western Europe. An insulated glazing unit, consisting of two glass panes bound together into a single unit with seal between the edges of the panes, was patented by Thomas Stetson in 1865. This concept was later developed into a commercial product in the 1930's. Further development concluded to the modern IGU.

A modern Insulated glass units consists of multiple parts. First of all, the two glass panes, who are spaced apart by an aluminium spacer. This spacer is filled with a desiccant to prevent moisture building up in the construction. The spacer and the glass panes are glued together with the primary sealant, in this case Butyl. The secondary sealant seals off the rest of the construction and is the first layer to keep moisture out of the construction. Modern Insulated glass units are filled with a gas between the glass panes, to reduce thermal conductivity. This is most often Argon but can also be Krypton. The glass panes can also be treated with a film to reduce sun transmitted through the glass. IGU's can also be made with three layers of glass increasing the insulating capacity even more.
As stated before, the functionality of the IGU is dependant on the size of the cavity filled with air or gass between the glass panes. The insulating quality and value is determined by three factors; radiation, convection and conduction. Radiation is not dependant on the width of the cavity and is therefore a constant. As to be seen in Figure 8.

Heat transmission is measured in W / (m² * K) and expressed as α. The subscripts are cd, R and cv for conduction, radiation and convection respectfully. To find the optimal insulating panel, the sum of the heat transmission must be as low as possible. The heat

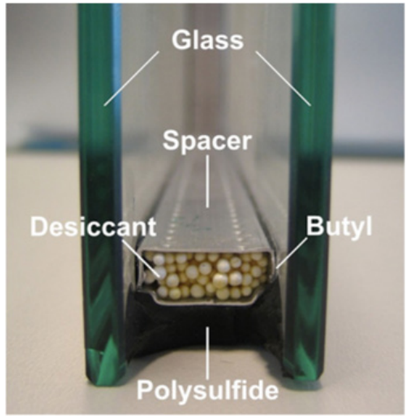

Figure 8. Classic insulating glazing unit (Norfinch glass & mirror MFG. Ltd 2024)

transmission through conductivity is defined as:

$$\alpha_{cd} = \frac{\lambda}{d}$$

Whereby is the thermal conductivity, and d is the thickness of the cavity.

Convection is governed by the cavity depth. Van der Linden (2018) gives a value of ∂cd = 0.25 W/(m².K) for a cavity of 12mm. The width of this cavity dictates the amount of conduction that takes place in the IGU. The bigger the cavity width, the heat has to pass through more air or gas. This reduces the conduction in the panel. However, increasing the width of the cavity will eventually lead to the air more freely moving around, causing convection. It is stated that for cavities larger than 20mm, the reduction of heat transport through conductivity is cancelled out by the increase of heat transport through convection. Together they are given as αcd + αcv = 1 W / (m2xK). It is assumed that αcd = αcv = 0.5 W (m2.K).

The heat resistance of the IGU Rc can now be calculated as:

$$R_c = \frac{1}{\alpha_{cd} + \alpha_r + \alpha_{cv}}$$

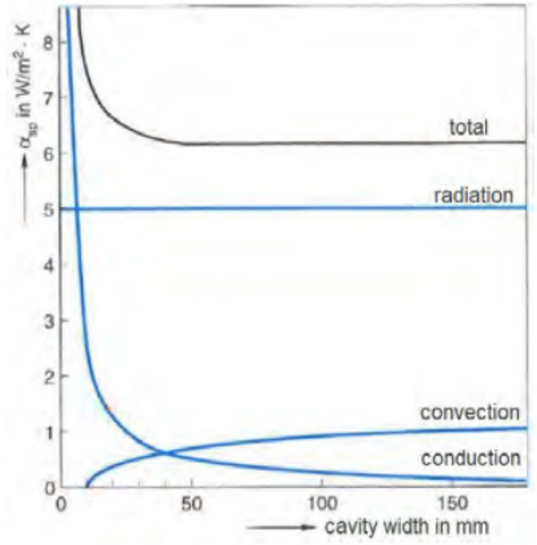

Figure 9. Relation of insulated glass unit cavity width to radiation, convection and conduction. (van der linden 2018)

2.5 Pressure in an IGU

For the IGU to function, the edges around the cavity, glass and spacer are hermetically sealed. The sealing of the edge ensures that no air can escape as this would lead to failure of the insulating value of the glass unit. By bending the IGU, the volume of the cavity might change. This causes fluctuation of the pressure inside the cavity. The air pressure inside the cavity is advantageous for the structural performance of the panel, as it helps the load distribute the load over the inner and outer pane. This can be advantageous in the case of wind loads, when the displacement of the first panel puts pressure on the gas, which displaces the second panel. This can prevent the first and the second pane from making contact under wind loads.

The final key aspect to an airtight cavity is thermal expansion / compression. Swifts in temperature can get quite high in the cavity of an IGU. The IGU basically working as a greenhouse, thus increasing the temperature differences between high and low temperatures. The effect of the gas expansion in the cavity on the adhesives can be seen in Figure 10 The fluctuation in temperature and therefore in pressure leaves an permanent deformation of the panel.

This causes stress on the adhesives between the spacer and the glass panes. Good adhesives are able to adsorb these deformations and stresses.

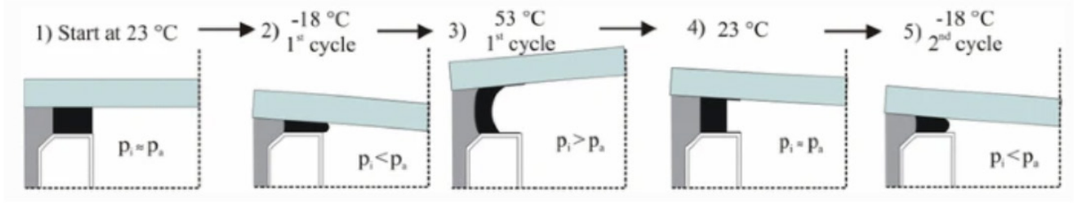

Figure 10. Movement of the primary adhesive caused by gass contraction and expansion (Buddenberg, S, Et al. 2016)

3

Glass as a structural material

3.1 Structural glass

Structural glass is a relatively new development in the building industry. Where products like wood, steel and concrete have been used for centuries, glass as a structural load bearing material has only been implemented since the last 30 - 40 years.

Structural glass is glass that is subjected to external forces without the use of a structural frame. Where in most architectural applications, forces are being carried by the frame around the glass, in structural glass, the glass itself is subjected to the force. Structural glass is used for aesthetic reasons, as frames are not required, giving the structural a clean and transparent look. (Figure 11)

Structural glass is used in different applications:

- Glass floors
- Glass roofs
- Glass façades
- Glass staircases

Annealed float glass is cooled in a gradual manner, allowing the glass to be cut without shattering. The production of float glass in these controlled conditions provides a perfectly elastic, isotropic quality. The theoretical tensile strength derived from this glass is exceptionally high, and may reach up to 32 GPa (Overend. M, 2022.) However, the strength of glass in reality is defined by much more than just the theoretical tensile strength.

Figure 11. Apple store New York, this picture shows the unmatched transparancy a structural glass structure can provide. No big other load bearing

3.2 Surface Flaws

Strength of glass is more defined by its surface imperfections. After the glass is formed, little cracks start to appear on its surface. The real characteristic strength of float glass lies more around 45 MPa. This decrease in strength is result of stress concentrations around the glass surface imperfections. Surface imperfections propagate under tension but not compression. That is why glass' compressive strength is much larger than its tensile strength. However, the compressive strength is generally irrelevant for glass in structural applications, as transversal tresses arising from Poisson's ratio effects or from buckling tend to cause indirect tensile failures and dominate the design. (Overend. M, 2022).

Flaws on the surface of glass are a product of time, that's why, when designing with glass, the design strength is calculated with load duration.

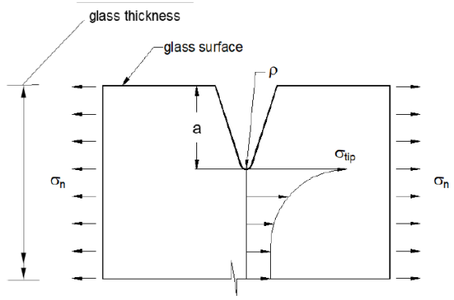

Figure 12. Stresses at glass' surface flaws (Overend, 2022)

Surface flaws on glass can create huge stress concentrations. With flaws, outer layers on the glass surface can allow for far greater displacement than the tip of the flaw. When glass is cold bend, one face of the glass is subjected onto tension, the other under compression. The face under tension is the weak link in this process. As can be seen in Figure 12. Qtip can be calculated by the following formula.

$$\sigma_{tip} = k_{shape}\sigma_n\sqrt{a/\rho}$$

whereby:

$k_{shape} = Shape\ of\ the\ flaws$
$\sigma_n = Tensile\ stress\ perpendicular\ to\ the\ crack$
$\rho = Radius\ of\ the\ tip\ of\ the\ crack$
$a = depth\ of\ the\ crack$

This equation can be expressed in terms of stress intensity Ki;

$$K_I = Y\sigma\sqrt{\pi a}$$

Whereby

$Y = factor\ accoutning\ for\ crack\ geometry\ and\ location$

When KI exceeds the plain strain fracture toughness, fast fracture will occur.

As discussed earlier, surface flaws on glass can grow when the glass is subjected to tensile forces. When grown to big, these surface flaws cause the glass to fail and crack. This is called stress corrosion. Because of the growth of these flaws, the tensile strength decreases with time. Therefore, a load duration factor

called Kmod is applied when determining the strength of glass.

The Kmod can be determined with the following formula, where fref is the tensile strength at the reference time tref (generally taken as 3s) and n is the static fatigue constant ≈ 16 for normal conditions. The variation of (kmod) or relative strength with time, for a constant stress history is shown in Fig ?. The dashed line is the sub-division of stress corrosion into long, medium and short term load durations (Table 6.2), which makes it easier to apply in practise.

$$\frac{f_g}{f_{ref}} = \left(\frac{t_{ref}}{t_f}\right)^{1/n} = k_{mod}$$

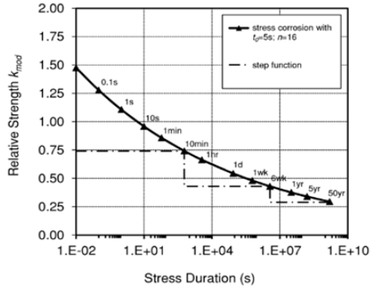

Figure 13. Relative strength vs Log10 stress duration (overend, 2022)

Surface flaws cannot propogate in compression, but since true compression is almost never achieved, or because of poisson's ratio effects, tension will always arise in certain parts of the glass' surface. Therefore, the design strength of glass is mostly defined by the tensile strength. Which is on its own defined by the surface imperfections, and the load duration. Table 1 shows the chemical composition of regular float glass. One of the big advantages of glass is that it is fully recyclable. The more cullet is added to the molten glass batch, the lower the footprint is. As to be seen in the table, silica sand has a relatively low carbon footprint. Mostly Soda Ash has a high carbon footprint in the glass composition as it is an energy intensive production process.

3.3 Chemical composition

Chemical Structure of Different Glasses: Glasses are amorphous (non-crystalline) solids typically formed by cooling a liquid without allowing it to crystallize. The most common type, soda-lime glass, is composed mainly of silica (SiO_2), with sodium oxide (Na_2O) and calcium oxide (CaO) added to lower the melting point and improve workability. In borosilicate glass, boron oxide (B_2O_3) replaces some of the silica to enhance thermal and chemical resistance. Lead glass contains lead oxide (PbO), which increases the refractive index and density, making it useful for optical applications. Each glass type maintains a disordered silicate network, but the inclusion of various oxides modifies its properties by disrupting the Si–O–Si linkages and introducing non-bridging oxygens.

Chemically strengthened thin glass, is typically made from aluminosilicate glass. This type of glass consists of a network of silicon dioxide (SiO_2) in which some of the silicon atoms are substituted by aluminum (Al^{3+}), forming a more robust aluminosilicate framework. The glass is strengthened through an ion-exchange process, where smaller sodium (Na^+) ions in the glass surface are replaced by larger potassium (K^+) ions from a molten salt bath. This substitution creates compressive stress at the surface and tensile stress in the interior, significantly enhancing the glass's resistance to scratches and cracks while preserving its transparency and thin profile.

Glass Type	Primary Composition	Density (g/cm^3)	Young's Modulus (GPa)	Shear modulus (Gpa)	Tensile Strength (MPa)	Hardness (vickers)	Bending strength (Mpa)	Poisson's ratio	Thermal Expansion (10^{-6}/K)
Soda-Lime Glass	SiO_2 (70-75%), Na_2O (12-15%), CaO (10-12%), MgO, Al_2O_3	2.44–2.49	68,2–71,7	28-29,5	31 - 34,2	439-484	31-35	0,21-0,22	8–10
Borosilicate Glass	SiO_2 (~80%), B_2O_3 (10-13%), Na_2O, Al_2O_3	2.2–2.3	63–65	30,8-32,3	35–50	500–600	35-100	0.20	3–4
Aluminosilicate Glass	SiO_2, Al_2O_3 (15-20%), Na_2O, K_2O, MgO	2.5–2.7	70–75	28-35	50-100 - 300-700Mpa	600–700	50-120 (400-700)	0,20-0,25	4–6

Table 1. Chemical composition of different glass types derived from (Oikonomopoulou, 2019)

Type of glass	Standard	$f_{g,k}$ N/mm²
Float glass	EN 572-2	45
Polished wired glass	EN 572-3	33
Drawn sheet glass	EN 572-4	45
Patterned glass	EN 572-5	33
Wired patterned glass	EN 572-6	27

Table 2. Characteristic design (tensile) bending strength for soda lime silicate float glas

3.4 Strengthening of glass

There are two primary methods to improving the structural properties. Tempering and chemical strengthening. During the glass tempering process. Glass undergoes an intense heating process, followed by a rapid cooling process. This sudden and quick change in temperature makes the outer layers of the glass pane contract. The rapid contraction in the outer layers causes compression on the surface, while tension is formed in the core.

This method is often used for glass applications where fall through, or shatter safety is required, like roofs, and large windows.

During chemical strengthening, float glass is submerged in an molten alkali salt bath of approximately 300 - 450 degrees Celsius. In this process, smaller alkali metal ions (typically sodium ions, in the glass surface are replaced by the larger alkali metal ions (commonly potassium ions) found in the bath. The larger alkali metal ions squeeze themselves in the gaps left by the sodium ions. The surface of the glass is now also in a state of compression, while the core is in compression.

Simultaneously, the compression of the surface further closes micro-cracks and thus suppress the initiation of crack propagation, making the influence of surface flaws on the glass' strength smaller.

The advantage of chemically tempering is that it is applicable to thin glass, whereas the tempering process is not. Furthermore, chemically tempering offers better optical quality as it leaves less distortion in the surface compared to the tempering process.

Engineers work with design strengths to calculate the maximum capacity of glass products. According to European standards, specifically CEN/TS 19100 and EN 16612, the characteristic bending strengths for different types of soda-lime-silicat glass are:

- Annealed glass: 45MPa
- Heat-strengthened glass: 70MPa
- Thermally toughened (tempered) glass: 120MPa

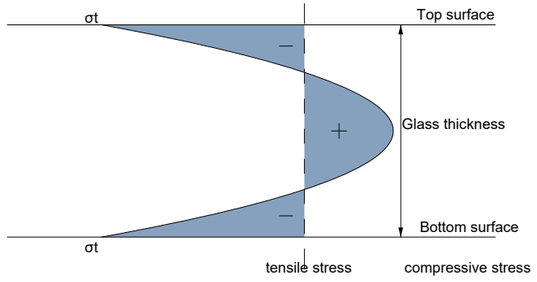

Figure 14. Section of heat strengthened glass (Datsiou, 2014)

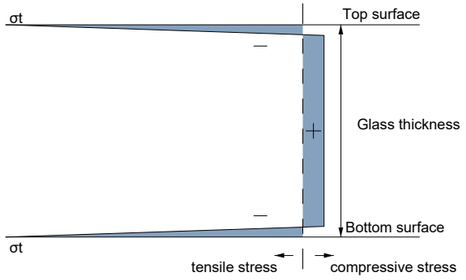

Figure 15. Section of chemically strengthened glass (Datsiou, 2014)

3.5 Laminated glass

In many situations, glass is laminated to make it safer during breakage. Laminating two glass panes with a PVB interlayer ensures the glass doesn't shatter everywhere, but makes the glass "stick" to the interlayer. PVB or polyvinyl butyral is an adhesive plastic layer between the two glass panes. Lamination prevents glass from shattering after breaking. The glass shards stick to the PVB interlayer, reducing injury risk. Lamination is applied to glass where it is an requirement for glass to remain in place after breaking; for example, glass roofs, or high rise windows/façades. Laminating the glass has no observable effect on the crack propagation, but has a significant influence on the post-fracture performance. (Overend, M. 2022).

While the lamination of glass panes in cold bent façades is a very important factor to increasing safety, laminating thin glass panels is worth a research project on its own. Including the lamination of glass does not fit in the scope of this research. Therefore, the equivalent thickness of laminated glass as a monolithic pane can be calculated.

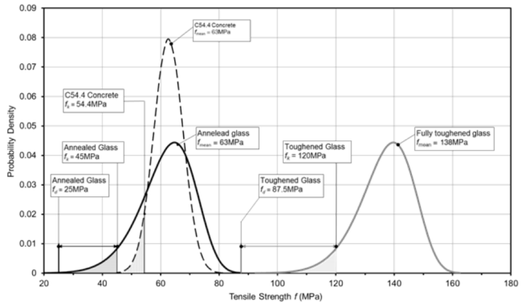

Graph 1. Probability density functions of tensile strength of annealed glass and fully toughened glass (Haldimann, L Et al. 2008)

$$h_{eq,\delta} = \sqrt[3]{(1-\bar{\omega})\sum_i h_i^3 + \bar{\omega}\left(\sum_i h_i\right)^3}$$

Equivalent thickness for calculating the bending deflection.

$$h_{eq,\sigma} = \sqrt{\frac{\left(h_{eq,\delta}\right)^3}{h_i + 2\bar{\omega}h_{m,i}}}$$

Equivalent thickness for calculating the bending stress in the I plane.

Where $0 \leq \varpi \leq 1$ represents no shear transfer (0) and full shear transfer (1); h_i is the thickness of the glass plies; $h_{m,i}$ is the distance between the mid-plane of ply i and the mid- plane of the laminated glass unit, ignoring the thickness of the interlayers (Overend, M. 2022).

Figure 16. Laminated Glass (BAsystems.co.uk, retrieved 2025)

3.6 Curved glass façades

There are three methods in creating a curved glass façade: division panelling, hot bending or cold bending.

Division panelling
A seemingly round surface can be divided into many smaller flat surfaces. This theory can be applied in façade design. A round glass façade would be made out of flat glass panels. The higher the division rate of panels on the total façade, the smoother the surface can result in. This method is often used in projects which have tight budgets, as flat panelling is a cheaper option. However, a completely smooth surface can never be created using flat panelling, and therefore the true desired effect of a curved façade is often not achieved.

Hot bending glass
Bending glass panes is not a new concept. Bending glass in its heathened state has been around since the late 19th century. Manufacturers use a mold and an oven to shape the glass into a certain shapes. There are two types of curved glass using heat: hot bending glass, and tempered curved glass. In both situations the mold and the glass are heated up to around 580 and 630 degrees Celsius. While in this state, the glass has high flexibility and can be curved into many shapes, synclastic or anticlastic. The glass is curved or bent in its desired shape. Hot bend glass is cooled slowly, giving minimal distortion to the glass and providing better optical quality.

Tempered glass is cooled rapidly, this is a technique called quenching. By rapidly cooling the glass, the outer layers contract way faster than the internal layer, creating tension in the pane.

The hot bending technique for façade construction has positives and negatives. The positive side of hot bending is that almost every imaginable shape can be produced using this method. For façade application this often means anticlastic (double curved) shapes, with possibly a very small curve radius. This offers great design flexibility for architects and façade designers. The smoothness of the shape can be completely controlled, also meaning that the glass can be very well distributed over its surface. This ensures very good optical quality of the curved glass panes.

Another positive is that hot bent glass is stress free. As the curving geometry is achieved in the liquid state of the glass, no more stresses will form in the glass in its cold state.

Negative aspects of hot bending glass are its inefficient production process. An already completed glass pane has to be cut into shape firstly, then reheated back to its liquid state to achieve its desired shape. This adds an extra, energy inefficient step to the production process. Moreover, the same panels often get made twice, to make sure there is an replacement should the panel break during transportation or instalment.

If every panel to be made has a unique shape, unique molds have to be used, making the production non scalable and not easily automated. These steps increase carbon offset, time, and decrease flexibility of a project.

Figure 17. Hot bent façade of ELbphilarmonie Hamburg, (Schielke, 2017)

3.7 Cold bending glass

Cold bent glass uses an already finished glass pane product. The curve of the façade is defined by an existing framework. The glass panels need to be bent according to the shape of that frame. This process requires more force to bend the glass into the desired shape, because the glass is in its elastic state, the glass wants to bend back to its original state, producing permanent tension in the glass and on used adhesives. How far a piece of glass can bend into a curve depends on the thickness of the glass. Cold bending glass façade panels is applied in curved glass façades where the individual panels have a small curve radius. The bending stiffness of the panels dictate the maximum allowed curvature of the cold bending of the panel. Cold bending on site is much cheaper and faster option than hot bending because uniform panels can be delivered on site, where they are bent into place. Cold bending can be done in many forms. A single curved geometry is often cold bent with a maximum curvature with a radius of 3 meters.

A more common method of cold bending being used in architectural applications at the moment is Single corner cold bending. Hereby one corner of the façade panel is pushed out of plane, creating a slight curvature on the plane of the glass. A newly explored option for cold bent façades is free-form cold bending. Whereby the advantage of free form cold bending is that more extreme curved geometry façades can be achieved.

A big difference between single corner and free-form cold bending are the edges. Single corner cold bending can be achieved with straight framing members.

Spherical and concave/convex free-from curves are based on flexible framing members, whereby the glass is pressed on to the spacer, and kept in position by adhesives. The glass, with its inelastic nature wants to bend back in to its original flat state, therefore producing big stresses on the adhesives and on the flexible spacers.

Another possibility in cold bending is creating an anticlastic shape. Which could also be approached as double corner cold bending. In theory, anticlastic shapes also have straight framing members, which would make it easier to produce than free-forms with curved framing members.

Figure 18. Cold bent glass façade (Credit Libanais beirut, 2013)

3.8 Cold bending of glass façade panels

Cold bending of glass panels is an interesting and effective way of creating large curved façades. However, the maximum bending capacity of a panel is pane is largely determined by its glass pane thickness. Therefore bending capicity is limited. The relationship between thickness and bending capacity can be explained through flexural rigidity (D), a mechanical property that governs a plate's resistance to bending. The flexural rigidity formula is derived from the Kirchhoff-love plate theory (1888) for a glass plate this would be:

$$D = \frac{Eh^3}{12(1-\nu^2)}$$

D: Flexural rigidity of the plate [N · m]
E: Young's modulus of the material [Pa or N/m^2]
h: Thickness of the plate [m]
ν: Poisson's ratio of the material [–]

The flexural rigidity is dependant on the Young's modulus (E), the poisson"s ratio (v) and the thickness (h). The thickness of the plate has a large influence to the flexural rigidity. Twice a thicker plate, means 8 times a stiffer panel. A quick conclusion would be that a thinner glass plate would be more flexible and thus better perform in cold bending applications. However as previous work shows, thin glass has its own drawbacks - namely:

- Reduced capacity to resist transverse load
- Limited ability to be warped without buckling
- Increased deflection under transverse load

Thus, in the realm of cold warping there exists an optimal thickness for a given size, geometry, and required load resistance (Bensend, A. 2018).

However, cold bending of façades panels is dependant on many aspects. The behaviour of the frame is equally important as glass while cold bending a panel. Combining all these factors creates a stiff façade panel whereby substantial amount of force must be applied to shape it into its desired position. This prolongs installation time per façade panel installation on the building site.

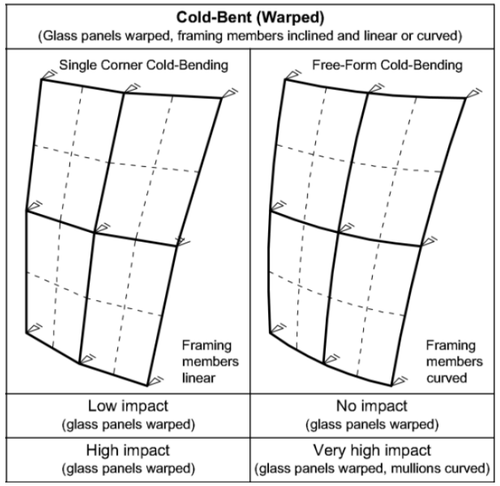

Figure 19. Single corner cold bending v free form cold bending. (Meinhardt, 2017)

When a flat façade panel is bent into its desired shape the frame of the panel is deformed. The frame twists around its own axis as can be seen in figure 20 (Rahimzadeh, K et al. 2023). After the façade panel is installed these deformation will remain. The next façade panel will arrive flat next to the previously installed panel. The flat panel now has to interlock with the previously installed, and now deformed panel as. The discontinuity between the frames creates a challenge in interlocking both the panels with each other. Panels not interlocking leaves opportunity for flaws in air and water tightness of the façade. To address these issues, Himzadeh, K. et al. (2023) controlled the angle at which an facade panel edge was cut by using a compound miter. This allowed them to prefabricate each panel with the exact geometry that would connect them to the previous and next panel without twisting. However, although the edges themselves might be adjusted to the possible twisting, the glass itself is still twisting. This could compromise the structural silicone bite, and/or the interface with the exterior mechanical cap, if included. Therefore, a middle ground was explored.

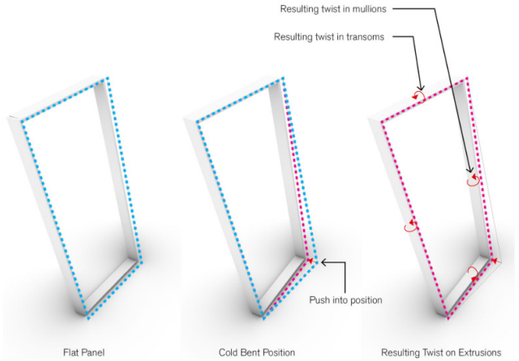

Figure 20. Diagram indicating how framing elements are twisted during the conventional flat-panel cold-bending process. By K. Rahimzadeh et al. (2023)

3.9 Maximum achievable curvature by cold bending

The maximum achievable curve of a glass panel is largely dictated by the thickness of the glass. The maximum achievable curvature of a glass pane can be calculated with the following formula:

$$\sigma = \frac{E \cdot t}{2 \cdot R}$$

$\sigma = stress\ in\ the$ glass $(Pa\ or\ N/m^2)$

$E = young$'s modulus of glass (around 70Gpa)

$t = thickness\ of\ the\ glass\ pane\ (m)$

$R = radius\ of\ the\ curvature\ circle$

The maximum bending angle θ_{max} can then be derived geometrically

$$\theta_{max} = \frac{L}{R}$$

$L = arc\ length\ (m)$

$R = Radius\ of\ curvature\ (m)$

For a glass pane with regular mechanical properties of 1.5 meter long, and 6mm thick, this would result in maximum curvature radius of 4.2 meters. Providing a curvature of figure 21.

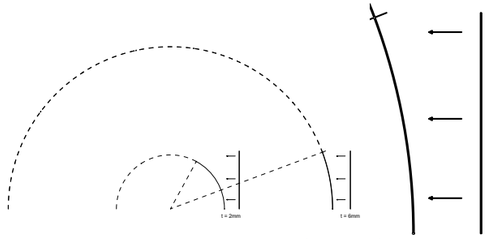

Figure 21. Maximum cold bending Radius.(own work)

3.10 Visual distortion

During both the production and cold bending process, glass can develop distortions in its surface that affects its optical quality. Visual distortion in glass surfaces arises from variations in thickness, residual stresses, bending processes, or surface irregularities. These distortions can impact both the functional and aesthetic aspects of glass, influencing reflections, transmitted images, and overall clarity.

One common cause of visual distortion is the manufacturing process itself. For subsequent processing techniques for float glass such as tempering, chemical strengthening, lamination, and cold bending can introduce stress variations and surface deviations that lead to optical distortions. Roller wave distortion, often observed in tempered glass, occurs due to contact with rollers during heat treatment, creating periodic waves that interfere with reflections.

Chemically strengthened glass, unlike thermally tempered glass, undergoes an ion-exchange process where smaller sodium ions in the glass surface are replaced by larger potassium ions when immersed in a molten salt bath. This creates a compressive stress layer that enhances strength and durability without the visible distortions typically associated with tempering. Since chemically strengthened glass does not go through the heating and cooling cycles of thermal tempering, it exhibits fewer optical distortions and is preferred for high-precision applications such as display screens and aircraft windows.

Imperfections on the surface of large glass façades are the easiest to notice. Especially when orthogonal shapes are reflected on the façades.

Figure 22. Roller wave distortion (Abbot, M. et al, 2001)

In applications where glass is cold-bent for structural or aesthetic purposes, visual distortion becomes more pronounced. Cold bending induces internal stresses that can lead to ripple formations or localized warping, particularly along constrained edges or diagonals. The extent of distortion is influenced by factors such as glass thickness, support conditions, and applied loads. When the distortion exceeds acceptable limits, it can cause unwanted reflections, image distortion, or even visibility issues.

Accurate measurement and analysis of visual distortion are essential for quality control in glass applications. Various optical techniques, such as grid reflection analysis, Moiré interferometry, and laser scanning, are used to quantify surface irregularities and assess optical performance. Understanding and mitigating visual distortion through optimized manufacturing techniques, improved installation methods, and precise measurement tools ensures that glass retains its clarity and functional integrity in demanding environments.

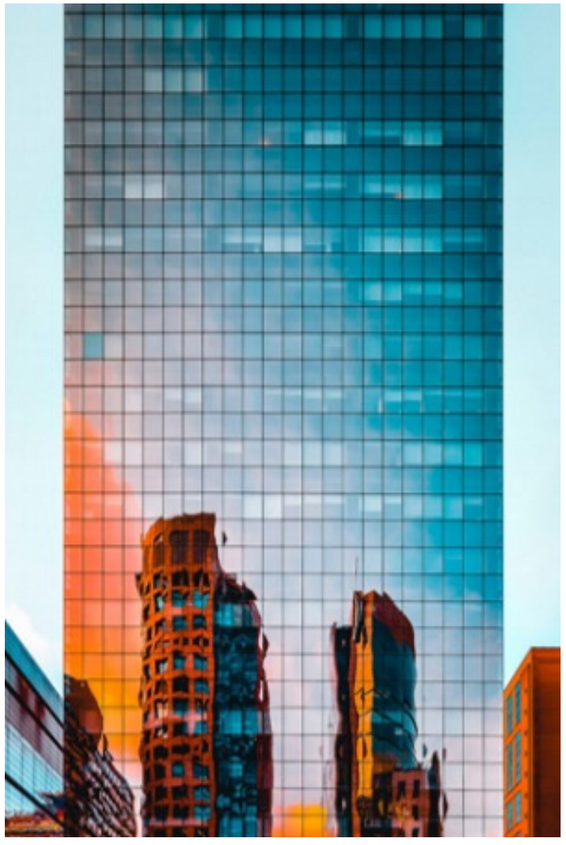

Figure 23. Roller wave distortion (Glassonweb, 2019)

3.11 Curved glass shapes

A flat plane is prone to deflections more easily than a three-dimensional plane. Adding a third dimension ads an axis for forces to be transferred through. For glass façades, the applied load comes mostly in the form of wind loads, or impact loads. Making glass safe against impact loads can be achieved by either tempering or chemically strengthening the glass, as explained before. Minimizing deflections as a result of wind loads is usually achieved by the thickness of the glass pane. Should thin glass be used in for example a high rise façade, minimizing against wind loads could be achieved by altering the shape of the pane.

For thin glass improving the structural properties of the panel will likely not be enough to overcome large deflections of the panel. Bending the panel out of plane will likely give the panel more stability and stiffness. A flat plane can be formed into many shapes. We can categorize these shapes into three subdivisions; synclastic shapes, anticlastic shapes and monoclastic shapes.

In order to improve structural stiffness in the glass plane, one of these shape definitions could provide the best outcome. Single curved shapes are likely not ideal to improve structural stability of the glass plane. The single curve on the surface would likely concentrate the stresses of the entire surface on a too small part of the glass plane. Synclastic and monoclastic shapes both have a more complex shape. The surface shapes are both defined by the bending of at least two curvatures. The difference being the direction of the centre points of the curve. The structural quality of these shapes is that the internal stresses of the plane are more equally divided over the surface.

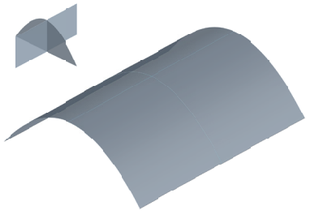

Figure 24. Monoclastic shape, single curvature. (own work)

A Monoclastic shape is characterized by bending in only one direction.

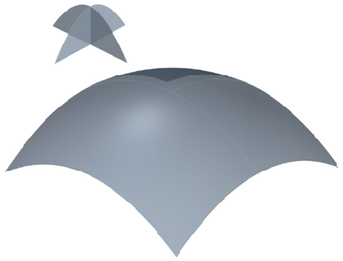

Figure 25. synclastic shape, two curves in the same direction. (own

A synclastic shape consists of curvatures that bend in the same direction along two principal axes. This means that the curvatures are either positive or negative, and that the shape of the surface will resemble a bowl or a dome.

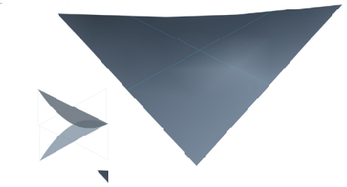

Figure 26. Anticlastic shape, two curves in the opposite direction

An anticlastic shape is defined by two curves who have their centre points at the opposite side of the surface. Anticlastic shapes, (Hypar or saddle) shapes can be achieved both with curved and straight edges.

04

Previous research

4.1 Hypar buckling phenomenon

Multiple studies done on cold bending of thin glass have been conducted. In this section, relevant these studies are evaluated to find if lessons can be learned, and improvements can be made.

Studies performed by Galuppi (2014), Young (2019) and van Driel (2022) involved shaping thin glass into a hyperbolic paraboloid (hypar) shape. Due to the curvature, membrane forces would be activated in the glass during loaded conditions. The hypar would provide a stiff surface as the double curved shape equally distributes much of the stress over the entire plane. However, both van Driel and Young concluded that pushing the glass into a hypar shaped proved to be very hard. Multiple issues arose during the testing phase.

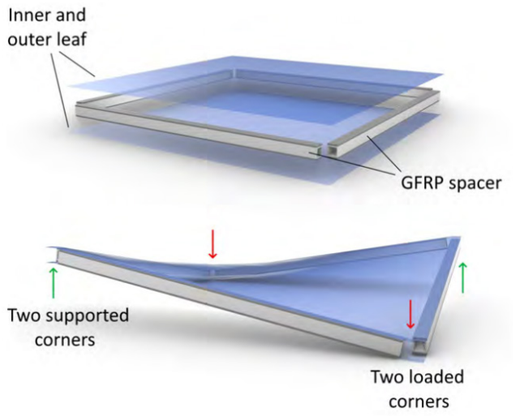

Figure 27. 3D visualation of the panel that is used in the test setup of van Driel. (van Driel, 2022)

Plates buckling

The Kirchoff-love theory that predicts that when a rectangular plate is subjected to force at two corners, a hyperbolic paraboloid would form. However, experiments have provided evidence that a particular form of instability occurs above a certain limit of the distortion: one of the principal curvatures becomes dominant with respect to the other. The glass plate would form a single curve and the edges would take on a curved shape. Research by Galuppi (2014) made a model that would predict this phenomenon. The results are shown on the right.

At a certain deflection the hypar shape would snap. This snap causes the straight diagonals to curve, whereby the double curved hypar shape would turn into an single curved shape. This is called the Buckling phenomenon.

Galuppi, L (2014) shows Three stages of forming a hypar glass shape. In this model, a square glass plate of 2000x2000mm, 10mm thickness is used. Figure 28 shows a four-point supported glass plate with pre-scribed displacement of the corners of 10mm (scale factor 50). This displacement is small considering the size of the panel (2000x2000mm). In this situation, the plate is in a hypar shape with straight edges.

In figure 29 the corner displacement has increased to 70mm. The surface still resembles a hypar shape, except with more curvature near the corners. Furthermore, the edges are not straight and have formed in an S shape.

In figure 30 The glass plate has turned into an almost single curved shape.
Galuppi concludes that the buckling of the surface is caused by the curvature of the supposed to be straight edges.
To combat this behaviour Galuppi (2014) modelled a stiff edge around the perimeter of the glass. The finite element model shows that the stiffened edges delay the buckling phenomenon. Therefore it was recommended to test this numerical theory physically.

Panes touching

A finite elements model of two glass panes connected with an GFRP frame was modelled. The model showed that the panels move towards each other. This means that at quite low corner deflections the panels would touch. The exact moment being dependant on the thickness of the glass and the type of adhesive used.

While the research conducted by van Driel does not serve the same porpuse as this research, a large paragraph of the thesis is about creating a finite elements model that could accurately simulate the bending of the IGU.

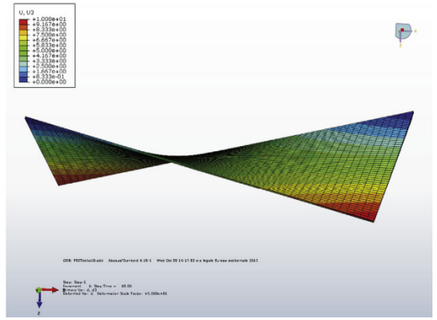

Figure 28. Four-point supported glass plate with pre-described displacement of 10mm (scale factor 50) L. Galuppi et al. (2014)

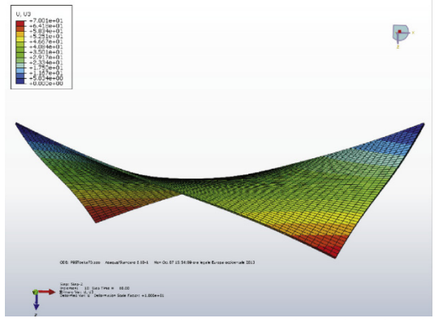

Figure 29. Four-point supported glass plate with pre-described displacement of 70mm (scale factor 10) L. Galuppi et al. (2014)

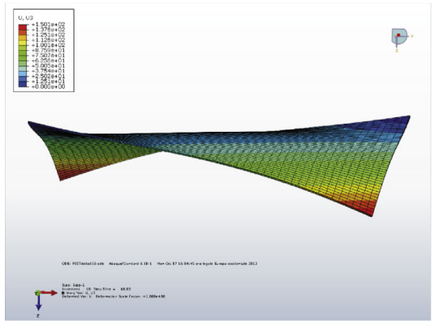

Figure 30. Four-point supported glass plate with pre-described displacement of 150mm (scale factor 3) L. Galuppi et al. (2014)

Staaks (2003) tested rectangular glass plates during cold twisting. One element that could be concluded from the research is that the relative thickness of the plate influences the timing and nature of the displacement of the centre of the panel. The lower the relative thickness of the plate, the more snappy the buckling will occur. Staaks used a single corner deformation, which is the equivalent of a double corner deformation.

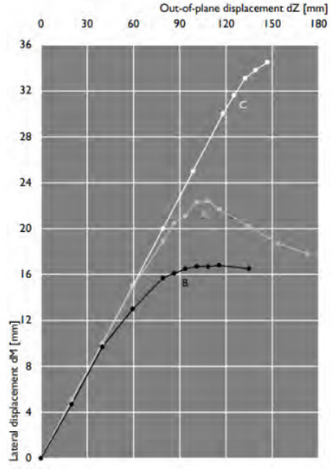

Figure 31. Graph of the displacement of dM and dZ in the situation drawn in figure 32B It can be observed how for specimen A, the discplacement of the centre snaps at a certain point, meaning that the pane turned into a single curved shape instead of a hypar. With the relatively thicker plate B, this buckling occurs a bit earlier and more gradually.

Specimen	Dimensions	Thickness
A	1721 × 1688 mm	8 mm
B	1779 × 1800 mm	10 mm
C	2066 × 1088 mm	10 mm

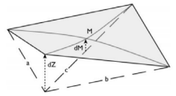

Figure 32. A (left) and B (right). shows the dimensions of the specimen and a sketch of the experiment setup.

4.2 Adhesives & sealants

Applying the right adhesive is important and influential to finding a properly bending IGU. When an IGU is bent, the adhesive must keep the glass and spacer attached whilst performing perfectly impermeable, as argon gas must not escape the cavity. The sealant also has to offer slight flexibility, as during the cold bending process, shear stresses cannot be too high as they will be redirected towards the glass and spacer. Thus it is necessary to find the adhesive with the right properties for this research.

This section takes reference from multiple research papers mentioned in "Investigations on the cold bent behaviour on the cold bending behaviour of a double glazing unit with a rigid edge spacer frame" written by Tim van Driel in 2022. The source research papers from Fedoseeva and Young were not available during the writing process of this thesis. The research performed by van Driel (2022) tried cold bending two thin glass panes connected to a GFRP spacer into a hypar shape. The research propagates on earlier research performed by Young (2019), where a single glass pane with an GFRP rigid edge was cold bent into an hypar.

A study performed by Fedoseeva (2017) researched different adhesives and their performance when used for joining glass to a GFRP frame. Three adhesives from three different manufacturers were considered. Each with large variations in strength and stiffness.
The following adhesives were tested involved in the research:

- 3M Scotch-Weld Epoxy Adhesive DP490
- Kömmerling Körapox EP 40619 & EP 42091
- SikaForce, 7666

The basic stiffness properties of the adhesives were tested through tensile dumbbell tests and double lap shear tests (figure 33, 34)

The basic stiffness properties as a result of the dumbbel test are shown in table 3.

Adhesive bulk properties	DP490	Körapox	SikaForce
ν	0.38	0.38	0.45
$E_{adh,bulk}$ [MPa]	1427	298	286
$G_{adh,bulk}$ [MPa]	517	108	98.6

Table 3. Bulk properties of different adhesives (Fedoseeva, 2017)

The value of the poisson's ratio (v) of Körapox and SikaFore were deemed incorrect and omitted. The value for DP490 was taken form Nhamoinesu (2015). The value for Körapox was assumed to be equal to the value of DP490, and the value for SikaForce is speculated by van Driel (2021) to be taken from the manufacturers.

Figure 33. Set-up of the tensile dumbbel test. (fedoseeva, 2017)

Figure 34. Set-up of the double-lap shear test. (fedoseeva, 2017)

The double-lap shear test was done to determine the shear stiffness and shear adhesion strength. Every adhesive type was loaded until failure. The results found that DP490 failed al 19.9 kN, Körapox failed at 7.3 kN and SikaForce failed at 2.30kN. Therefore DP490 performing the best and being the strongest. The research provided a disclaimer stated that the mixing possibly was not done thoroughly and could have an influence on the results.

In research performed by Young (2019), three separate tests on a Glass fibre reinforced polymer (GFRP) connected to glass. Two of the three samples were made with DOWSIL 795. The other one was made with The Körapox also used in the research performed by Fedoseeva. DOWSIL 795 has a much lower stiffness than Körapox, with a tension adhesive strength of 45 and 60 MPa at respectively 25% and 50% extension. (DOW, 2022). In theory DOWSIL 795 would develop less stress in the adhesive at the cost of overall stiffness of the panel (van Driel, 2022).

To compensate for the lower stiffness, DOWSIL 795 was applied in a 5mm thickness as opposed to the 2mm thickness of the Körapox. In the test, wire gauge transducers were placed on the panel to measure vertical displacement. Two out of the three tests lead to meaningfull results. During the first test with Körapox peeling of the adhesive occurred at a position where stress levels were not expected to cause this failure. This has been suspected to be caused by poor mixing. The second panel (using D795) fell from the test setup leaving no meaningful result to the test.

A picture of the test setup can be seen in figure 35. The results of Körapox and DOWSIL 795 can be seen in Table 3

Figure 35. Experiment test setup. Young (2019)

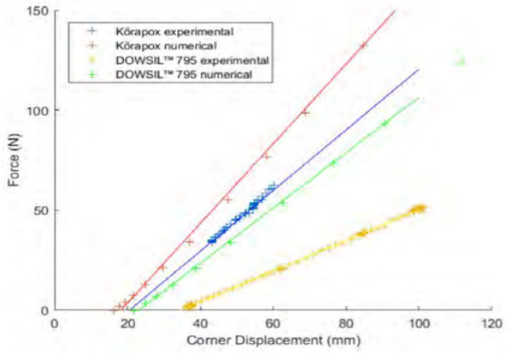

Figure 36. Numerical and experimental test data for adhesives during cold bending (Young, 2019)

From the research performed by Fedoseeva, the DP490 proved to be the strongest adhesive. However, for the panel, Körapox was concluded to have the right combination of strength and stiffness. Therefore Young performed the experiments with Körapox, where it was discovered that it was still to stiff. A more flexible alternative was required for the research.

After consultation with Dow, van Driel (2022) chose to use DOWSIL 993 Structural glazing sealant. This adhesive is widely used in structural glazing applications. And has strength and stiffness properties that make it a popular choice for cold bending. The research concluded that adhesive DOWSIL 993 performed well during the tests. However, the GFRP spacers used in the experiment were not stiff enough. After more stiff spacers should be used in following research, DOWSIL 993 should be evaluated again to find out if it can withstand higher stress levels.

4.3 Interlayers

Another study by Zhang, et al. (2021) tested single corner cold bending on 9 tempered glass panes with a size of 2200 x 1200mm with a pvb interlayer. Thickness' of the panes was 5, 6 and 8 mm but same panes with the same thickness were used to laminate . The aim of this experiment was to research the mechanical response and the properties of cold formed laminated tempered glass panes after applying with a wind load. Their method consisted of using two clamped edges and to free edges to allow for the single corner displacement. The displacement for the free corner point is 30 mm and 60 mm respectively. This gives a curvature of 0.6% and 1.2% respectively.

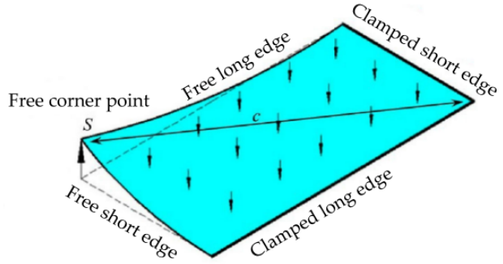

Figure 1. Cold bending and load action mode.

Figure 37. Cold bending and load action mode (Zhang, et al. (2021)

The most important findings include:

• The maximum stress of a PVB laminated tempered glass pane with single corner cold bending appears near the corner point in the short edge direction. This is located near the edge of the pane and this is unfavourable to the stress of the glass pane.

• The influence of the cold bending stress is defined by these three aspects (In order of influence)
  • The cold bending curvature
  • the thickness of the glass pane
  • The thickness of the PVB interlayer

• When the cold bending curvature is large and the glass thickness is large and the interlayer thickness is small, the bearing capacity of the glass is panes is controlled by the cold bending stress. Therefore, the cold bending curvature should be limited.

• When there is single angle warping cold bending, the maximum value of the load stress coupled with the cold bending stress is located in the center of the glass pane.

• The load stress curve and load deflection curve of the cold-formed glass panes show a slight nonlinear relationship under the later load.

• The thickness of the PVB interlayer has little effect on the chance in the stress and the deflection equivalen effects of cold bending and load coupling.

4.4 Spacers

Using the right spacer material is important to the cold bending process. The ability of IGU edge seals and spacer bars to cope with high deflections is not only important for long term cold bending deflections, but also for short term deflections due to wind loads. (Beer, B. 2019). Traditional spacer bars are made out of aluminium and stainless steel, but relatively new spacers available on the market are Silicone foam spacers and thermo plastic spacers (TPS).

The glass is continuously subjected to bending stress throughout its lifetime, which affects the bearing capacity of the glass plate. The sealing spacer materials and glass plate bend and deform together; there is mutual restraint between them that produces an interaction. If the interaction is too large, the large relative slippage between the glass plate and the sealing spacer materials may be too great, resulting in failure of the insulating glass. Thus, studying the stress distribution in the cold bending process of insulating glass is necessary for safe application of cold bending technology.

TPS spacers usually consists of a one component polysibutylene with included desiccant material. These spacers do not include metal stiffner. And the whole spacer is a homogeneous flexible material. Therefore, these spacers tend to be able to withstand higher deflections of the insulating glass units compared to metal spacer bars. As this reduces shear stresses which helps avoid edge seal failure, it can be concluded that they improve on long-term functionality.

The Research published on trying to bend an IGU into a hypar shape required high stiffness at the edges of the glass to delay the buckling effect as explained before. Therefore in the research performed by van Driel (2021) GFRP spacers were chosen because of their excellent tortional stiffness. Other considerations were aluminium, steel and timber.

4.5 Cold bending distortion

As explained before, optical distortion in the glass' surface can occur during the production process. As long as the distortion amount is below the accepted limit, this does not necessarily form an issue. According to EN12150-1:2000 the allowable limit for roller wave distortion on thermally toughened glass is 0.5 mm over a length of 300mm.

How the glass reacts to cold bending in anticlastic shapes has a big impact on its surface quality.

Datsiou. K (2016) performed research on how the surface quality of monolithic glass panes during anticlastic cold bending by pushing two corners and supporting two corners, much like van Driel (2022) and Young (2019) did afterwards.

Findings where that the buckling effect, where one diagonal straightens while the other flattens has significant impact on the quality of the glass' surface. Even at stress levels much lower that the breaking strength, a local instability occurred where ripples form in the glass before fracture. How and when ripples occur is strongly influenced by the boundary conditions of the corners in the bending setup. Corners of this particular test setup were supported with clamped, pinned or roller supports and bent by pushing the other two corners.

The main findings of the paper include that cold bending distortions can occur without failure, compromising the optical appearance of the glass panes. The distortions grow with plate thickness, aspect ratio and load magnitude. Plates thicker than 4 mm or smaller in size are more prone to visible distortions. The next page displays a flowchart designed by Datsiou, (2016) for determining the acceptance of distortion of monolithic cold bent glass plates.

To use this chart, surface distortion has to be measured with very specific instruments. The use of these instruments likely lies out of scope for this research.

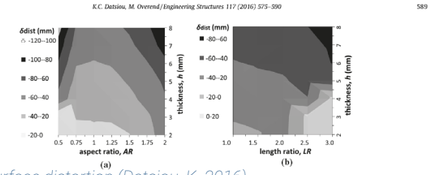

Figure 38. Surface distortion (Datsiou, K. 2016)

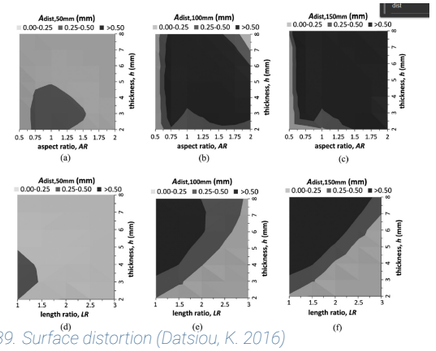

Figure 39. Surface distortion (Datsiou, K. 2016)

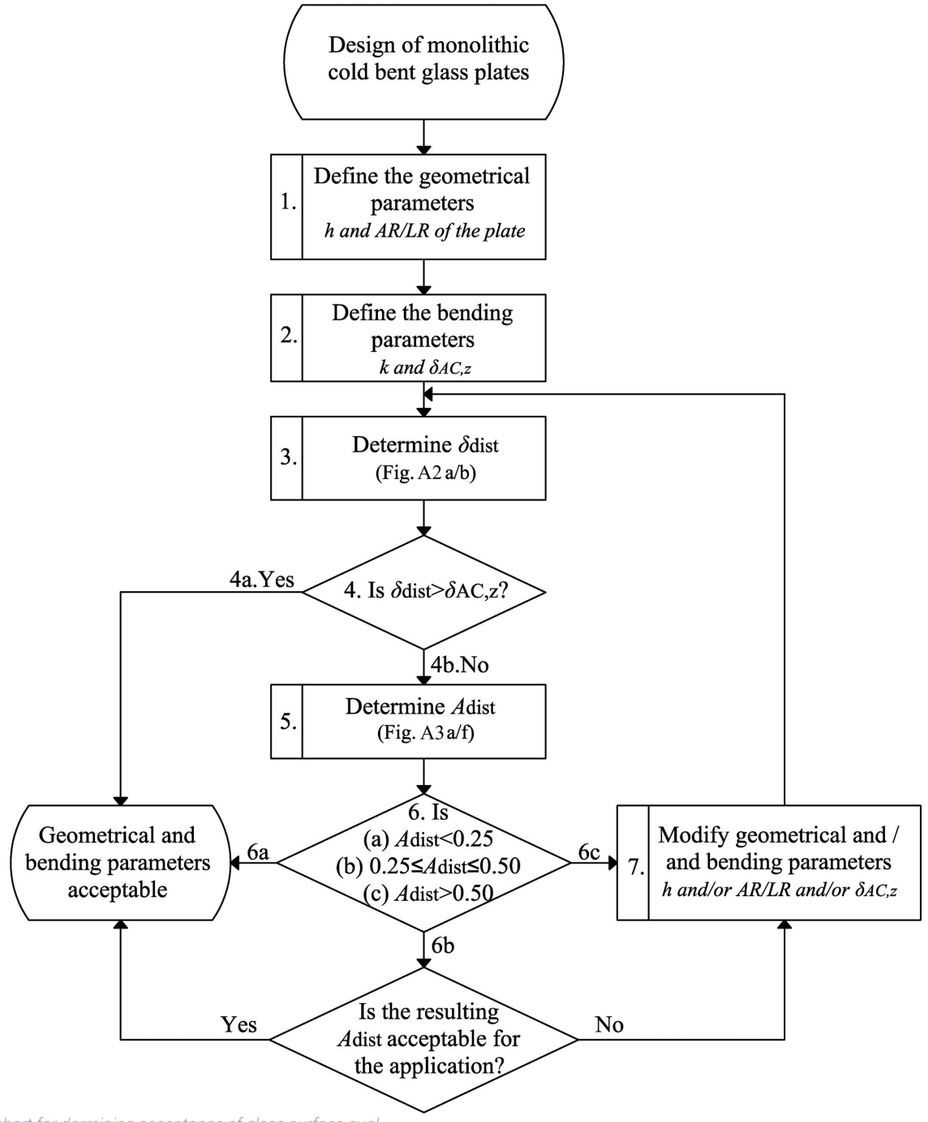

Figure 40. Flowchart for dermining acceptance of glass surface quality distortion (Datsiou, K. 2016)

4.6 Summary and considerations

As can be concluded from previous research, the way glass bends into shape during cold bending is highly dependant on the composition of the entire product. Single glass panes are able to cold bent without other limitations than the glass pane itself. It is concluded by Zhang, x. Et al (2021) that lamination has little effect to the cold bending capabilities of glass panes.

Further research conducted by Galuppi (2014) concluded that cold bending a monolithic glass pane into a hypar shape proved to by only possible at low displacement before the edges of the glass start buckling behaviour, and a shape more resembling of a single curved shape is achieved. The recommendation was made to enhance stiffness of the edges of the glass panes.

Young (2019) built further on this research and added GFRP profiles to a single glass pane and tried cold bending it into an anticlastic shape. van Driel (2021) added a second glass pane to the construction, thus creating an insulated glass unit. This IGU was tried to cold bent into anticlastic shape, and it was concluded that it was difficult or impossible to get close to a hypar.

The conclusions of this previous research proved that trying to cold bent glass into a hypar shape shows little promise for glass applications. Therefore, the anticlastic shape was discarded, and focus was put on free form glass curvatures, whereby the spacer does not necessarily require to stiffen the edges of the glass panes.

Research was conducted in finding the best fit for constructing a flexible insulated glazing unit. The conclusion of the research found that for flexible cold bending:

- Thinner glass sheets are a requirement to increase the maximum curvature allowed during the cold bending process.

- A warm edge spacer is flexible at room temperature and thus accommodates to the shape of the panel during cold bending. Warm edge spacers often include a primary adhesive in the product, making the requirement for another primary adhesive obsolete.

- To achieve maximum flexibility, a secondary sealant with highly flexible capabilities after hardening has to be applied

The required three main components were selected by reaching out suppliers and discussing what is available and achievable for this master thesis' research. The following materials were chosen

- 10 x 1.1mm Glanova Thin glass sheets - after consolidation with NSG/Pilkington.

- 99 metres of the Triseal spacer from edgetech with dimensions of 20.2 by 7.3 millimetres. Included is a Polyisobutylene primary adhesive - after consolidation with Edgetech/superspacer.

- Kömmerling Ködiglaze S as a secondary sealant. Chosen because of its, and its required tools for application's availability at the faculty. It must be noted that while Ködiglaze S is not specifically made for cold bending, its material properties and its influence on the design allowed for this choice.

05

Material selection & pro-totype fabrication

5.1 Spacer

For a spacer bar, a polymer foam spacer is chosen as to accommodate for high flexibility in the panel. Contact was made with Superspacer to inquire whether one of their spacers would suit the flexible thin glass IGU. After Consultation, the Triseal spacer was chosen for its high flexibility and strong integrated primary adhesive. A width of 20.2 millimetres is chosen as a thick spacer could prevent issues like glass panes touching as occurred during research conducted by van Driel, (2021). The spacer consists out of flexible silicone foam, an acrylic adhesive and a primary butyl seal.

The roll of spacer was sent by Superspacer with a total length of 99 metres. The Triseal spacer has an integrated primary adhesive. The spacer is sealed off in an vacuum tight wrapping after production and during shipping. This ensures that the spacer foam doesn't dry out. The adhesive is covered by a plastic wrap.

Figure 41. Vacuum wrapped Triseal spacer (Picture taken by author)

5.2 Secondary sealant

For the secondary sealant, it was advised to use a two component silicone sealant. Using a two component sealant ensures faster curing than a single component silicone.

At the faculty of Architecture, a large stash of sealant was available for use in the lab. This sealant has been used by a previous student to seal of an insulated glass unit. The sealant is Ködiglaze S, produced by Kömmerling. This sealant specifically made for insulating glass applications. An automated dispenser is advised for applying an even and well distributed layer of sealant. Ködiglaze S needs to be applied in a 1:10 ratio.

The Airflow One pneumatic dispenser is capable of applying this ratio and is available at the faculty. This pneumatic dispenser needs to connected to a compressed air tank to push out the pistons.

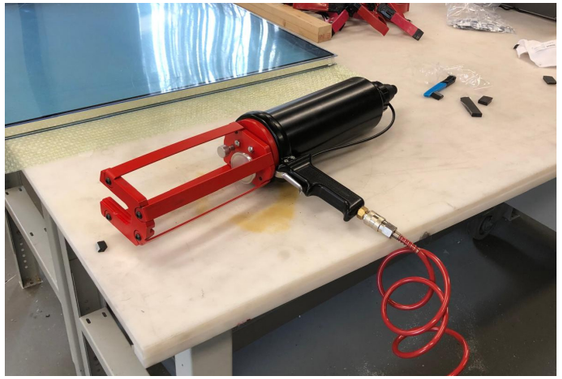

Figure 42. Innotech Rott Airflow one pneumatic dispenser (Picture taken by author)

5.3 Assembly

One pane of glass is put on the table, on a soft underlayer to prevent damaging of the glass. First of all the glass is brushed off to remove any dust particles from the glass' surface. Then the glass is cleaned with Isopropanol and a microfibre cloth. The isopropanol removes any stains or fat from the surface of the glass. This is important for not having any stains on the inside of the IGU where it can never be cleaned. The edges are cleaned extra carefully, as having any grease or stains on the surface compromises the ability for the spacer to glue to the glass.

Then the spacer is taken out of its vacuum sealed wrap. The sealing of the wrap prevents the spacer from drying out and thus the wrap should be sealed again after use.

The spacer is applied separately per side of the pane. A piece slightly larger than 80 cm (the size of the edge of the pane) is cut off. Edgetech provided a small piece of wood designed for applying the spacer by hand. The wooden piece has an indent which provides the distance required to place the spacer from the edge of the glass. The small surface at the edge of the pane is designed for applying the secondary seal.

After applying the first side of the spacer to the glass, the edge of the spacer has to be cut in a 45 degree angle. The wooden piece provides guidance for making the 45 degree cut.

The next piece of spacer is cut off from the roll. For this piece, another 45 degree angle is cut from the edge. The two pieces now connect together and will form a connection that can be sealed off easily. The next part of the spacer is pressed on the glass. This process is repeated until the spacer goes all around the pane.

Figure 43. Application of the Triseal spacer (Picture taken by author)

Figure 44. Application of the Triseal spacer (Picture taken by author)

The corners are still slightly separated and therefore have to be sealed off. Edgetech provided small butyl strips than can be applied to the corner. It is important that the butyl on the side of the spacer makes a continues bond along the edge. This is the primary adhesive that holds the glass and the spacer together, and is simultaneously the first impermeable seal to close off the cavity.

Then the second pane of glass is cleaned with the same method of the first pane. The glass is then pressed on the spacer. Clamps are applied to the glass in small intervals to create an equalized pressure along the edge. Because of limited supplies, each side was pressed separately. The corners are pressed with a stronger clamp to spread out the butyl layer over the gap. A continues bond can be seen in the picture.

After the glass is properly glued to the spacer, the IGU can be sealed off. For application of the Ködiglaze S, the Airflow one pneumatic dispenser is attached to a pressurized air tank. The Ködiglaze is put in the dispenser and the plastic silicone mixer is put on the cans. This mixer makes sure the two components are mixed in the right 10:1 ratio.

The cavity is completely filled up with silicone to make sure the spacer and glass are fully sealed. The excess silicone is scraped off and the panel is left to dry for at 3 days.

A total of 6 IGU's are constructed
- One plexiglass IGU
- Two regular Glanova thin-glass IGU's
- Two "laminated" Glanova thin-glass IGU's
- One Blacked out Glanova thin-glass IGU

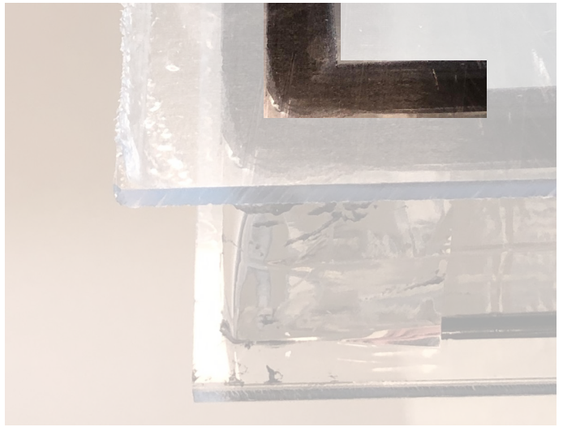

Figure 45. Continues seal of the polyisobutylene primary adhesive (Picture taken by author)

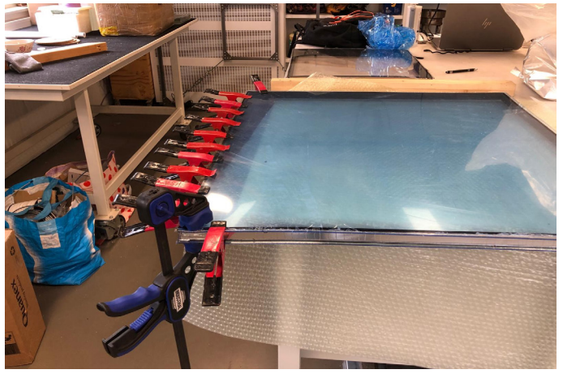

Figure 46. Clamping of the glass to the spacer (Picture taken by author)

Figure 47. Application of the Ködiglaze S (Picture taken by author)

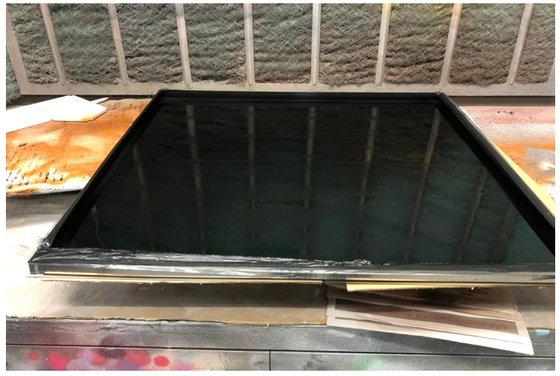

Figure 48. Black spray panted IGU, one inner pane is spray panted so that the reflection of the glass pane can be clearly observed (Picture taken by author)

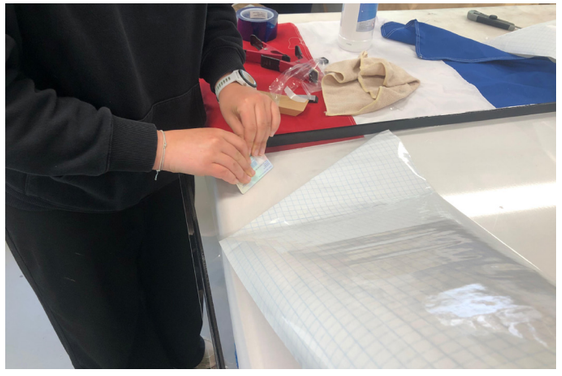

Figure 49. Lamination of one of the two laminated IGU's. Bookcover foil was used for its adhesion and strength. On these IGU's one innerpane and another outer pane were laminated. (Picture taken by author)

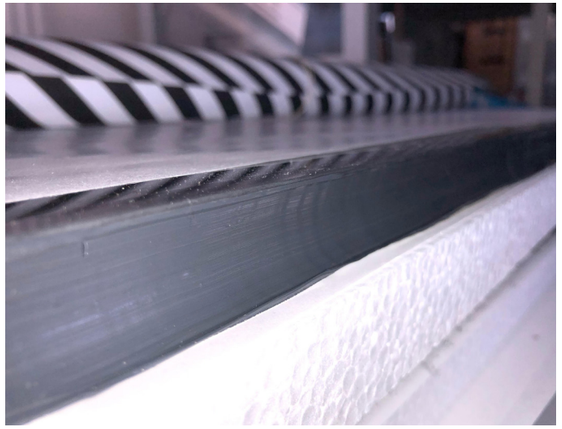

Figure 50. Finishing of the Ködiglaze S (Picture taken by author)

5.4 Cold bending setup

For testing the flexibility of the panels, single corner cold bending is used as a physical testing mechanism. During single corner cold bending of a glass pane, three corners are clamped, and one corner is pushed out of plane. These tests are performed to validate the results of the numerical model. If the glass behaves the same way during the tests as in the numerical model, the model can be considered as realistic. The model can then be further optimized with materials and sizes not possible for the scope of these physical tests.

First, wood is sawn up to for a frame that has an inner gap dimension of at least 80 by 80 centimetres. As stated before, this setup will utilize single corner cold bending. That means that 3 corners have to clamp the glass, while one corner is designed to apply a displacement to the glass in that respective corner.

With that setup in mind, four corner elements are made. 3 corner elements are clamps, wherein the glass can be clamped. The clamps are made with multiple spacer-rings to accommodate for different thickness' of panels.

The corner element is made with a bench dog holddown clamp. With this clamp, a displacement can be pushed by fixing the red piece, and screwing down the bolt. The current screw wire is replaced by a larger steel rod to accommodate for larger displacement.

Finally, polyethylene foam is used as a buffer between the clamps and the glass. This foam is often used as wrapping material for parcels. The material is compressible up to a certain point, where after it is very hard to push through. This material is ideal as a soft buffer between the glass and the steel as it will distribute high stress points at contact elements.

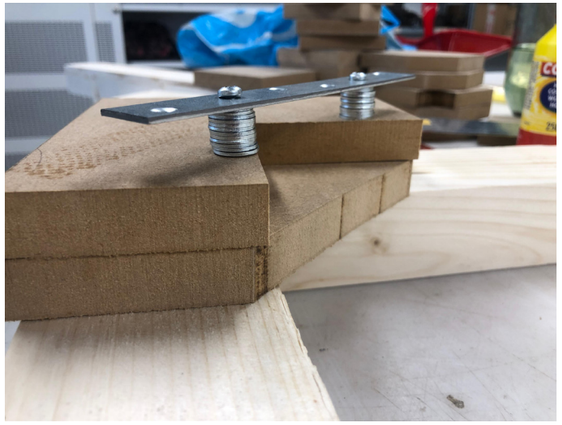

Figure 51. Final Design of the clamp (picture taken by author)

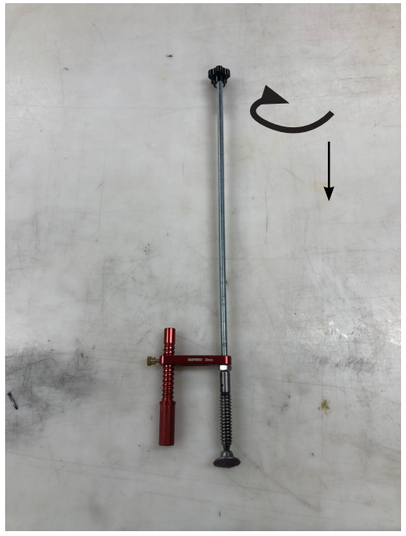

Figure 52. Configuration of the pushing screw (picture taken by author)

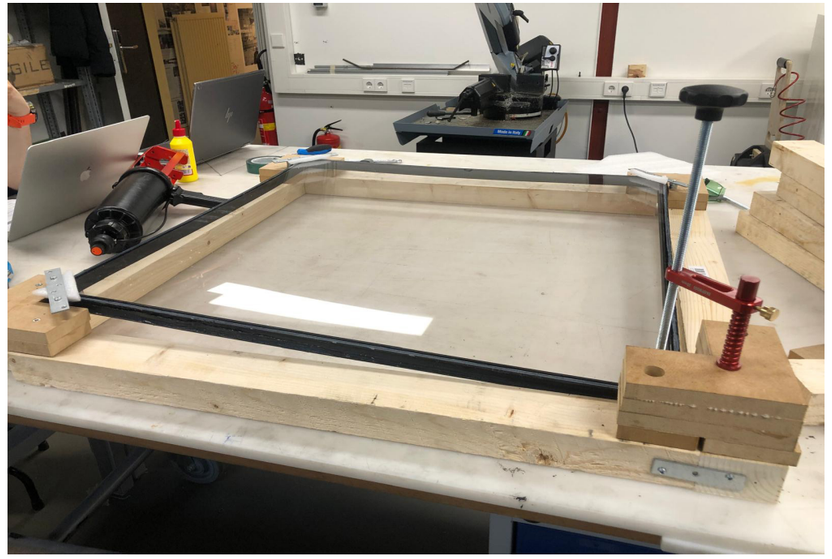

Figure 55. Final Bending rig configuration (picture taken by author)

Figure 54. Tip of pushing screw, ball joint accommodates movement of the glass (picture taken by author)

Figure 53. Clamped plexiglass panel (picture taken by author)

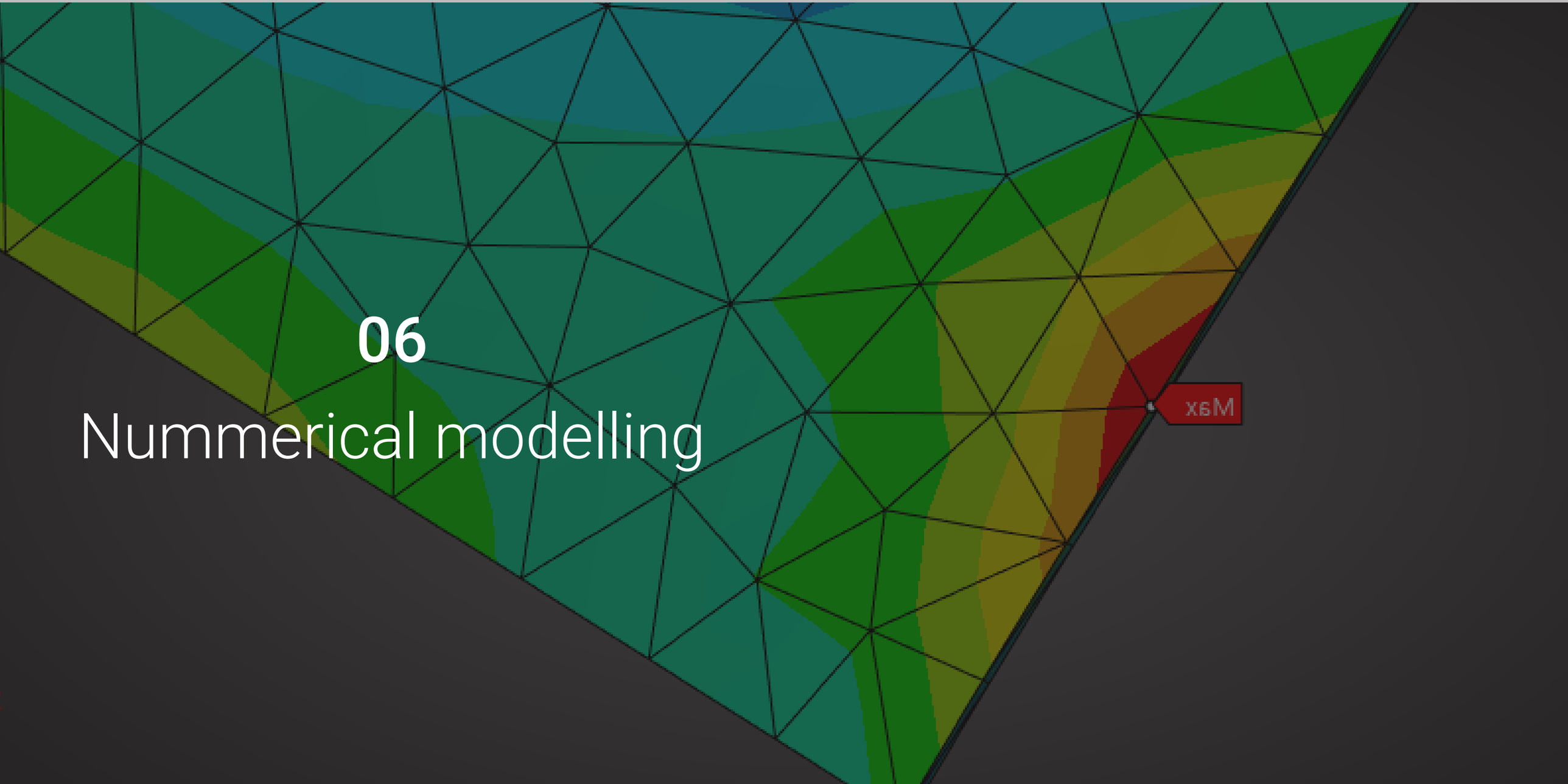

06

Nummerical modelling

6.1 Numerical model 1 - glass pane

First, a model will be constructed that only consists of the glass panes. This way, the stresses in the glass can be modelled. It is predicted that the glass will be the deciding factor on the maximum bending curve. It is helpful to solely model the glass first to gain an understanding on how the glass performs on its own. Other materials and parts of the IGU change the shape the glass will take when it is cold bent. This means that stresses will be distributed differently and could cause stress concentrations at different location. Setting up the right Finite elements model with correct boundary conditions is important for creating accurate results of bending the single glass pane.

The model of the glass pane consists out of a single solid square element with dimensions of 800 by 800 millimetres, the same as the physical test setup will be. For the glass, glanova thin glass by NSG group is used. This glass is used for smartphones, automotive exterior glass, solar cells and much more. This glass can be made from 0.33mm to 2mm thick and is made with the float process.

The plate has been given a thickness of 1.1 millimetres. A new material is created in ansys' engineering data with the properties derived out of the table, namely a Young's modulus of 75,4 MPa, a poisson's ratio of 0.24 and a compressive strength of 700Mpa.

Defining the tensile strength is very important to this research as that is when the glass will break under its tensile forces. Samples of the ordered glass were tested with a Scalp 5, but because of insufficient knowledge about the depth of the chemical strengthening layer, accurate data could not be derived. A tensile design strength is estimated in the table provided by Eckersley O'callaghan and has been set at 260 MPa. This number is likely derived from tests performed by the company itself. This is the maximum tensile stress they use during their design process. Therefore this number is what this thesis will also use.

Parameters		Unit	NSG glanova®
Glass properties	Optical transmittance	%	≥ 91
	Refractive index (λ=587,6 nm)	—	1.51
	Density	g/cm³	2.48
	Young's Modulus	GPa	75.4
	Poisson's Ratio	—	0.24
	Dielectric constant @1GHz	—	6.9
	Coefficient of thermal expanssion (50-350°C)	x 10^{-7}/°C	91.8
Viscosity	Softening point	°C	742
	Annealing point	°C	552
	Strain point	°C	508
Chemical strengthening	Compressive stress	MPa	600 - 800
	DOL	µm	15 - 25
	Vickers Hardness (before chemical strengthening)	Kgf/mm²	528
	Vickers Hardness (after chemical strengthening)	Kgf/mm²	583
Dimensions	Thickness	mm	0.33 - 2

Table 5. Mechanical properties of NSG glanova glass (HPM.NSG.com, derived 2025)

		Leoflex glass (LG)	Saflex DG41 (SAF)	SentryGlas (SG)	
Density	ρ	2480	1080	950	kg/m³
Young's modulus	E	74000	1007	612	MPa
Shear modulus	G	30000	341	211	MPa
Poisson's ratio	v	0.23	0.476	0.449	-
Tensile bending strength	σ_b	260	32.4	34.5	MPa
Maximum size	A	1.5x1.85	2.46x3.2	1.2-200	m
Thickness range	t	0.55-2	0.76	0.89	mm

Table 4. Physical properties of AGC Leoflex Glass and interlayers (Eckersley O'callaghan, derived 2025)

Comparing the compressive stress and the tensile stress makes clear that the tensile stress for glass is much lower than the compressive strength. Therefore the maximum tensile stress of 260MPa should not be exceeded.

The Mesh

The mesh in ANSYS significantly affects the behaviour of a model by influencing accuracy, computational time, and result stability. A finer mesh, with more elements, provides higher accuracy because it captures small details and stress concentrations more effectively. However, it also increases computational time and resource usage. On the other hand, a coarser mesh runs faster but may lead to less accurate results, missing important features such as localized stresses.

The type and shape of elements also play a role. Hexahedral elements, which are brick-shaped, tend to be more accurate and stable but are harder to generate for complex geometries. Tetrahedral elements, which are pyramid-like, are easier to mesh around complicated shapes but may require a finer mesh to achieve the same accuracy. Poorly shaped elements, such as those that are overly stretched or distorted, can reduce accuracy and cause numerical errors.

In areas where stress concentrations are expected, such as sharp edges, holes, or contact regions, a finer mesh is needed to capture the details correctly. If the transition between fine and coarse mesh regions is too sudden, it can introduce artificial stress points, so a gradual change in mesh density is preferred.

If the mesh is too coarse, the simulation may struggle to converge, meaning the results do not stabilize. To find the right balance, a mesh independence study is useful—this involves refining the mesh gradually until the results stop changing significantly.

Different types of simulations have specific meshing needs. For example, in glass fracture analysis, a fine mesh is required to capture stress distribution and crack propagation accurately. On the square plate, four triangles are drawn to distribute the displacement and load condition.

The is generated around these cut off corners, instead of the entire surface being divided into a square mesh, the surface is now divided into triangles. The smaller the mesh object size is, the more accurate the models calculations will be. An optimal mesh size is chosen to accommodate for the computers maximum calculating power.

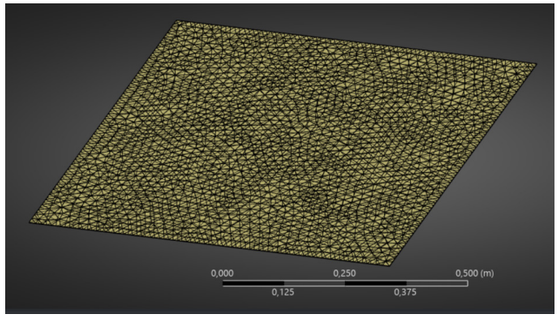

Figure 56. Meshing elements of the modelled monolithic glass pane (own work)

The boundary conditions of the plate are defined at four corners. The four corners of the plate are given a remote displacement. 3 of these corners are set at zero movement for the X, Y and Z direction. One corner is given a displacement, which means that the corner will be moved in the Z direction with a set amount. These boundary conditions are set at triangles on near the corners of the plate. This is done to distribute stresses over a larger surface than just the corner. Standard earth gravity has been assigned to the surface, since this will also play a minor role in the real life test setup.

There are multiple ways to setup the bending of the glass plate. Deformation in the Z direction at one corner can be used. Also applying a force at the given corner is a possibility. For this method, a deformation at the corner is chosen. Furthermore it is important that large deformations are enabled. This ensures that after steps of deformation, the model is reconfigured to calculate the stresses in the deformed model. This is done in multiple steps ensuring a more accurate analysis result.

Since the surface is now divided into multiple parts which have a more complex geometry than just a square, an accommodating mesh has to be construct-

Corner A (OPPOSING)		Corner B	
X-Component	0	X-Component	0
Y-Component	0	Y-Component	0
Z-Component	0	Z-Component	0
X-Rotation	free	X-Rotation	0
Y-Rotation	free	Y-Rotation	0
Z-Rotation	free	Z-Rotation	free

Corner C		Corner D (Displacement	
X-Component	0	X-Component	0
Y-Component	0	Y-Component	0
Z-Component	0	Z-Component	-0,2
X-Rotation	0	X-Rotation	0
Y-Rotation	0	Y-Rotation	0
Z-Rotation	free	Z-Rotation	free

Table 6. Situation of the boundary condition (Own work)

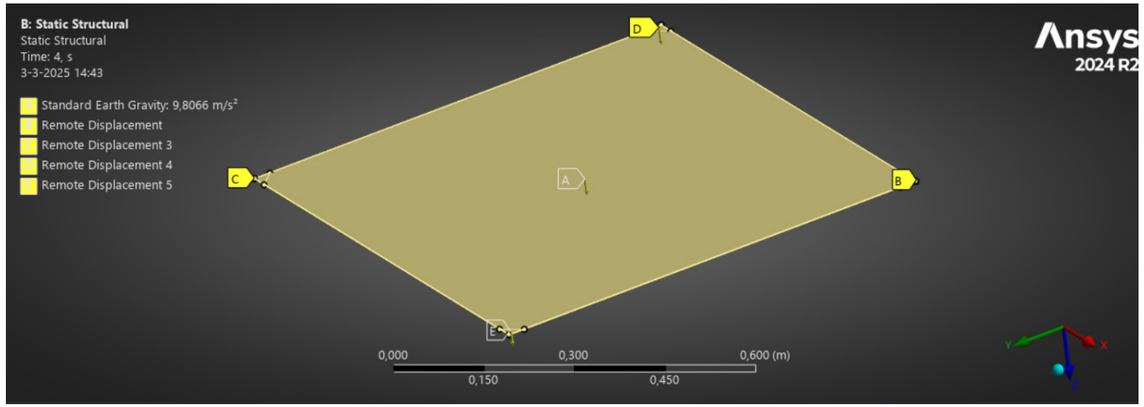

Figure 57. Situation of the boundary condition (Own work)

Iteration 1

The first iteration the corners of the panel are clamped with triangle surfaces. The clamping of the corners makes sure there is no movement allowed along the X, Y and Z axis. However, when one corner of the pane is pushed down on the Z axis, the edges of the glass will slightly move on the respective X and Y axes. The triangle shaped clamps proved not to be a realistic model.

Iteration 2

In the second iteration the triangles clamping the glass are disbanded into sides to allow for movement along certain edges. The loaded corner is loaded with a surface load, this spreads the stresses more evenly along the surface, as a point load would concentrate the stress at the mesh element in the corner.

The opposing corner A is restricted in its movement in the X, Y and Z direction, but does allow for rotation in these directions. Corners B and C are clamped at the side the arrow points at. This makes sure the panel does not deform and 'stretch' during bending.

This iteration is not perfect as there is a large stress concentration at the downside of the panel at the loaded corner created by the edge of the pressurized surface.

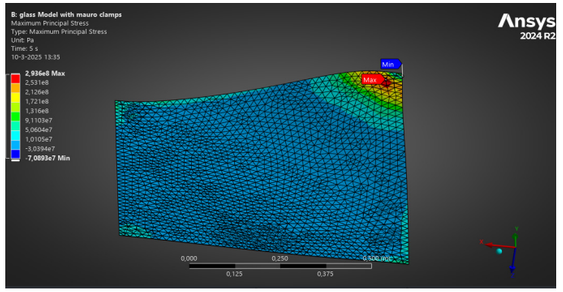

Figure 61. Schematic of the glass pane deforming during cold bending (Own work)

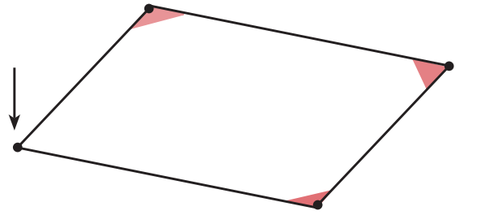

Figure 58. Schematic of the first iteration (Own work)

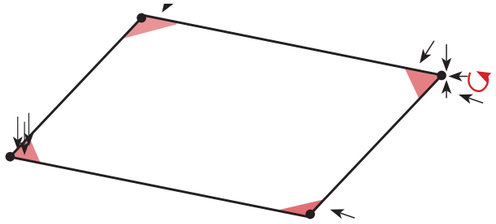

Figure 59. Schematic of the second iteration (Own work)

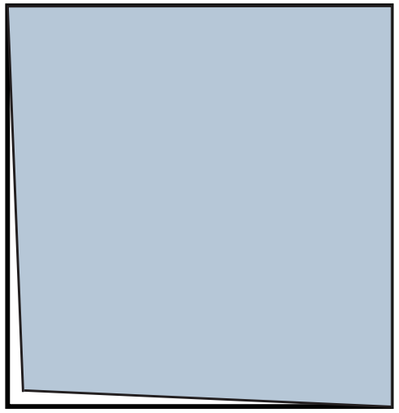

Figure 60. Schematic of the glass pane deforming during cold bending (Own work)

Iteration 3

The third iteration is largely the same as the second iteration. The difference is that the displaced corner is allowed rotation. This removes the stress concentration at the underside of the panel. Stress concentrations are now located at the edges of the pane near the clamped connections.

The maximum amount of displacement of the corner achieved with this simulation is a deformation in the Z-direction of 17,9 centimetres. The maximum principal stress at this deformation is 2,49*10⁸ Pa. Which is 249 MPa, slightly below the maximum threshold of 260 MPa, the value derived from EOC maximum design strength table.

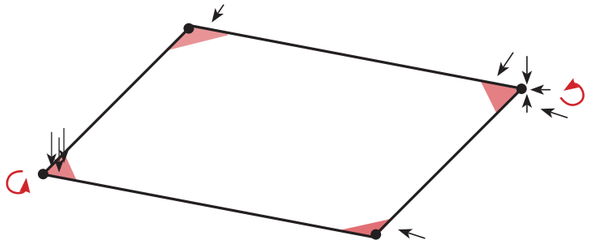

Figure 62. Schematic of the third iteration (Own work)

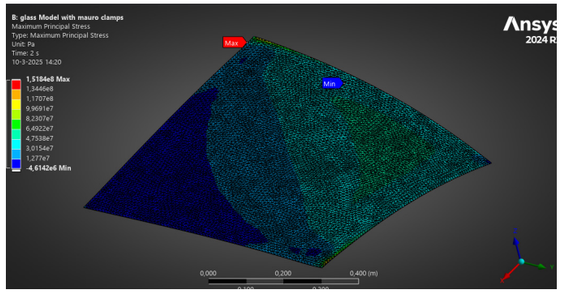

Figure 63. Third Iteration during deformation (Own work)

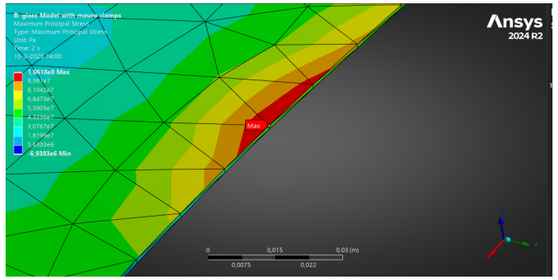

Figure 64. Zoomed illustration at maximum stress location (Own work)

SITUATION D	Corner A (OPPOSING)		Corner B			Corner C		Corner D (Displacement	
	X-Component	0	X-Component		0	X-Component	0	X-Component	0
	Y-Component	0	Y-Component		0	Y-Component	0	Y-Component	0
	Z-Component	0	Z-Component		0	Z-Component	0	Z-Component	-0,2
	X-Rotation	free	X-Rotation		0	X-Rotation	0	X-Rotation	0
	Y-Rotation	free	Y-Rotation		0	Y-Rotation	0	Y-Rotation	0
	Z-Rotation	free	Z-Rotation		free	Z-Rotation	free	Z-Rotation	free
Test 01	**1.1mm**	**Deformation (Tabular)**	**Max Stress (Pa)**	**Min Stress (Pa)**	**Weak springs**	**Large Deformations**			
		5,01E-02	5,98E+07	-1,46E+07	OFF	ON			
		0,10063	1,29E+08	-3,19E+07					
		0,17858	2,49E+08	-6,04E+07					
		0,20548	2,94E+08	-7,09E+07					
		0,20548	2,94E+08	-7,09E+07					
		0,20548	2,94E+08	-7,09E+07					

Table 7. deformation calculations (Own work)

6.2 Numerical model 2 - IGU

The setup of the numerical model is of great importance to the results. Results can only be trusted if they are derived from an accurate and realistic model. Therefore, the numerical model should be modelled as closely as possible to the physical test setup.

Global dimensions. The modelled IGU has a width and length of 800 by 800 millimetres. These sizes were partly chosen because of availability of the manufacturers glass, and because of the size of glass that could be handled during physical tests.

The IGU contains four corners,

- Corner A: Adjacent clamped corner 1
- Corner B: Opposite clamped corner
- Corner C: Adjacent clamped corner 2
- Corner D: Loaded corner.

The clamped corners are made by de constructing the corners into small surfaces on the edges.

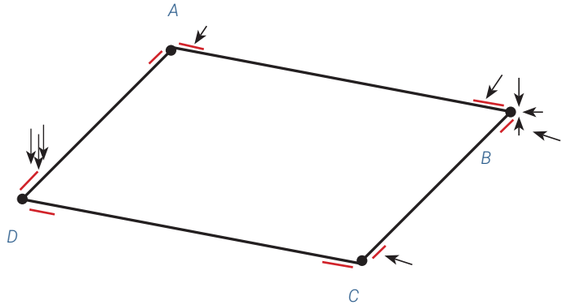

Figure 65. Schematic of the boundary conditions of the IGU model (Own work)

6.2.1 Spacer: uniaxial tensile Test

Edgetech was contacted to obtain the mechanical properties of the spacer to use for modelling. Unfortunately Edgetech could only provide the density of the spacer which is 0,7 g/cm³. Materials like these are too complex to be modelled as an isotropic elastic material. Therefore hyper-elastic models have to be used. These models depend on parameters. Since the parameters of this material are unknown they have to be derived and calculated from test data.

To obtain mechanical properties that could somewhat be used for Finite Elements Modelling multiple experiments were executed.

The first experiment is a tensile test. With a tensile test, a part of the spacer is slowly pulled outwards. The machine registers the pulling force and the displacement per minute is set as a constant. The machine therefore outputs a Force/strain graph.

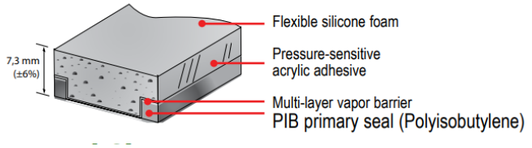

Figure 66. Composition of the Triseal (triseal data sheet, derived 2025)

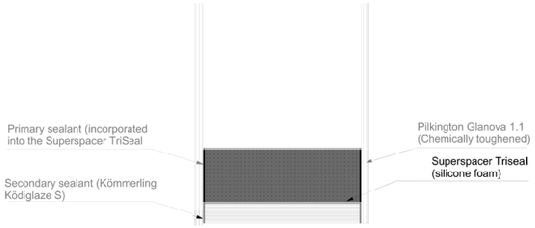

Figure 68. Triseal spacer in the IGU (Own work)

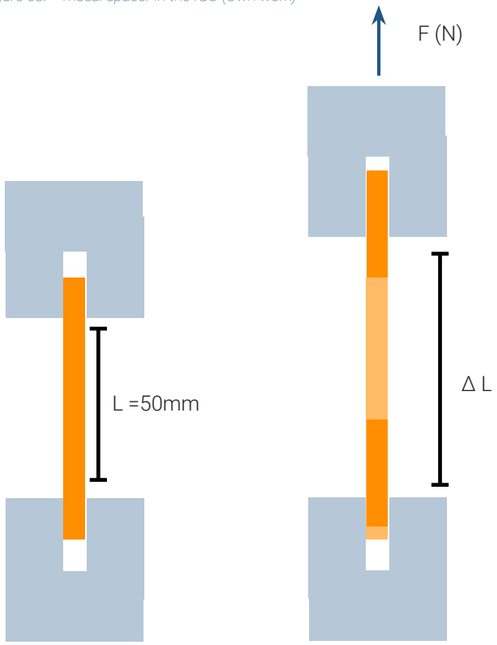

Figure 67. Schematic of the tensile test (Own work)

Figure 69. Tensile test setup: initial position (own work)

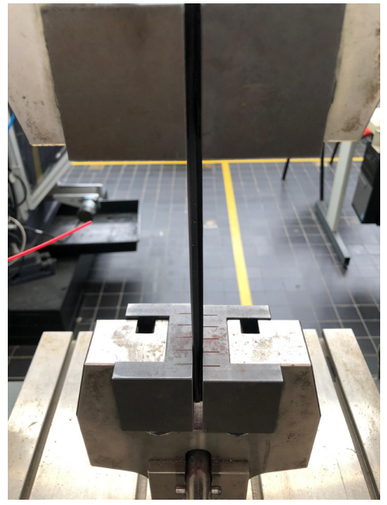

Figure 70. Tensile test setup: Sample under tension (own work)

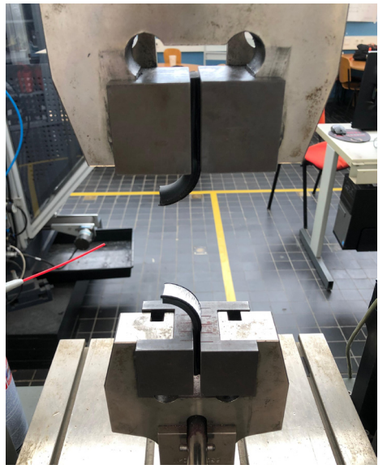

Figure 71. Tensile test setup: Sample after breaking (own work)

Figure 72. comparison of spacer before and after tensile test (own work)

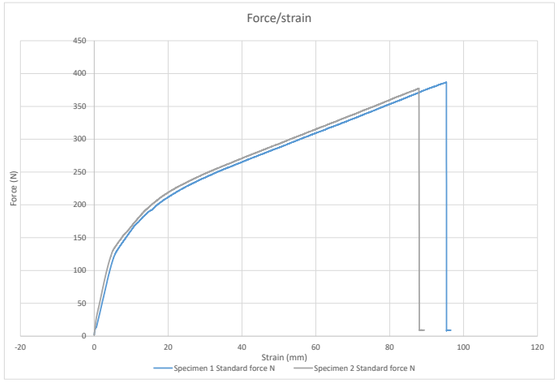

Graph 2. Force strain diagram for sample 1 & 2 (Own work)

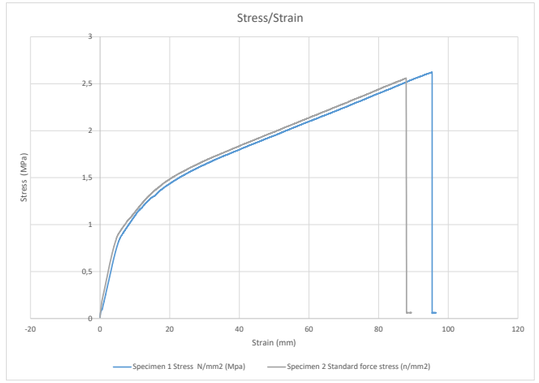

Graph 3. Stress strain diagram for sample 1 & 2 (Own work)

The two specimen were put in the tensile machine with a free length of 50mm. From there the machine starts pulling on the specimen with a displacement of 10 millimetres per minute.

The graph shows that both samples are in the elastic region until around 120N. This can be observed by the linearity of the curves. This means that the material will form back to its original size up until this point.

After the linear part of the diagram, the line starts to plateau. It shows that less force is necessary to stretch out and deform the material. This is the plastic region of the spacer. All stretched deformation on the sample will remain, the material will not stretch back to its original size.

As can be seen in the Force/Strain diagram, the first sample broke at 96,5 mm strain. The second specimen broke a bit faster, at 88,9 mm strain. Both specimen show great tensile strength, almost stretching twice as far as the original length of the unclamped part of the sample. By dividing the Force applied on the spacer by the surface size of a section of the spacer, the stress can be determined.

$$\sigma = \frac{F}{A}$$

$$A = 20{,}2 * 7{,}3 = 147{,}46mm^2$$

The spacer has dimensions of 20.2mm width, and 7,3mm height. The area size is 147,46 square millimetres. The strain is divided by the area and this creates a stress data column. This data is plotted against the strain which creates the stress/strain graph.

The young's modulus of the sample can be determined by calculating the slope of the elastic region of the graph. The graphs show a clear linear elastic line between 50 and 100 Newtons. Therefore the data between these rows were taken and the derivative was calculated.
For the calculation of the Young's modulus, the strain expressed in millimetres cannot be used. In the formula for calculating the Young's modulus strain is expressed as a ratio.

$$E = \frac{\sigma}{\varepsilon}$$

$$\sigma = Stress\ (Mpa)$$

$$E = Young's\ modulus$$

$$\varepsilon = Strain\ (\frac{mm}{mm})$$

$$\varepsilon = \frac{\Delta L}{L_0}$$

$$\Delta L = difference\ in\ length$$

$$L_0 = original\ length\ of\ sample\ (mm)$$

The strain (mm) has to be divided by 50 (the original length of the sample's free space between the clamps.)

The linear (elastic) part of the graph remains between the same rows with values.

Specimen 1 has a derivative of 8,1519. Specimen two has a derivative of 8,7376. Another specimen was tested, but not until breakage point and with a different tensile deformation/min value. This specimen also went beyond its elastic region and had a derivative of 7,6265
The average derivative of these samples is 8,172 making this the average Young's modulus of the samples.

This value is used on the model and results with these values prove the material way to flexible. A possibility to why the material behaves to flexible in simulations is the behaviour of the foam during the tensile tests. Materials like foams show visco-elastic behaviour, meaning that the material will slowly creep back to its original state. The visco-elastic part of the graph can not be used for calculating the Young's modulus.

A hyper-elastic model is required to model the spacer as the strain and stresses on the material during the cold bending are to complex for an isotropic elastic model to handle.

There are many different hyper-elastic models to choose from in ansys and all have different strengths and weaknesses. Six hyper-elastic models were considered for this material.

- Neo-Hookean
- Mooney-Rivlin
- Ogden
- Yeoh
- Arruda-Boyce
- Gent

These models can be used by filling in the required parameters, like the initial shear modulus and the incompressibility parameters. The second and more accurate option is to use test data uploaded to ansys.

In ansys the following experimental is available for input

- Uni-axial Test Data
- Biaxial Test Data
- Volumetric Test Data
- Simple Shear Test Data
- Uni-axial Tension Test Data
- Uni-axial Compression Test Data

ansys can then fit this data to the stress strain curve, and can calculate the required parameters itself.

The stress strain data from the tests was loaded into the Uni-axial tension test data under the hyper-elastic experimental data section. The stress strain data sheet that came out of the experiment had around 10,000 lines of data recorded for sample 3 (the most accurate). This dat is too much for ansys to handle on these computers so the data sheet was altered. For every 10 rows of data, only one row was kept, reducing the amount of lines from ~10,000 to 1000. These values were implemented into ansys. Another required parameter is the temperature during the experiments.

These type of materials behave differently under different temperatures and therefore it can be valuable to perform experiments at different temperatures.

The temperature during the tests was not recorded, but since the experiments were performed inside a normally climate controlled hall, the standard temperature value of 22 degrees Celsius is taken.

Many types of hyper-elastic models were tried

Some models perform fine with solely uni-axial tension tests.

Mooney-Rivlin, Neo-Hookean, Gent and Yeoh have all been tried to run the experiments with. Mooney-Rivlin proved not to be a right fit for this type of material and was discarded after simulations failed to complete.

Simulations ran with yeoh did complete but proved to be not a perfect fit as it does not have enough parameters to calculate a representative model for this particular spacer material. Eventually, The Yeoh hyper-elastic model was chosen. Like other hyper-elastic models, orders can be chosen, essentially defining how many parameters have to be filled in

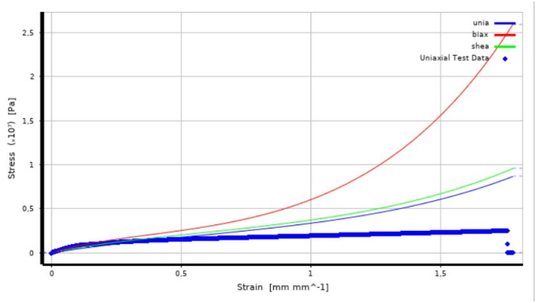

Graph 4. Yeoh third order calculated stress/strain graph from data (Own work, derived from Ansys engineering data)

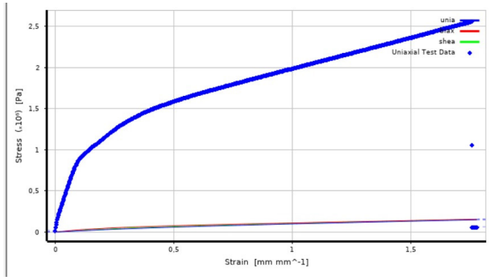

Graph 5. Yeoh first order calculated stress/strain graph from data (own work derived from Ansys engineering data)

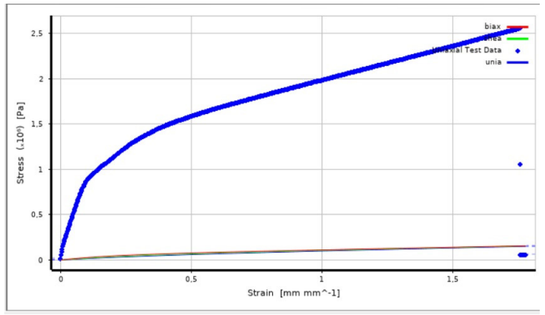

Graph 6. Neo-hookean calculated stress/strain graph from data (Own Work derived from Ansys engineering data)

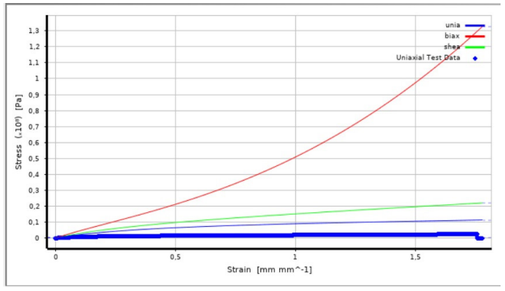

Graph 7. Mooney-rivlin 2 parameter calculated stress/strain graph from data (own work derived from Ansys engineering data)

6.2.2 Spacer: double lap shear Test

To obtain more information about the mechanical behaviour of this material, shear tests have been performed. Two pieces of spacer are sandwiched between three steel plates. This configures a shear test sample whereby the average of the sample is in the same plane, namely the central axis which makes it compatible with shear tests. This is also called a double-lap shear test.

A total of four samples were tested. The samples were compressed by the top cylinder, which results in shear forces in the samples until a displacement of 2mm.
One of the four samples was displaced further as to see what would happen in high strain situations with the material. As an be observed in picture the strain is not absorbed by the spacer, but more by the primary adhesive. Therefore the data up to 2 millimetres is more representative for the spacer foam itself. Ideally, the spacer was placed between 3 glass sheets instead of 3 steel sheets. For the bonding between the primary adhesive and the sheet would have been exactly the same as in the IGU. Unfortunately, using glass in shear test experiments comes with its own issues, namely the glass buckling/breaking before enough shear is recorded, or the glass breaking in tension.

The experiments provided two data outputs. The displacement (Up to 2mm) and the corresponding force required for this displacement.

The displacement is divided by the width of the samples,

Figure 73. Set-up of the shear test experiment. picture A, before. Picture B;high shear deformation (own work)

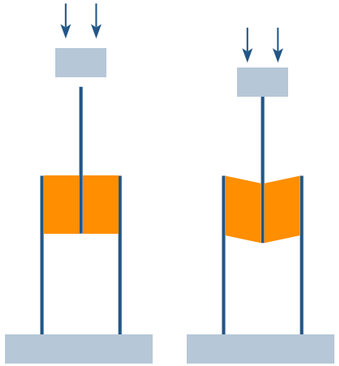

Figure 74. Diagram of the double lab shear experiment (own work)

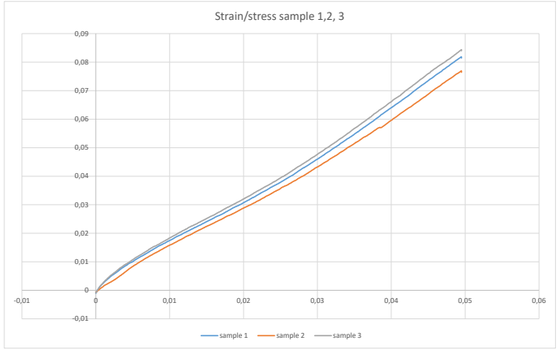

Graph 8. Strain/stress data derived from double lab shear test experiment (own work)

$$\gamma = \frac{\delta}{2t} = \frac{2}{2 * 20{,}2} = \frac{2}{40.4} = 0{,}0495$$

$$\gamma = shear\ strain\ (\frac{mm}{mm})$$

$$\delta = displacement\ (mm)$$

$$t = thickness\ of\ the\ sample\ between\ steel\ plates$$

$$A = 7{,}3\ mm * 40\ mm = 292mm^2$$

$$\tau = \frac{F}{2A} = \frac{50}{2 * 292} = \frac{50}{584} = 0{,}0856MPa$$

$$A = surface\ of\ the\ glued\ area$$

$$F = Force\ pushed\ downwards\ on\ the\ double - lap\ sample$$

$$\tau = shear\ stress\ (MPa)$$

These two rows of data were curve fitted into ansys under the shear test data. This data was then used in the Yeoh first order model which were converted to graph 8. Observe how the green line derived from the test data is very close to the green line derived from ansys, hyper-elastic calculations.

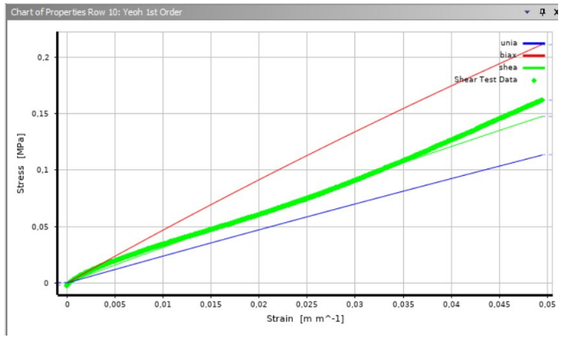

Graph 9. Ansys curve fitting model of the shear test data in model: yeoh 1st order. (Own work)

6.2.3 Primary adhesive

The TriSeal spacer does not consist out of only one material. The primary adhesive that is a separate component in regular insulated glass units is implemented in the TriSeal spacer. Although the spacer as a whole was tested on its Young's modulus, the adhesive strip has to be modelled on its own.

The polyisobutylene adhesive is a really small strip along half of the edge of the spacer. The polyisobutylene (or PIB) is modelled as a component with 1 millimetres depth and half the thickness of the spacer.

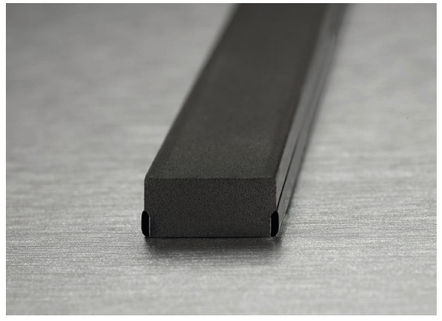

Figure 75. Section of the spacer with the PIB strips at the side (Edgetech. com, 2025))

The exact mechanical properties of this polyisobutylene layer are not known, even after consulting with Edgetech themselves. PIB behaves much like a rubber and is known for a few important mechanical properties.

- PIB is a soft, flexible and stretchable polymer, especially at room temperature.
- PIB is an amorphous model, which means its exhibits non-linear elasticity.
- PIB is a nearly incompressible material, a key trait for many hyper-elastic models, meaning the poisson's ratio would approach 0.5.

Differences between rubber and PIB are:
- PIB's gas permeability is much lower that typical rubber, which means it doesn't let any gas through, making it an ideal sealant for insulated glazing.
- PIB is very resistant to aging dye to saturated backbone.

A normal isotropic elastic model is not sufficient for highly flexible material like PIB, so again a hyper-elastic model is recommended. Since the deformation of the primary adhesive is relatively small. The Neo-Hookean, Mooney-Rivlin or Gent models are recommended.

Cwyl, M. Et al (2021) performed research long-term performance of polyisobutylene and silicone in warm edge glazing systems. Since the glazing system used in this research is a warm edge system, values will be derived from this paper to form accurate values for the parameters of the Neo-hookean model.

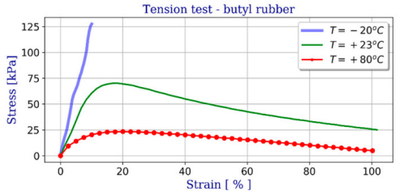

Graph 10. Tension test data, butyl rubber for glazing (Cwyl, m. Et al, 2021)

The Young's modulus is derived from this stress/strain diagram.

Although the linear part of this stress/strain diagram is merely a small hardly readable part, for 23 degrees Celsius, until 50kPa seems linear. The strain % is measured at 7%. The Young's modulus is then calculated as

$$E = \frac{\sigma}{\varepsilon}$$

$$E = Young's\ modulus$$

$$\sigma = Stress\ (Mpa)$$

$$\varepsilon = Strain\ (\frac{mm}{mm})$$

$$E = \frac{50.000}{0{,}07} = 0{,}714MPa$$

With the Young's modulus, the initial shear modulus can be calculated

$$\mu = \frac{E}{2(1+v)}$$

$$\mu = Initial\ shear\ modulus$$

$$V = Poisson's\ ratio = 0{,}49\ (nearly\ incompressible)$$

$$\mu = \frac{0{,}714Mpa}{2(1+0{,}49)} = 0{,}24MPa$$

And finally the incompressibility parameter D_1 can be calculated

$$D_1 = \frac{3(1-2v)}{E}$$

$$D_1 = Compressibilty\ parameter$$

$$D_1 = \frac{3(1-2*0{,}49)}{0{,}714*10^6} = 8{,}57*10^{-8}\ Pa^{-1}$$

These are the two required input parameters for the Neo-Hookean model.

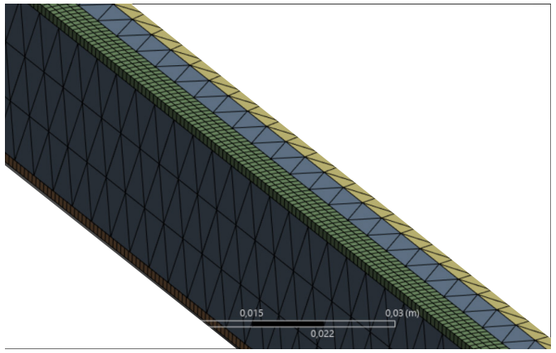

Figure 76. Model and meshing of the spacer (Own work)

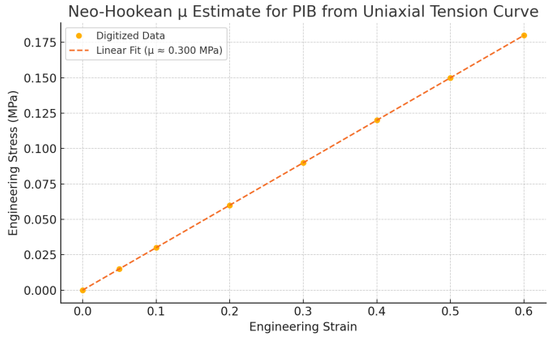

Graph 11. Neo-Hookean estimate μ for PIB from Uniaxial Tension Curve

6.2.4 Silicone sealant

Modelling the sealant correctly is important to the overall mechanical behaviour of the IGU. Silicone materials, particularly those used in glazing sealants and flexible adhesives, exhibit hyper-elastic behaviour due to their polymeric structure. Accurately modelling silicone is essential for predicting its mechanical response under deformations. For this model, the Arruda-Boyce model will be used, as it is well-suited for characterizing the non-linear stress-strain behaviour of silicones.

The silicone sealant to be modelled is be the same as used in the physical constructed IGU. Ködiglaze S from Kömmerling. This sealant comes in 2 connected tubes. Both component A and Component B have a density of 1,37g/cm³. (Technical data sheet). Ködiglaze S has a tensile yield strength of 2,10N/mm or, 2,1*10⁶ Pa.

As stated, the Arruda-Boyce hyper-elastic model is used for the modelling of the silicone. The Arruda-Boyce hyper-elastic model is commonly used for rubber-like and silicone materials, making it ideal for modelling Ködiglaze S in Ansys. This model accounts for non-linear elasticity and the molecular chain behaviour of polymers under deformation.

In Ansys' engineering data, the Arruda-Boyce model is applied from the hyper-elastic models. The parameters here are:

- Initial Shear Modulus MU
- Limiting Network stretch
- Incompressibility parameter D1

The values for this model for Ködiglaze S are derived from "*Finite element analysis of timber-glass walls* (Beer. B, Et. Al, 2016). This paper experimentally investigated timber-glass composite walls. Multiple adhesives were used in this research, whereof the visco-elastic and elasto-plastic properties were tested by uni-axial tests. (Overend et al. 2011).

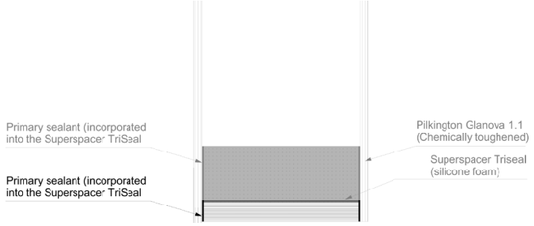

Figure 77. Secondary sealant in the IGU (Own work)

The used values were derived from the following table. Where the silicone is Ködiglaze S.

- The initial shear modulus (MPa) is 0.7066
- The limiting network stretch 2.90*10¹¹.
- The incompressibility parameter d1 (1/MPa) is 0.2143

This provides the following stress/strain diagram.

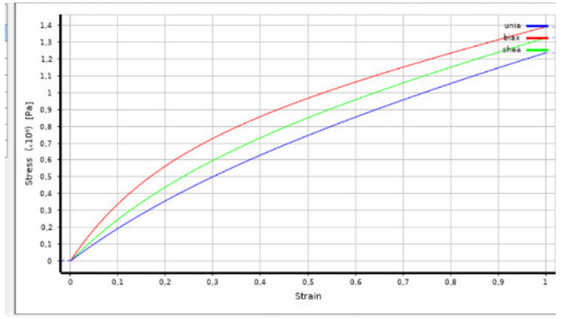

Graph 12. Stress strain data calculated from parameters derived from Ber, Et. Al, 2016)

The preferred mesh element type is the hexahedral element, an alternative is tetrahedral elements for complex geometries. For large-strain behaviour, enhanced strain formulations is activated in material settings. Near contact interfaces, the mesh size should be small, to around 0.5 to 1 mm. For high strain areas the mesh size should be around 1 to 2 mm, for bigger volumes the mesh size can be higher, but there are no such areas in this model.

At least 3 mesh elements should be generated across the thickness of the applied adhesive to properly calculate deformations. Therefore, a small mesh size is used with elements of 2 mm.

Table 5 Selected material models for each type of adhesive

Adhesive	FE model designation	Material model (Ansys designation)		
		Hyperelastic—Arruda–Boyce (TB HYPER BOYCE)		
Silicone	S3a (M)	Initial shear modulus μ	Limiting network stretch λ_L	Incompressibility parameter d_1
		(MPa)	(–)	(1/MPa)
		0.7066	2.90E+11	0.2143
	S3a (EP)	Elasto-plastic model with isotropic hardening (TB MISO)		
	1B (EP)			
		Hyperelastic—Ogden (TB HYPER OGDEN)		
Polyurethane	S3a (M)	Material constant μ_1	Material constant α_1	Incompressibility parameter d_1
		(MPa)	(–)	(1/MPa)
		0.9126	14,486	0.3
	S3a (EP)	Elasto-plastic model with isotropic hardening (TB MISO)		
	1B (EP)			
Epoxy	S3a (M)	Uniaxial tensile test data (TB EXPE UNIAXIAL)		
	S3a (EP)	Elasto-plastic model with isotropic hardening (TB MISO)		

Table 8. Material models for each type of adhesive (Beer, B. Et Al, 2016)

6.2.5 Clamps

The IGU is clamped in three corners. There are multiple ways to make a clamped connection in a Finite Elements model. One way is by creating a remote displacement. With a remote displacement the movement can be determined in direction X Y and Z, as well as rotation in these vectors. Using these remote displacements as a clamped connection allowed for zero movement in the glass, while during testing, the glass should allow for some, at least minimal movement to not concentrate any stresses around the clamped connection. Therefore, load blocks were used to distribute the reactionary forces of the clamps to a larger area.

Experiments conducted by Young (2019), and van Driel (2021) also modelled support blocks to distribute loads. As this simulation should represent reality as much as possible. The square support blocks used by van Driel and Young are replaced by triangular shaped support blocks. This more accurately represents the part of the glass that leaves the clamps as this clamps under 45 degrees.

To make the model as close to reality as possible, the support blocks were divided into two materials. Structural steel and expanded polyethyrene. The Structural steel was used to create a clear absolute boundary for the glass to move.

This foam like material is used to reduce stress concentrations arising from clamping the glass with just steel. A small imperfection in clamping the steel to the glass could result in a high stress concentration where the glass could break. Furthermore, the foam allows for small movement of the glass during the cold bending as it presses into the foam.

The material properties of the polyethyrene used in the tests is not exactly known, therefore the properties were approached using multiple tests. The polyethylene was modelled using an isotropic elastic model requiring input for the Young's modulus and the poisson's ratio.

The Young's modulus for low density foams can tipically range from 10 to 1000kPa. Poisson's ratio of this foam can range from 0.1 to 0.3. The polyethylene is placed between the glass and the metal sheet. The metal sheet is screwed towards the glass to provide a better clamp, compressing the polyethylene. The polyethylene therefore is already in a compressed state during the experiments. Therefore values for the Young's modulus and the poisson's ratio taken for a more compressed foam material, meaning a poisson's ratio of 0,3 is more accurate, as the polyethylene is not much more compressible in this state.

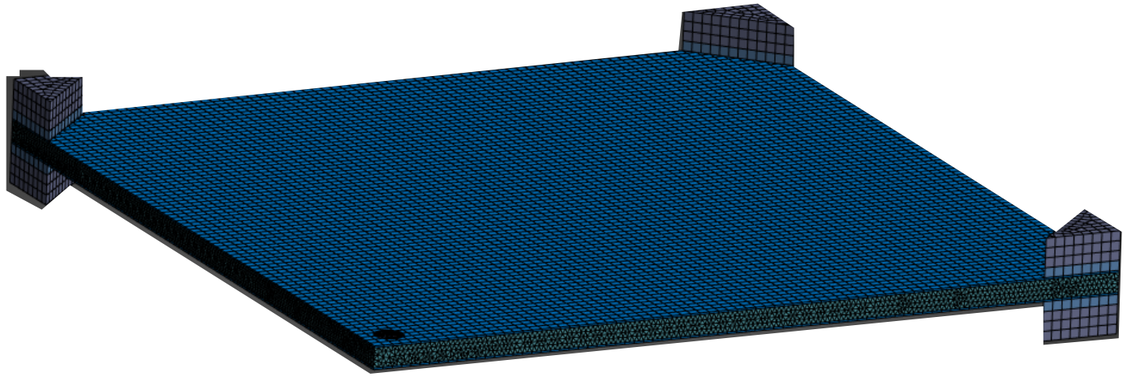

Figure 78. IGU with triangular clamps (own work)

6.2.6 Contact points

In finite element simulations, contact points between different elements have to be defined. There are five different contact settings in ansys mechanical.

Frictionless: allows sliding without any resistance to tangential motion.
Frictional: sliding with resistance, governed by a friction coefficient ranging from 0 to 1.
Bonded: the default setting, acts like surfaces are glued together which means: no sliding and no opening.
No separation: surfaces can slide relative to each other but can never separate.
Rough: Simulates infinite friction, practically means frictional with the friction coefficient set to >1. This means no separation + no sliding.

As a default, all contact points are set to bonded, meaning the elements will not disconnect and rather push or pull all the forces back onto the materials. This contact definition can be applied for most elements of the IGU, since these parts are glued together.

The bonded contact points in the model are:

- Glass to primary adhesive (PIB)
- Glass to spacer
- Glass to secondary adhesive (Ködiglaze S)
- Spacer to primary adhesive
- Spacer to secondary adhesive
- Structural steel support block to expanded polyethylene foam.

An important contact point in this particular model is the glass to clamp connection. When the displacement is applied to the free corner of the glass, the other three corners will move slightly in the direction of the free corners. Therefore the "frictional" contact is chosen. The friction coefficient is determined by the normal contact force. The friction coefficient μ determines the maximum tangential force before the two solids start to slip.

$$F_{tmax} = \mu * F_n$$

$$F_{tmax} = maximum\ tangential\ force$$

$$\mu = friction\ coefficient$$

$$F_n = normal\ contact\ force$$

It is difficult to exactly determine the exact friction coefficient that corresponds with the real test setup. Therefore a more general value of the friction coefficient is taken for this specific situation. A friction coefficient of 04-0.6 can b used for this specific situation as the tight clamping of the panel does not allow for much deformation of the panel, but the softness of the polyethylene foam does allow for some deformation. A friction coefficient of 0.6 gives the following output and seems accurate for the tests.

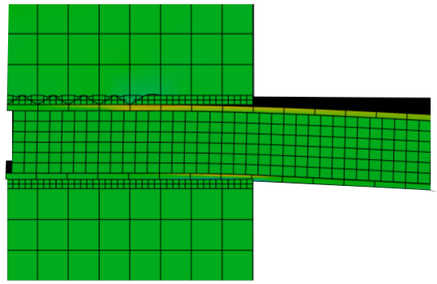

Figure 79. Clamped connection with frictional contact (own work)

6.3 Nummerical model 3: Plexiglass IGU

To validate the numerical model of the thin-glass IGU, a test setup with a real thin-glass IGU needs to be measured and evaluated. The original plan was to use AGC's falcon glass. Unfortunately AGC was not willing to sponsor this years research topics so a different supplier had to be reached out to.

Consultations with different glass producers took place whereby fortunately, pilkington was willing to provide chemically strengthened thin-glass. After consulting with Pilkington's engineers, Glanova chemically strengthened thin glass was chosen as the ideal product for this application. Unfortunately this specific glass is only produced in Japan which increased communication and delivery times. Ultimately the thin glass arrived too late to perform tests with.

Instead a different material had to be used for the validation of the numerical model. PMMA was used as a substitute of thin glass. PMMA is a flexible transparent polymer. A sheet of PMMA, although more flexible than thin glass could simulate the bending of the real thin glass panel the best. A thickness of 2 millimetres was chosen for the PMMA panes, as it would more closely simulate the stiffness of the 1.1 millimetre thick glass panes.

Accordingly, a finite elements model was made with the PMMA panes. The only difference between the two models being the thickness of the panes and the material properties.

Since PMMA is more flexible than the glass, the IGU will bend further before breaking. The importance of this model is the extrusion of data at precise coordinates.

	A	B	C	D	E
1	Property	Value	Unit		
2	Material Field Variables	Table			
3	Density	1,19	g cm^-3		
4	Isotropic Secant Coefficient of Thermal Expansion				
6	Isotropic Elasticity				
7	Derive from	Young's Modulus an...			
8	Young's Modulus	2,798E+09	Pa		
9	Poisson's Ratio	0,37			
10	Bulk Modulus	3,5872E+09	Pa		
11	Shear Modulus	1,0212E+09	Pa		
12	Tensile Yield Strength	Tabular			
13	Tensile Ultimate Strength	Tabular			

Table 9. Material properties of PMMA plexiglass

6.4 Results setup

Ansys solutions of maximum principal stress, and maximum principal elastic strain provide tabular data with the maximum stress and strain achieved in the entire model. To see data of stress and strain at particular points on the surface, probes can be inserted on the model. Multiple probes are set to provide clear answers.

- Probe 1: maximum stress and strain at the edge of the support block on side one
- Probe 2: Maximum stress and strain at the edge of the support block on side 2
- Probe 3: maximum stress at the inner side of the pane , directly below the displaced surface.

Probe 3 should correspond to the values of the global maximum principal stress, as that seems to be the place of the highest stress concentration

Furthermore, probes are set at locations where strain gauges will be placed to test if the model corresponds to the physical prototype. These probes are placed a bit further than the locations with the highest stress concentrations, as there has to be room for physical placement of the strain gauges

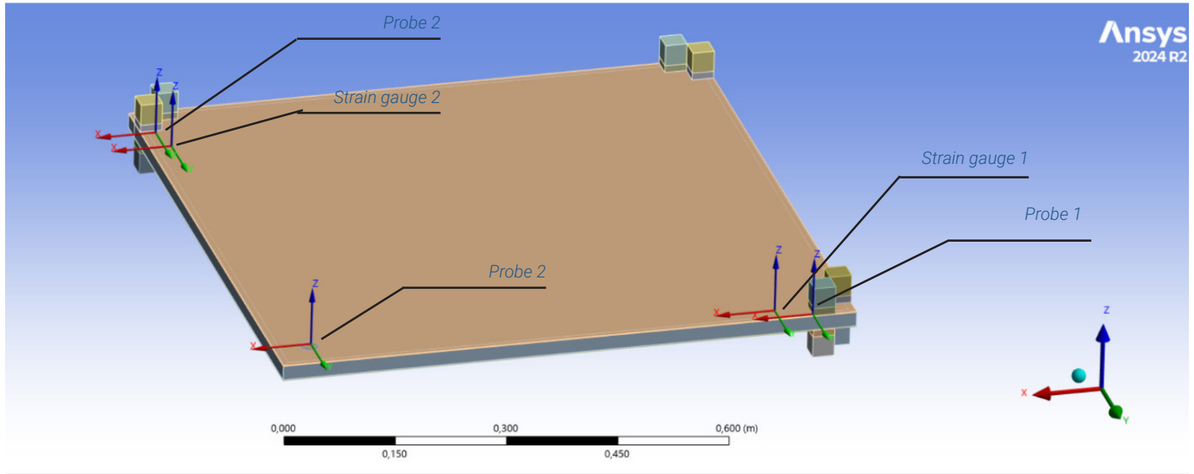

Figure 80. Result setup comparable with real tests (Own work)

6.5 Results - Plexiglass IGU

In figure 81 the deformation result of the plexiglass IGU can be seen. The deformation is set at the vertex of the free corner and is calculated with a step for every centimetre of displacement. This steps are divided into 5 sub-steps for more accurate results.

Shape

The deformation of the panel is set to 10cm. The deformed shape of the panel is actually a clear single curved surface. The edges of the panel are seen to slowly curve over the length of the panel. The stiffness of the spacer is not high enough in order to support a double curved (hypar) shape. This also partly can be attributed to the behaviour of plexiglass instead of real glass. The plexiglass behaves way more flexible rather than thin glass, and especially for the first few millimetres and centimetres of the displacement this makes a different on shape of the surface of the IGU.

Stresses

Figure 82 shows the maximum principle stresses that occur in the IGU. The largest stress is recorded at the vertex of the displaced corner at the opposite side of the panel. Activating the displacement at the vertex will give a high stress concentration as all the stress is calculated on the nearest mesh element. The maximum principle stress value derived from this corner is not of great value for this research. During proposed cold bending of the panel, the displacement is always activated at a larger area than the displacement is at a single vertex area. Therefore it is more interesting to look at other locations with high stress concentrations.

Other large stresses mostly occur along the edges of the glass pane, where they increase near the glass leaving the clamps. The glass leaving the clamped area creates an initial cantilevered situation. The bend-

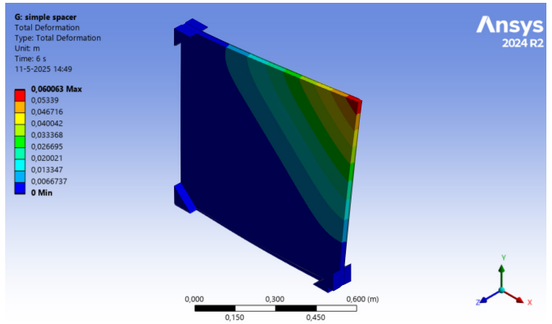

Figure 81. Total deformation of the panel under single corner bending (Own work)

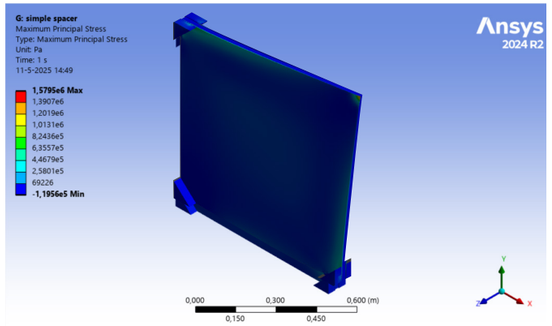

Figure 82. Maximum principal stress in panel in deformed state (Own work)

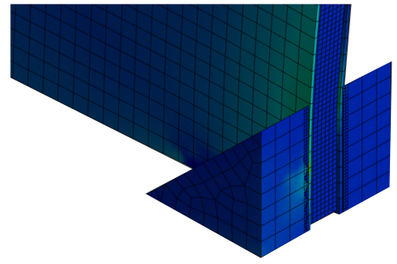

Figure 83. Stress concentration at plexi-glass leaving the clamps (Own work)

ing moment is the largest at this location, and this creates the largest stress at the upside of the pane.

Strain

Figure 84 shows the strain vectors according to strain size. As can be seen in the location of the strain obviously corresponds with the locations of the stress. What can be observed more closely in this model is that there is a field of strain in the middle of the pane. This is the area where the bending of the panel occurs on the surface of the glass. It can also be observed that strain gets recorded at the bottom edge of the IGU, this is interesting, and by taking a closer look, it is noted that both fully clamped edges of the IGU bend in the opposite direction as the deformed corner.

These strain vectors are important because they determine the right location for the placement of the strain gauges in the test experiment. It is beneficiary for the placement of the strain gauges to be near high-strain areas. The strain gauges can collect more data and this way the gauges will be more resistible against dissimilarities and noise.

As concluded from this image, strain gauges will be applied near the two clamped corners near the free, deformed edge. This is where strain is large, and this is an accessible location for application of the gauges.

Another location for a strain gauge to be applied is near the edge of the clamped side of the IGU, near the location where it bends in the opposite direction. Applying a strain gauge here will determine if this opposite movement of the bottom edge occurs in the experiment aswel. Graph 11 shows the strain data at the locations the strain gauges will be placed during the tests.

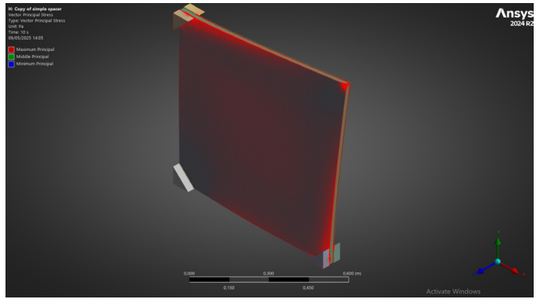

Figure 84. Strain vectors on panel in deformed state (own work)

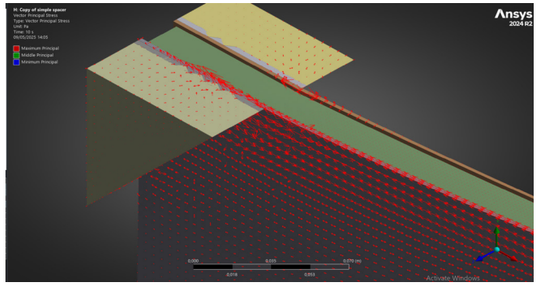

Figure 85. Strain vectors on panel in deformed state (own work)

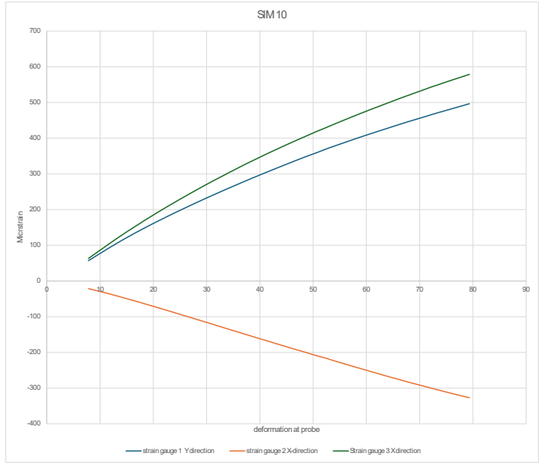

Graph 13. Strain/deformation graph of the three strain probes in the numerical model.

6.6 Results - Thin-glass IGU

The thin glass IGU model the same as the plexiglass model, except for the two plexiglass panes that have been swapped with Glanova 1.1mm thin glass panes. This model is deformed until 16 centimetres of deformation at the vertex of the deformed corner. This number is chosen as it would almost certainly include the maximum principle stress possible for the glass, 260MPa. (Eckersley O'callaghan, N.B)

The deformed shape of the thin-glass IGU is practically the same as that of the plexiglass IGU. This is expected as both the plexiglass and the glass are quite flexible, whereas the spacer is the structurally a large component of the panel.

Opposing to the plexiglass, in this model the maximum principal stress becomes very relevant. The prediction is that the Glanova chemically strengthened thin-glass will break at this point. As can be seen in the picture, the highest recorded stress is at the mesh where the glass leaves the clamps.

In this model the maximum principle stress reaches a value of 458MPa at a displacement of 16 centimetres. This number is obviously too high for the glass to reach. 260MPa (the approximated maximum tensile bending strength for chemically strengthened thin-glass) is reached at a displacement of ~ 9,4 centimetres displacement at the corner.

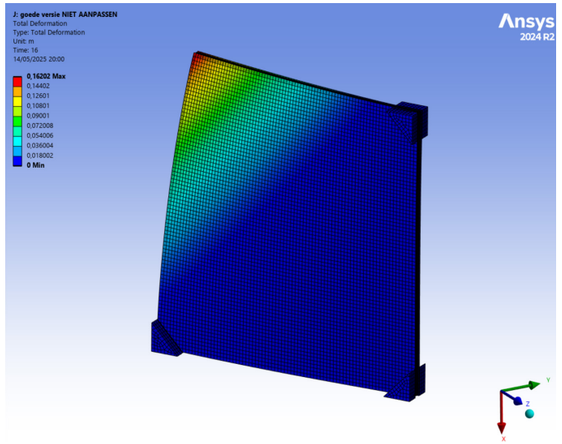

Figure 86. Deformed shape at 16cm deformation at corner (own work)

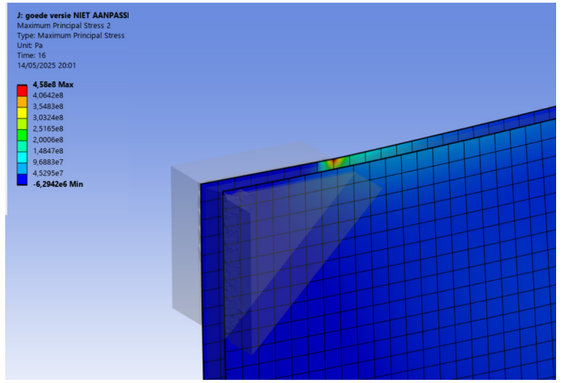

Figure 87. Maximum stress location (Own work)

This result can be compared with design bending strength in the ASTM E1300 - standard practice for determining load resistance in glass.

- Annealed glass ~45MPa -> 3,1 centimetres displacement
- Heat-strengthened glass: ~ 85MPa -> 5,3 centimetres displacement
- Fully tempered Glass ~ 120MPa -> 7,4 centimetres displacement
- **Glanova Chemically strengthened glass ~ 260MPa ->15,4 centimetres displacement**

If this model is correct and could the thin-glass IGU really bend this far will be confirmed after validating the tests.

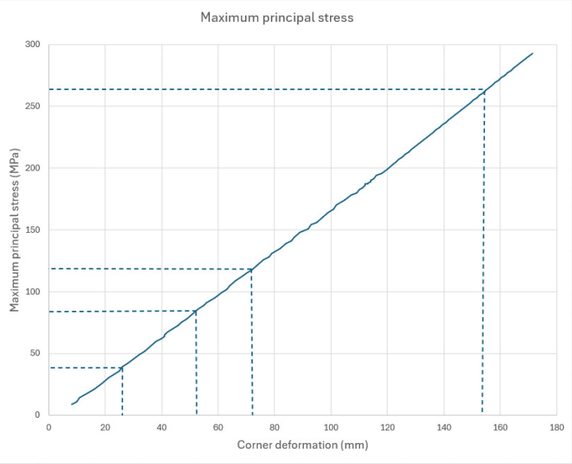

Graph 14. Maximum principle stress of thin glass pane during deformation (own work)

6.7 Discussion of the results

The values derived from this finite element model could for multiple reasons vary from the results derived from the real tests. Modelling a physical set-up could derive in various ways from the finite element model. The goal is to model as closely as possible to the real situation. This paragraph will discuss a few reasons as to why results could differ.

• Mesh size and computing time

The mesh size is very important in a finite elements model. The mesh determines the amount of calculations the program will perform for each task. The smaller the mesh size, the more accurate the results will be. The size of the mesh has a great influence on the computing time of the simulations. For the (plexi) glass panes, a mesh of 1cmx1cm has been used in this final product. Decreasing the mesh size to for example 5 by 5 mm would quadruple the amount of mesh elements on the panes, and therefore quadrupling the amount of computing time. For running the simulations, the laptop of the author was not satisfactory, therefore the PC's at the VR-lab were used to run every simulation on. These PC's contain a 12-core CPU and 32 Gigabytes of ram. These computers perform significantly better than the authors laptop. Unfortunately, these computers were not always available, since there are 2 computers with Ansys installed, and are meant to be used by the whole faculty.
With simulations already taking up to hours in the current state of the model, the mesh was left at the current size.

• Modelling of the foam support cushions

Accurately modelling the foam material between the clamp and the glass proved to be a real challenge. The exact material properties of the foam used in the test setup was unknown. How the foam behaves proved as a guide to model the support blocks. Precisely modelling this foam was a challenge, as making the foam too stiff, would cause high stress concentrations, and modelling the foam too soft would make an incorrect model, or cause distortions during computing, crashing the simulation.

• Friction Coefficient

The friction coefficient between the foam and the (plexi)glass panels is not a researched value but rather an educated guess. Multiple values were tried out and accuracy according to the real tests was observed. A friction coefficient of 0.6 seemed to be a realistic value. The realism of this value shall be proven during the real tests.

• Air pressure

When an Insulated glass unit is constructed, gass is placed inside the cavity to increase its thermal insulating value. The spacer has one, or preferrably two small holes. After the glass is connected to the spacer, the argon gass is injected into the cavity. The other hole is there to let the normal air escape out of the cavity. The gass is injected upto a slight overpressure in the cavity. The overpressure ensures a good distribution of the gass. The overpressure also accounts for the gass leaking in small amounts over time.

The cavity between the IGU is sealed off. The cold bent geometry of an insulated glass unit can provide a slight volumetric change of the cavity. Therefore giving the cavity a slightly higher or lower pressure on its surroundings. Because of time restraints, modelling of the air pressure was not included in the final ansys model. The influence on pressure in the IGU on the cold bending behaviour for this simulation and test is thus currently unknown.

07

Testing

7.1 Plexiglass measurement

The first bending test are performed using a prototype IGU made with plexiglass since delivery of the real chemically strengthened thin glass is scheduled to late for thesis admissions. These tests are compared to an ansys model also made with plexiglass. If the model and the test results of the plexiglass panel correspond, the plexiglass can be swapped out and the model should be reliable enough to make calculations for the thin glass IGU.

The plexiglass is useful for discovering the right setup for the single corner deformation tests since it is not as breakable as normal glass. The setup of the bending of the plexiglass and the real thin glass is largely the same, except for a few minor details.

The following paragraph explains how strain gauges are applied to the surface of the plexiglass panel.

7.2 Strain gauge application

3 strain gauges are applied to the plexiglass surface. These strain gauges are applied to areas on the surface where high strain is expected following the numerical model.

1: The strain gauges are outlined parallel to the edge of the IGU. This provides output of strain direction to a single axis, which can be compared to strain in a single direction derived from the numerical model. Measuring and noting the exact location of the strain gauge is important. The surface of the plexiglass is cleaned with isopropanol to make sure the adhesive perfectly connects the strain gauge to the plexiglass.

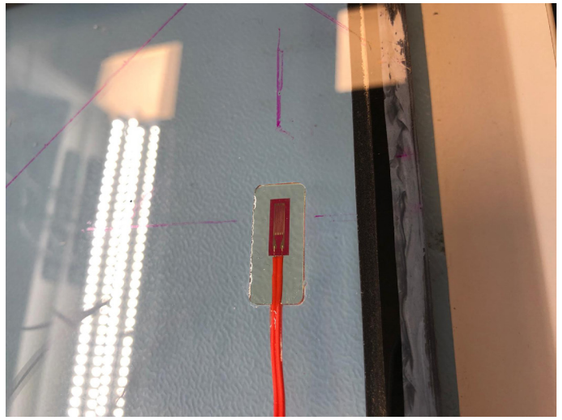

Figure 88. Alignment of strain gauge (own work)

On corner 1, two strain gauges are applied in perpendicular direction to each other, to accurately measure data in both the X and Y direction, making it possible to calculate the direction and total amount of strain roughly on this location. Strain gauge 3 is placed on the other corner.

The strain gauges are attached to an amplifier. The amplifier is set to 1 Volt for the strain gauges, this is to minimize swing in the strain value caused by minor deformations or temperature switches.
After the device is hooked to a converter which is connected to a PC, the strain gauges will start to warm up as electricity runs through them. Therefore the strain value must stabilize before performing any bending tests. After the strain gauges have stabilized, the strain gauges can be set to a zero-measurement. after this, the strain data is exactly the same in the graph as on the prototype.

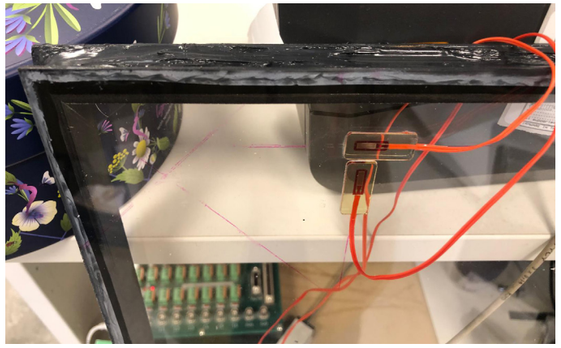

Figure 89. Double strain gauge setup in the corner (Own work)

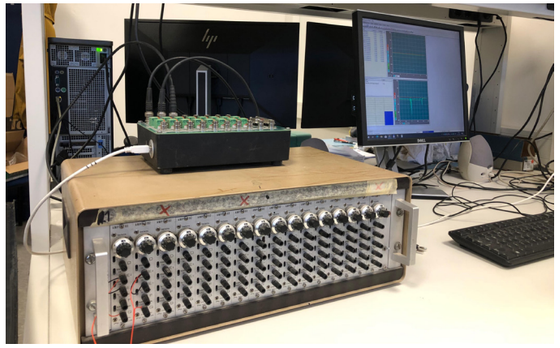

Figure 90. Used amplifier and converter (Own work)

7.3 Strain calibration

Each batch of strain gauges has a different K-factor. The K-factor (also called the gauge factor) of a strain gauge is a constant that relates the electrical resistance change in the gauge to the mechanical strain it's experiencing.

The first batch of strain gauges used has a K-factor of 2.12. Strain gauge 1 had a defect after pre-testing and was replaced. The second batch of strain gauges had a K factor of 2.12

To convert the resistance of the strain gauge and the K factor to micro-strain the following formula is used. For the first batch of strain gauges (2.12) the micro-strain/voltage is 1887. The change in voltage has to be multiplied by 1887 to gain an accurate output of micro-strain. For the second batch of strain gauges, this value is 1895.

A displacement meter is attached to the back of the IGU on the opposite side of the pushing mechanism. The displacement meter is hooked to the amplifier. Measuring displacement accurately is done so that the strain output data can be linked to an exact displacement, making it easy to compare the strain data of the prototype to the strain data from the model.

$$U = \frac{K * \varepsilon * E}{4} * A$$

$$U = exit\ voltage$$

$$K = Gauge\ factor = 2.12\ and\ 2.11$$

$$\varepsilon = strain$$

$$E = bridge\ voltage\ (v)$$

$$A = amplification = 1000$$

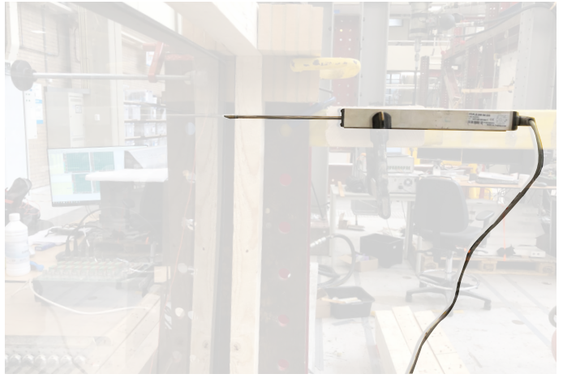

Figure 91. Displacement gauge setup behind the panel (Own work)

$$40 = 2.12 * 1000 * \varepsilon$$

$$\varepsilon = 0{,}01887 = 1887\ \mu Strain = 10\ volt$$

$$40 = 2.11 * 1000 * \varepsilon$$

$$\varepsilon = 0{,}01895 = 1895\ \mu Strain = 10\ volt$$

The final setup can be seen in figure 91. The setup is rotated 90 degrees from the original design. The original design had the IGU laying flat on its back. The flexibility of the plexiglass and the spacer made the IGU deflect under its own weight to much for this experiment. Conducting the experiments with a vertical standing IGU solves this issue. Fortunately it also helps the issue of the upper pane sagging more than the lower pane. The phenomenon of the two panes possibly touching is now possibly delayed. A difference between the designed setup for bending the thin-glass IGU and the plexiglass IGU is the screw down bending mechanism. The applied pressure on the surface of the point bending can cause extreme stress concentrations on the surface of the glass if the force is not applied equally on the surface. With a hand built prototype it is hard to evenly spread this force without creating extreme stresses. Therefore for the glass bending mechanism, the surface of the displacement press was wrapped in expanded polyethylene most commonly found in wrapping plastics. However applying a soft material to the displacement surface causes the IGU to bend back a bit and push into the displacement surface. This causes small errors in the strain measurements. Therefore during the plexiglass tests, the wrapping plastic was removed from the displacement surface.

Figure 92. Complete single corner bending test setup.

7.4 Plexiglass test results

The plexiglass IGU as shows above has been tested three times with the 3 strain gauges. During the tests, the pressure screw was displaced until 80, 100 and 120mm. The change in displacement is to see how the IGU would react to larger deformations each time. The three tests were recorded. Somewhere during the third test, the primary adhesive came loose from the plexiglass, where after the plexiglass IGU was no longer useful for anymore tests. It is predicted that this happened because the movement of the spacer against the movement of the glass was too large. This caused big shear forces on the PIB layer which ultimately failed. The bending of the edges of the glass exhibit a large pulling force on the PIB. This differs from the cold bending of IGU's with a more rigid frame, whereby most forces in the spacer are transferred to the middle of the surface of the glass.

Furthermore, the secondary glazing sealant, Ködiglaze S let loose from the PMMA plane and showed lare deflection on its own. Although the surface of the Plexiglass was cleaned with Isopropanol before applying the Ködiglaze, the adhesion might not have been sufficient.

The failure of both adhesives could be explained by the bonding between the silicone and the plexiglass. The PIB and Ködiglaze are engineered to bond on a molecular level to glass. Plexiglass of course has a completely different chemical structure, making the bonding different.

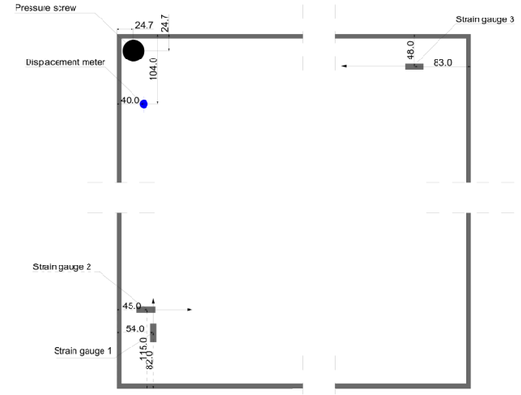

Figure 93. Schedule of the cold bending setup situation including locations of data points (own work)

Figure 94. The maximum bend deflection (own work)

Figure 95. Polyisobutylene layer letting loose from the PMMA pane. (Own work)

Figure 96. Secondary adhesive letting loose (own work)

The next graphs show the strain measured in micro-strain or µm. The graphs show that the strain gauges behave more or less similar in the three tests.

1. Strain gauge data

Strain gauge 1 and 3 gradually register more positive strain as the corner is displaced. Strain gauge 2 shows a negative strain while the corner is displaced. This means that this strain gauge is compressing. This can be explained by the movement of the entire panel. While the displaced corner is pushed "downwards" out of its plane, the two completely clamped edges start to bend upwards slightly. This can be observed in the simulations.

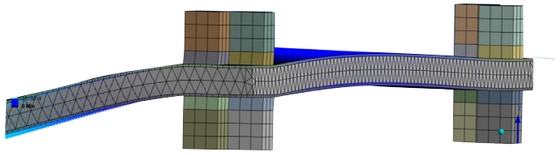

Figure 97. Opposite movement of clamped edge (own work)

Interesting behaviour can be observed as after a certain deformation, all three strain gauges start to register less strain.

- Strain gauge 1 registers a maximum strain of 253µm, Or $265*10^{-6}$ m.
- Strain gauge 2 registers a maximum strain of -217µm, Or $-217*10^{-6}$ m.
- Strain gauge 3 registers a maximum strain of 153µm, Or $153*10^{-6}$ m.

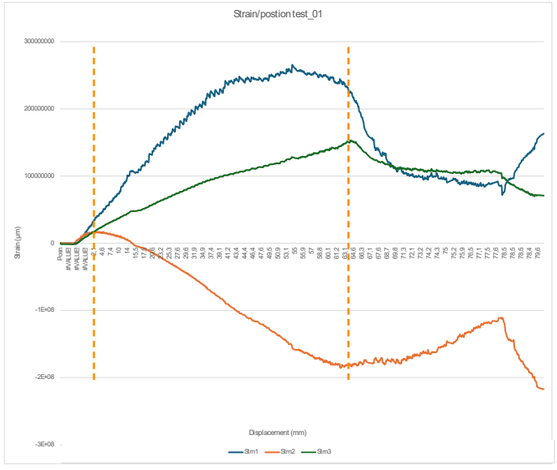

Graph 15. Strain gauge data plotted against deformation of the corner measured by the displacement gauge test_01 (Own work)

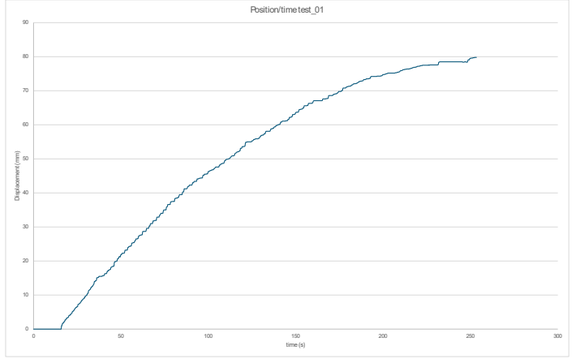

Graph 16. Displacement of the corner against time measured by the displacement gauge for test_01 (Own work)

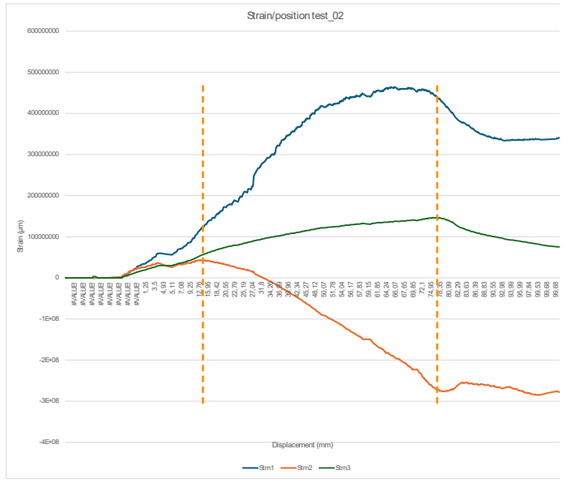

Graph 17. Strain gauge data plotted against deformation of the corner measured by the displacement gauge test_02 (Own work)

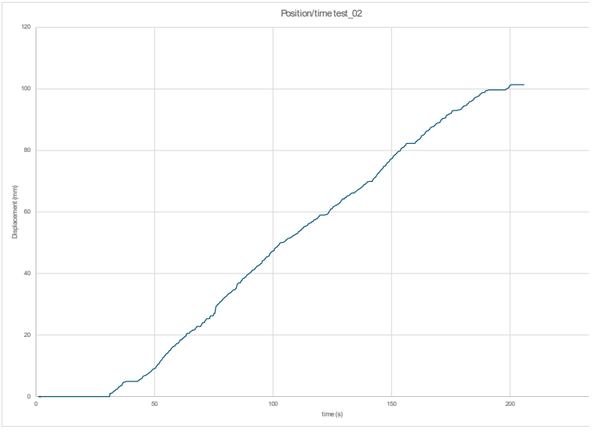

Graph 18. Displacement of the corner against time measured by the displacement gauge for test_02 (Own work)

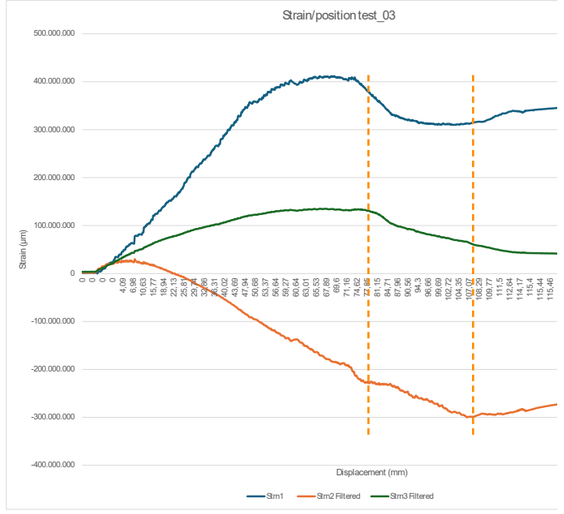

Graph 19. Strain gauge data plotted against deformation of the corner measured by the displacement gauge test_03 (Own work)

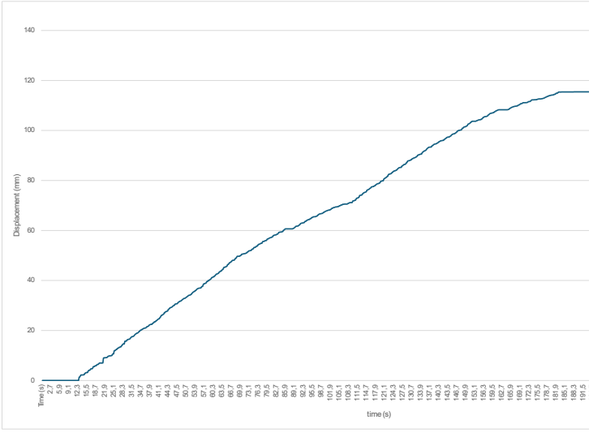

Graph 20. Displacement of the corner against time measured by the displacement gauge for test_03 (Own work)

It is clear that there is quite a significance difference between strain gauge 1 and 3. Ideally, these strain gauges should output the same data as the panel and boundary conditions are symmetrical. The difference in data could have a few causes.

1. The strain gauges are not placed on exactly the same place.
The author wanted to place strain gauge 1 and 3 on exactly the same place in their respective corners. Unfortunately the first applied strain gauge malfunctioned and had to be replaced by another. This strain gauge is now placed further from the edge of the IGU.

2. Asymmetry of the situation.
The panel is placed vertically, which ultimately means that the panel rests on the two bottom clamps and is free in the Y-direction (up or down) in the top two clamps, this could disrupt the data by a small amount.

3. Tightening of the corner clamps.
The corners are screwed down to clamp the IGU. The tightening of the screws was done with a simple hand screw. After reviewing the situation, making sure that every corner clamp was screwed and tightened the same amount would cause way more accurate deformations of the panel around the corners. If one corner is less tightly screwed than another, the whole panel would give more way, therefore reducing the amount of strain at a certain spot of the surface of the plexiglass.

2. Plexiglass surface buckling
As can be seen in the strain gauge graphs, the strain gets larger when the deformation gets larger until a certain point. This happens for test one, two and three respectively at a deformation of 64mm, 78mm and 76mm. This sudden shift in strain is believed to be caused by a buckling effect in the surface of the plexiglass. The shift in strain happened across al three tests and however it varies how much impact it has on the strain gauges and how the values shift multiple consistencies can be observed.

Strain gauge 1 is always the most impacted by this buckling effect. After a big initial dip in strain, strain gauge 1 starts to stabilize and then shows recovery thus increasing strain again.

Strain gauge 2 also clearly shows something happening during the common buckling point. Test 01 shows that strain gauge 2 slowly reacts to the buckling effect, crawling back from $-217*10^{-6}$ to $-110*10^{6}$. Test two shows a clear spike in strain after which the strain slowly increases until it starts decreasing again. Test three shows a slightly different reaction of the strain gauge to the buckling effect. A spike can be observed, much like test 02. After this initial spike the recorded strain keeps increasing until a corner deformation of 108mm. Here both strain gauge 1 and strain gauge 2 start recording strain in the opposite way of where they were moving.

Other interesting behaviour observed in strain gauge two is its initial rise in positive strain. The turning point for this initial rise is around 2 millimetres for the first test and at 13 and 7mm displacement for the second and third test. It must be noted that test 2 also shows signs of a buckle at a deformation of 4 millimetres.

Strain gauge 3 reacts much like strain gauge 1 and decreases recorded strain after the buckling effect. Similarly to strain gauge 2 it records a spike during the buckling effect.

3. Creep and dissimilarities.
There can be multiple causes for the difference between data output. One explanation of the difference in the exact location of the buckling effect is plasticity of the entire panel. Plexiglass on its own behaves very differently rather than glass. Plexiglass can show significant creep behaviour which is much larger than the creep that can occur in glass. Making glass creep insignificant compared to creep that can be observed in PMMA. Creep was observed during the physical experiments of the plexiglass IGU. After the first cold bent test, the panel bounced back after initially unscrewing the deformation push. After the initial few centimetres of removing the pushing knob, the IGU stayed in its deformed shape. The deformed IGU was then pushed back in its original state by pushing the displaced corner back.

It is very likely that the IGU was in a temporal state of plastic deformation, which essentially is visco-elasticity. A visco-elastic material gradually returns back to its original shape over time. This is very common behaviour for materials like polyurethane, silicone and elastomers. Both the PIB primary adhesive, the silicone foam spacer and the Ködiglaze are likely to be visco-elastic materials. Whereby it is very likely that the spacer caused to IGU to behave as a visco-elastic composition. Furthermore, the stiffness or rather the lack of stiffness in the plexiglass panes was not enough to pull the IGU back to a flat state.

After pushing back the deformed corner of the IGU, the edges still showed a curvature meaning the IGU was not yet fully recovered back to its original completely flat state. Because of time constraints, tests 02 and 03 were performed within decently quick succession of the first test. This inconsistency in the initial shape of the panel before the single corner cold bending could be the cause of the difference in the corner deformation at which the buckling of the surface of the IGU occurs.

The strain gauge outputs were zero measured before each experiment. This could explain larger dissimilarities between the strain data for each test. If the IGU was somewhat still “plastically” deformed at the time the next test took place, the strain gauges will record different strain.

Finally, when zoomed in on the graphs it can be observed that the lines for all the strain gauges during all the tests are nog very smooth. The small wiggling of the lines can be explained by the screwing mechanism for the displacement system. The pushing mechanism has to be manually screwed downwards, whereby it is performed with simple hand movements. Therefore the lines show small inclinations in the strain data.

Conclusions

The results of the tests seem usable for this part of the research. The strain gauges recorded the same behaviour for all the three times. Strain values, and deformations at which buckling effects happen do differ and is likely caused by the reasons mentioned above. Numerical data can still be compared to these graphs and if it shows roughly the same behaviour, the numerical model can be validated.

- The main surface buckling effect in the surface can be noticed from the graphs and happens in this situation at around 65 to 78 mm corner displacement.

- A secondary buckle can be observed in the fully supported axis. This buckle causes strain gauge 2 to move from tensile strain to compression.

Evaluation

- For further tests performed with thin glass it is important to make sure that all corner clamps are screwed equally tight.

- Fortunately, creep of the thin glass IGU is likely less significant as the glass is stiff enough to pull the spacer back to its original shape.

- The failure of the adhesives is less likely to happen with the thin glass IGU since both adhesives are designed for glass.

- To measure if the panel is indeed more symmetrical than recorded during these tests, placement of strain gauges one and three should be at the exact (mirrored) location of the central diagonal axis.

7.4 Comparison with FEM simulations

The behaviour of the panel and the strain values at certain locations are compared to validate the model.

Graph 21 shows the strain probes plotted against the deformation at the same location as the displacement gauge in the single corner bending setup. Strain probes are set at the nearest location possible as the strain gauges in the real panel are. Through constructing a new coordinate system in ansys, the exact location of the strain gauges can be put into the model.

In the numerical model the two strain probes measure almost the same strain, whereby strain probe 3 measures slightly more strain. This is expected as strain probe 3 is located more near the edge of the panel, where the strain and stress is higher than near the centre of the panel.

The data of the three tests are plotted against the numerical model in the next graphs. The first combined graph shows that while the general behaviour of the strain gauges are similar to the model, the data is actually quite far off. The buckling behaviour of the tests also does not appear in the numerical model.

Physical tests 02 and 03 show closer behaviour of the strain gauges to the model. Especially strain gauge one is almost completely similar to the model at test 03. At least until the buckling behaviour is recorded in the numerical model.

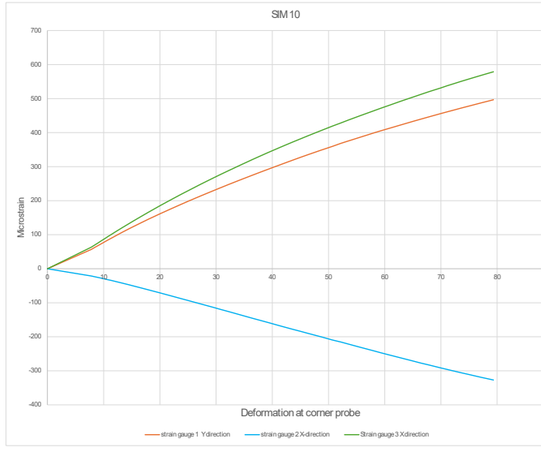

Graph 21. Strain/deformation graph of the three strain probes in the numerical model (own work)

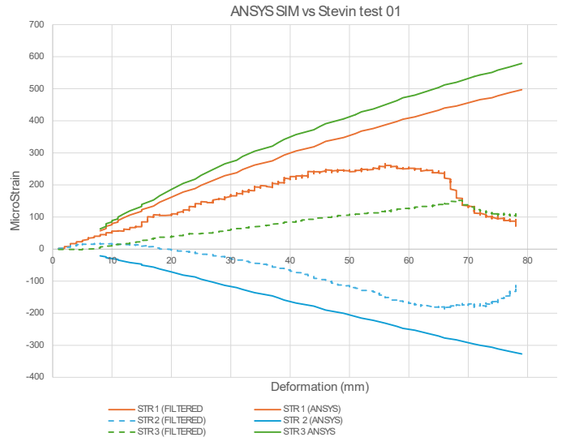

Graph 22. Microstrain/deformation ansys vs Test 01 (Own work)

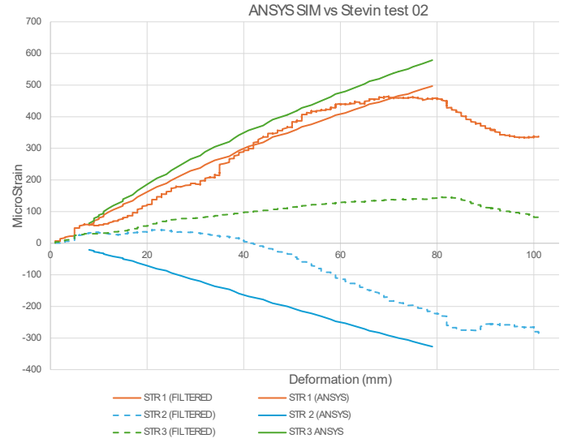

Graph 23. Microstrain/deformation ansys vs Test 02 (Own work)

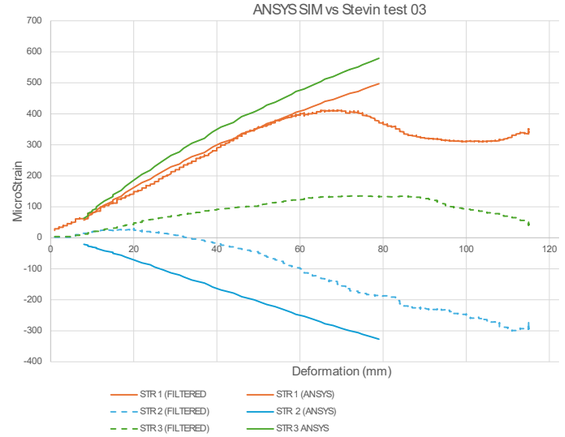

Graph 24. Microstrain/deformation ansys vs Test 03 (Own work)

While the strain gauges and the probes show the same general behaviour, the strain numbers are not exactly the same.

This could have multiple causes.

1. Bonding of the adhesive
The plexiglass IGU is modelled with a "bonded" contact point between the plexiglass and the primary adhesive + spacer. As explained in the chapter: numerical modelling, a bonded contact means that the two objects will not separate or glide. Wherein the physical model, as can be seen on figure 95. The primary adhesive PIB layer disconnected from the plexiglass pane and showed great shear deformation. This can possibly be attributed to the primary adhesive not being made for bonding with plexiglass and thus performing worse.

2. Clamping of the IGU
While constructing the experiment the plexiglass IGU is set in the test setup. The screws at the corner clamps are tightened. During the tightening it was noticed that the panel slightly compressed inwards, and therefore made a concave shape. This initial concave shape might have already put strain on the strain gauges. Before conducting the experiments, the strain gauges have been 0 measured. The strain recorded before this point is at that moment cancelled out. This could be a causation of the recorded strain in the tests being less high than the strain recorded in the numerical model.

3. Alignment of the strain gauges
The strain gauges are placed by hand and a small displacement could make the strain gauge not align exactly with the X or Y axis, although relatively speaking, this should have a small effect on the output of strain data.

4. Buckling
The buckling of the plexiglass surface recorded during the tests is very specific to the specific circumstances in the tests. This type of behaviour is very hard to accurately model and is often not recorded during simulations since the simulation is performed in a "perfect" setting. Real tests are often not "perfect" which can increase chance of buckling and other imperfections.

7.5 Thin glass test 01

The first panel was tested with the same panel configuration as the plexiglass test. The back panel broke first at a corner displacement of 280 millimetres. This test was only partly succesfull as the panel came loose from the clamp at roughly 115 millimetres displacent. This can be seen in picture 97. Therefore the 280 millimetres corner displacement is disregarded. This does not make the test useless, as the data recorded before the clamp failure is valuable. The 280 millimetres corner displacement also meant that the displacement gauge had to be removed, as it reached its maximum at 200mm.

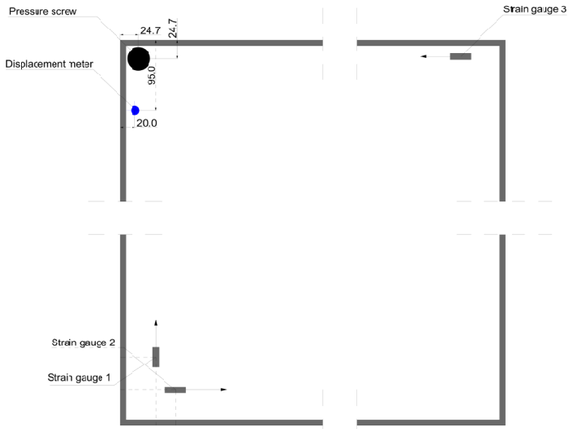

Figure 99. Panel leaving clamp. (Own work)

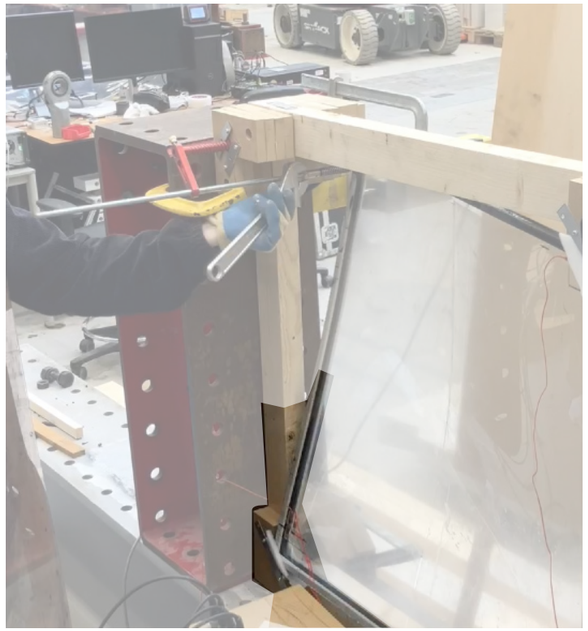

Figure 98. Schedule of the cold bending setup situation including locations of data points (own work)

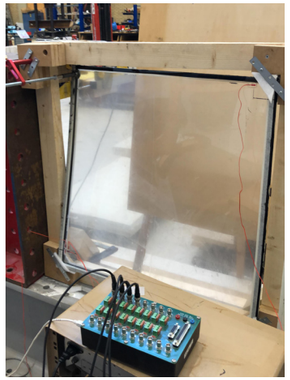

Graph 25 shows the strain recorded at the three strain gauges against the displacement. The maximum displacement of 200mm is exceeded, but not displayed in this graph. The graph shows that strain gauge one and three behave very similarly for the first 115mm, which is logical, as they are placed at an almost mirrored location. Untill 115mm, strain gauge three records a bit more strain, because it is located closer to the edge of the panel than strain gauge one. After 115 millimetres, the data of strain gauge 1 and 3 disperge because of the clamp failing. The dent in strain at 150mm can be explained by one of the clamps for the wooden frame to the steel profiles being removed as it limited the freedom for the panel.

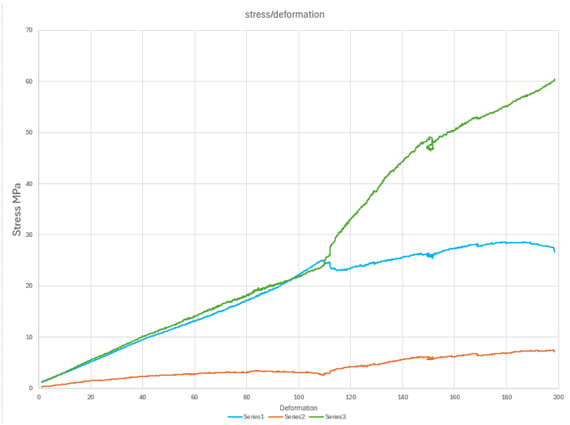

Graph 25. Glass test 01: measured strain against deformation (own work)

Graph 26 is zoomed in on the usable part of the test, where the strain gauges behave linearly. The dashed lines are the strain data from the model at the respective coordinates from the test. The lines do correspond decently, before deviating where the clamp failed. The difference in exact data can be explained by small dissimilarities between the model and the test, like the exact measurements for the clamps and the exact locations of the strain gauges. To make sure the clamp will not fail with the next test, the foam is replaced by cardboard. Cardboard is weak enough to not cause any stress peaks in the glass, and to distribute the stress. But it is stronger than foam and will give less way, making the glass' cold bending shape more predictable.

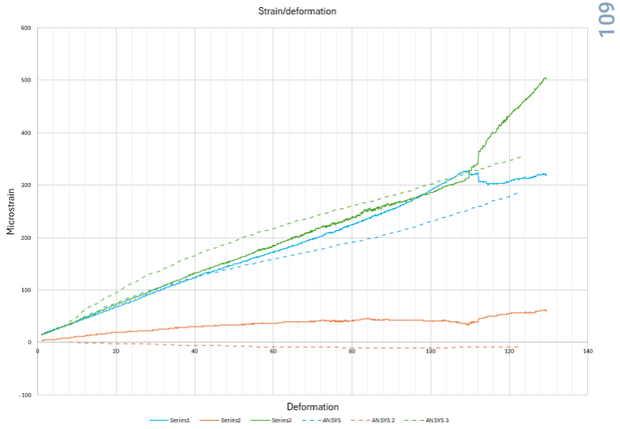

Graph 26. Glass test 01: measured and calculated strain against deformation (own work)

Graph 27 shows the strain is converted to stress by multiplying with the Young's modulus (75,4MPa). The stress behaviour is the same as the strain behaviour because the young's modulus is a constant. At these locations, relatively low strain is recorded during the initial phase of the bending test. After the failure of the clamp, a maximum stress of 60MPa is recorded at strain gauge 3. Which is higher than could be achieved with regular annealed glass, but is likely not the maximum for the Glanova as the pane broke at a different location than at the strain gauge.

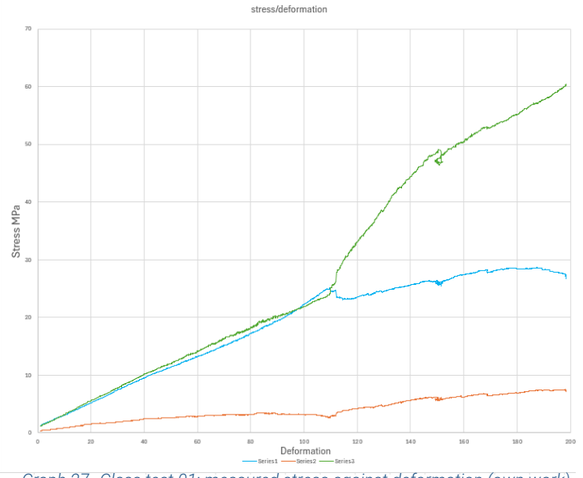

Graph 27. Glass test 01: measured stress against deformation (own work)

Graph 28 shows the maximum principal stress of the entire model is plotted against the stresses recorded at the strain gauges. If the maximum tensile stress of 260MPa is realistic, this would mean that in a better performed test, the glass would break at around 150-160mm corner displacement.

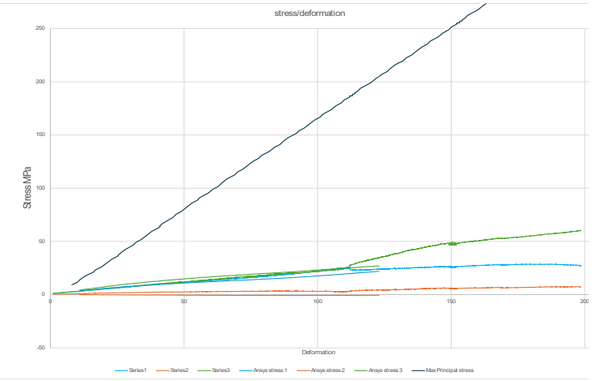

Graph 28. Glass test 01: measured stress vs calculated stress against deformation (own work)

7.6 Thin glass test 02

The second thin-glass panel was bend until a corner displacement of 18,5cm. This test the corners were clamped better than during the previous test, by tightening the screws further and using cardboard corner cushions instead of the polyethylene foam. The panel therefore stayed much better in its clamped position at the corners. Similar to the first test, the back panel broke first, likely at one of the two corners along the clamped diagonal. Again breaking at the same position as predicted by the model.

The setup of the strain gauges can be seen in figure 100
It was chosen to place all the three strain gauges at the same distance from the edges to test if the panel was clamped symmetrical

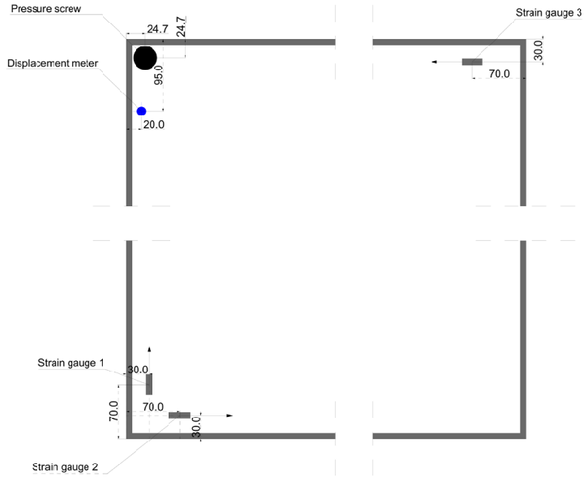

Figure 100. Scheduleofthecoldbendingsetupsituationincludinglocations of data points (own work)

Figure 101. Panel after breakage of the back panel (Picture taken by author)

Figure 102. Panel at the clamp after breakage of the back panel (picture taken by author)

Graph 29 shows the data derived from the strain gauges against the deformation at the displacement gauge. The graph shows that the corner from strain gauge 1 was clamped tighter than the corner from strain gauge 3, since strain gauge one records more strain than strain gauge 3. Interesting behaviour is observed at 80 millimetres displacement. Strain gauge one records a buckle in the glass' surface. The other two strain gauges do not record this behaviour. Similar to the other tests, strain gauge 2 records slight compressive behaviour.

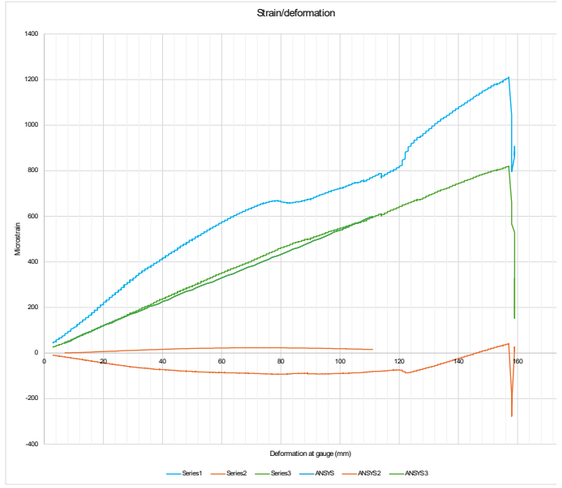

Graph 29. Glass test 02 measured strain against deformation (own work)

Graph 30 shows the stress calculated strain from the tests versus the stress from the simulations. The simulation could only run until a 110 milimetres corner displacement. It can be concluded that the panel was clamped slightly to loose since the maximum principal stress would rise to 300MPa in a linear extension of the simulated values. Clamping the panel slightly more tight would provide more accurate test data.

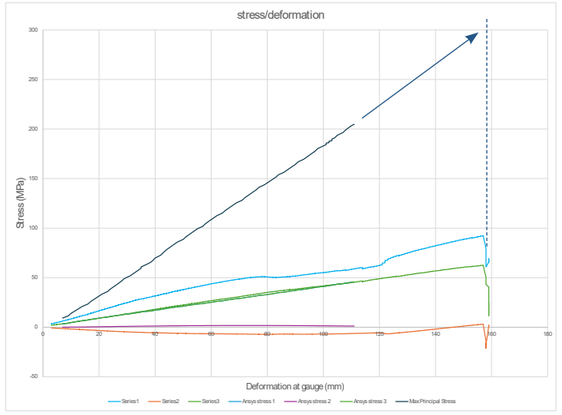

Graph 30. Glass test 02 measured strain against deformation (own work)

7.7 Thin glass test 03

For the third test, the clamps were moved slightly towards the centre of the panel. This would increase the tightness of the clamps and would decrease the risk of the clamps letting loose of the glass at high deformations. Unfortunately only one strain gauge was left available for testing. This strain gauge was placed on the Str 1 position in the previous tests. The strain gauge was placed very close to the panel leaving the clamp, that is why the recorded strain is very high at this location. The tightness of the clamps gave the panel little room to deviate which results in high strain concentration around this area of the panel. The strain of the strain gauge is plotted against the strain probe from the simulations at this location.

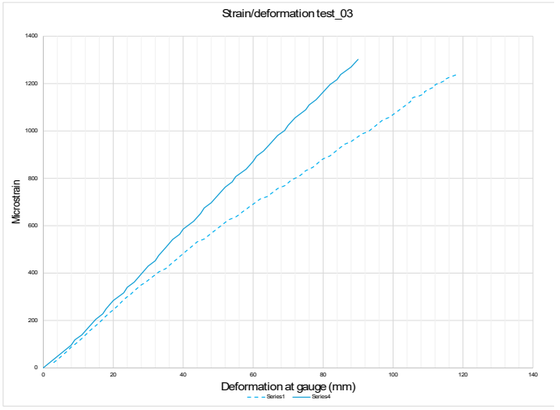

This panel was bend until a displacement of 163 millimetres where after the concave side of the panel broke first. Again the simulation was only run intull 90 millimetres deformation at the gauge, but the maximum principal stress show a generally linear behaviour of the maximum principal stress. If we extend this data, we see that the panel likely broke at a maximum principal stress of 260Mpa, which corresponds to the maximum allowed tensile stress of other chemically strengthened glass products. This deems the numerical model largely correct.

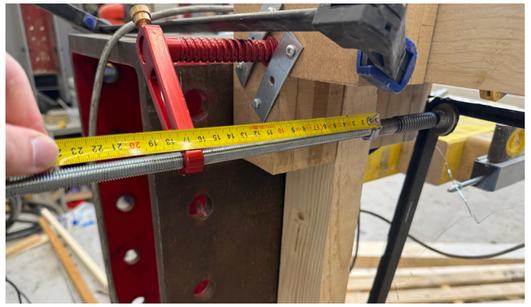

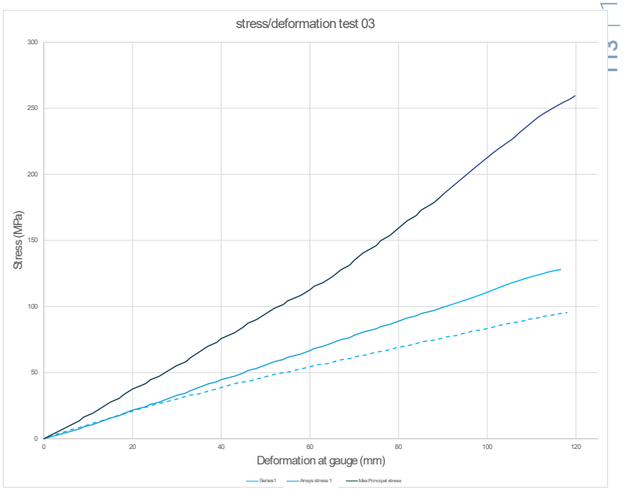

7.8 Discussion of the results

The results of the thin-glass IGU tests demonstrate both the mechanical potential and limitations of using chemically strengthened ultra-thin glass in cold-bent façade applications. Across multiple tests, the panels exhibited high tensile strength, with failure occurring at displacement values ranging from 16.3 cm to 18.5 cm. These results are consistent with the strain gauge measurements and the numerical simulations, which predicted maximum principal stress concentrations along the clamped edges and corners. The third test, which improved clamping conditions and strain gauge positioning, further confirmed this with a predicted breaking stress near 260 MPa, validating the predicted design strength for the Glanova thin glass.

If we compare the deformations at which the panels broke to the values at which other glass panels would brake we can conclude that the thin glass bends at least:

- 5,25 times further than Annealed glass
- 2,76 times further than heat strengthened glass
- 2,2 times further than fully tempered glass

Despite the promising strength values, challenges remain. The first test showed insufficient clamping, resulting in an unrealistic failure scenario. Only after refining the clamping setup were reliable and reproducible results achieved. The test setup also revealed that clamp positioning significantly influences stress distribution and must be optimized in design implementations to prevent premature edge failure.

Moreover, the strain values recorded during the tests align closely with the numerical Ansys model, reinforcing the accuracy of the simulation despite simplifications such as excluded cavity pressure modelling. However, in practice, air pressure changes within the IGU cavity and gas compressibility may slightly affect performance and need more advanced fluid-structure interaction modelling for comprehensive evaluation .

In conclusion, the results validate the feasibility of cold-bending thin chemically strengthened glass to significant curvatures, provided that the edge constraints are well designed. The successful correspondence between physical tests and simulations suggests that thin glass, when properly integrated into insulated glazing systems, could become a viable structural and aesthetic alternative to conventional glass products.

With the known data from the experiments, a scaling formula can be created to estimate the bending capacity of a thin-glass IGU depending on the panel's size. The relationship might not be linear and is dependant on at least

- Glass thickness
- Aspect ratio
- Spacer thickness

With the known inputs a formula can be created.

Panel size: 80 by 80 centimeters
Maximum cold bend deflection: 16,3 cm

$L = Side\ length\ of\ the\ square\ panel$

$D = diagonal = \sqrt{2} * L$

$B = corner\ deflection\ (in\ cm)$

$R = \frac{B}{D} = normalized\ deflection\ ratio$

$L = 80\ cm$

$D = \sqrt{2} * 80 = 113.14$

$B = 16{,}3\ cm$

$R = \frac{1.3}{113.14} = 0.144$

For this IGU design, it can tolerate a deflection of approcimately 14.4% of the diagonal length at one corner.

A formula can be constructed

$$Bnew = R * \sqrt{2} * Lnew$$

$$Bnew = 0.144 * \sqrt{2} * Lnew = 0.203 * Lnew$$

$$Bnew = 0.203 * 100 = 20.3\ cm$$

For a panel with size 100 x 100 cm, the predicted bending deflection at the corner is 20.3 centimeters.

08

Actualizing

Implementation of the panels is explored through a case study, Fenix Rotterdam. The Fenix museum in Rotterdam contains a unique hot bent glass roof structre accomodating the entrance and exit to the exterior part of the "tornado" on top of the roof of the museum. This chapter explored the possibility of using Thin-glass IGUs as a substitute.

9.1 Panel curve optimization

It was explored if a script could be made for surface panelization optiminization and failure visualisation. As a casestudy the roof of the Fenix building in rotterdam was taken. This roof features two entrances to the outdoor section of the "tornado". These glass entrances are made out of hot bend panels. A script was made mimicking these entrances to see if it was possible to divide the surface in panels that could be cold bend.

Firstly, an intensity study can be performed on the entire surface. Where surface curvature is high, the panels turn red, and where curvature is low, the panels turn blue. This allows designers to make changes to the curved façade in order to avoid high curvature sections in the design during the early design stage.

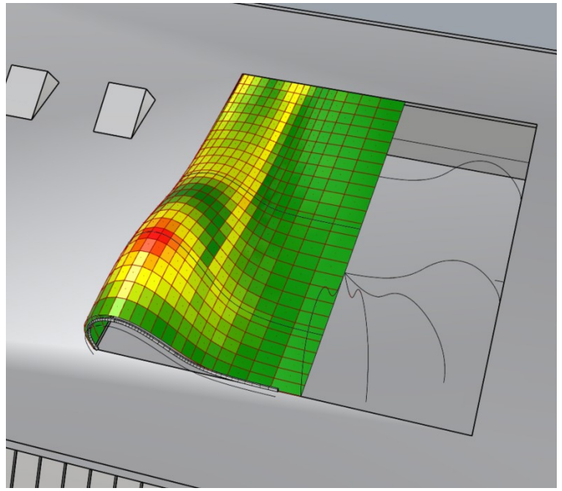

Figure 103. Panelized roof with surface curvature analysis (Own work)

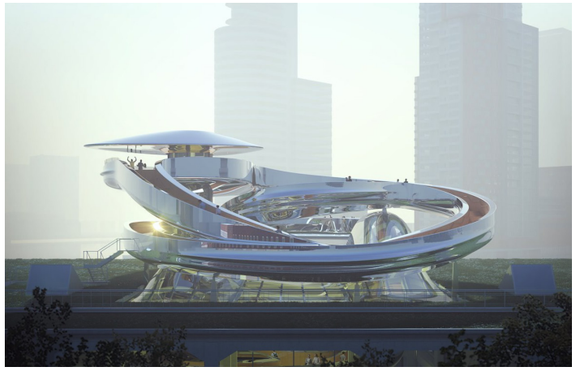

Figure 104. Fenix Rotterdam by Mad architects (Architectenweb.nl, 2024)

To analyze if a panel has to bend too far in order to fit onto the frame, the curvature radius of the tested panel is taken as a maximum allowable curvature. As concluded from the experiments and numerical modeling, the curvature radius can be calculated

$L = Side\ length\ of\ the\ square\ panel$

$D = diagonal = \sqrt{2} * L$

$B = corner\ deflection\ (in\ cm)$

$R = \frac{B}{D} = normalized\ deflection\ ratio$

$L = 80\ cm$

$D = \sqrt{2} * 80 = 113.14$

$B = 16{,}3\ cm$

$R = \frac{1.3}{113.14} = 0.144$

The k factor is 0.144 for the tested panel. This factor is taken to calculate the curvature radius.

First the surface was divided into into panels. Of these panels, the curvature radius is calculated by taking the end points of the shortest edge. The vector of the curve at these endpoints is rotated by 90 degrees. These vectors are used to start a line SDL. When these lines cross each other, a point is generated. Then, the line with the shortest distance to the end of the edge of the panel is taken. This distance is the curvature radius of the panel. Then the maximum allowed curvature radius is calculated with the following formula.

$$R = \frac{c}{8k} + \frac{kc}{2}$$

$k = deformation\ rate = 0.1441$

$c = chord\ length\ (panel\ diagonal\ or\ other\ span$

$R = radius\ of\ curvature$

An operator is implemented, where if the curve radius of the panel is higher than the maximu allowed curve radius, the panel is coloured red.

If the curve radius of the panel is lower than the maximum allowed curve radius, the panel is coloured blue.

This script works with just the curvature radius. This means that when panels scale larger, their curvature is sized linear. This means that larger panels can have thicker glass panes and can still ben bent to this degree.

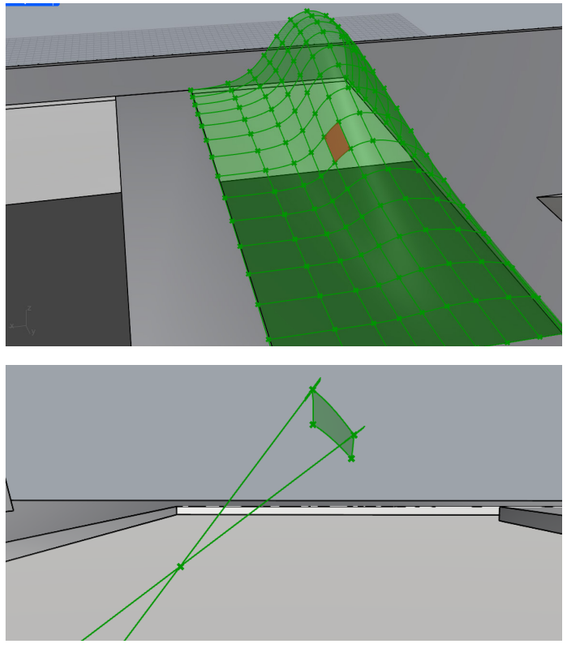

Figure 105. Curve radius of shortest edge of the panel.(Own work)

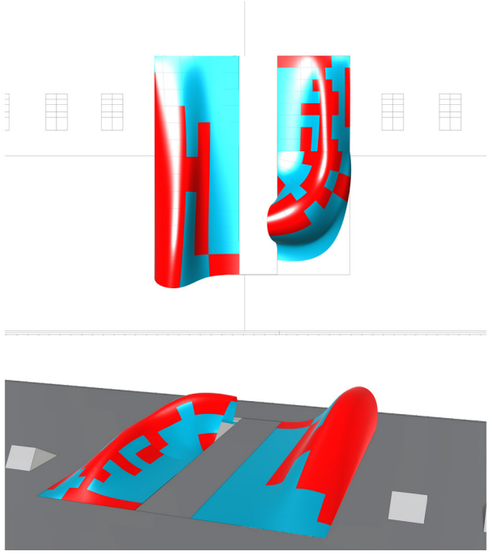

Figure 106. Few panels: thin tempered glass, maximum curvature k = 0.0642

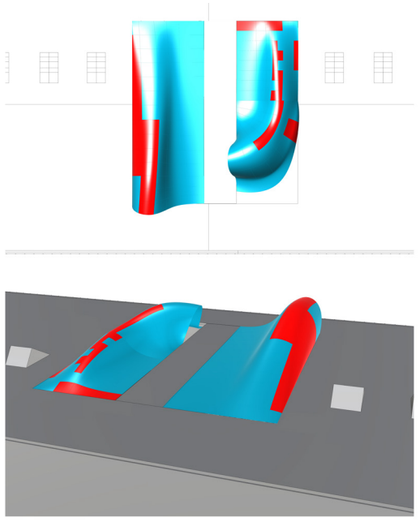

Figure 107. More panelized surface:: thin-tempered glass, maximum curvature k = 0.0642

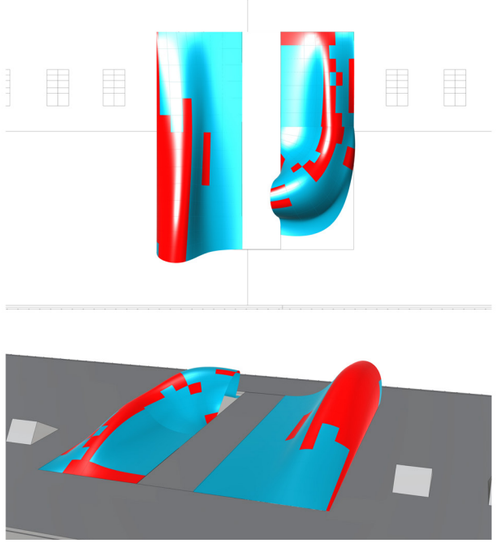

Figure 108. Few panels: thin chemically strengthened glass, maximum curvature k = 0.1441

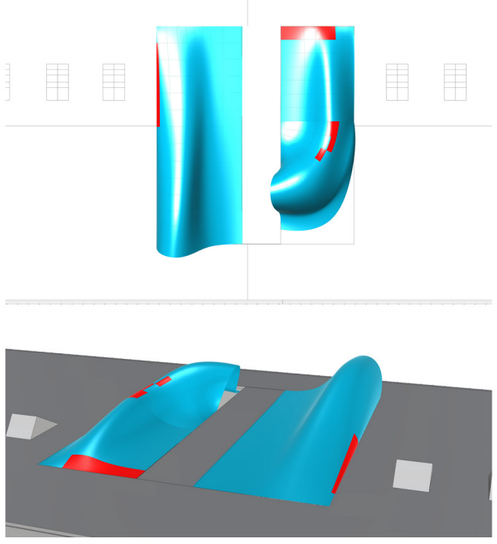

Figure 109. more panelized surface: thin chemically strengthened glass, maximum curvature k = 0.1441

9.2.1 Wind Loads

Wind loads are on of the most critical environmental forces that influence the structural design and performance of building façades. As buildings grow taller and more architecturally complex, the interaction between wind and the building envelope becomes increasingly significant. Wind exerts pressure and suction forces on the surfaces of a structure, and these loads must be accurately assessed and effectively managed to ensure the safety, durability and functionality of the façade system.

Façades serve as the primary interface between a building's interior and the external environment. They must resist wind-induced pressures while maintaining aesthetic appeal, thermal performance, and weather resistance. The impact of wind on a facade depends on several factors, including building height, shape, orientation, geographic location, and local wind climate. Additionally, the presence of nearby structures and topographical features can influence wind flow patterns and, consequently, the magnitude and distribution of wind loads.

NEN_19100-2 provides deflection limits for IGU's. Since this thin-glass IGU is continuously supported along all edges, a maximum deflection limit of L/50 is given. In the case of these 80cm by 80cm IGU that allows a maximum deflection of 1.6 centimetres at the centre of the panel.

The CEN/TS 19100-2 also provides a minimum nominal mechanical edge cover support depth "S" which in the case of IGU's should be at least 12 millimetres.

This support depth is modelled into the ansys IGU model. The maximum wind load of 2.07KPa is modelled as a pressure on the first pane of the IGU.

Table 9.1 — Typical deflection limits for glass components of deformation class 2 - SLS

	Support condition	Deflection limit of the support of the edges	Deflection limit at a free edge	Deflection limit at centre
IGU	Continuously supported along all edges	according to EN 13830:2015+A1:2020, 5.7		L/50[a]
	Continuously supported along 2 or 3 edges	according to EN 13830:2015+A1:2020, 5.7	L/150[c]	
	Point-fixed		L/150[c]	

[a] L is the length of the short edge.
[b] L is the distance between two point-fixings.
[c] L is the length of the unsupported edge.
[d] Either the deflection limit of l/100 at the edge or l/50 in the centre should be applied, not together. The decision whether to apply one or the other limit depends on the individual case.

Table 10. Typical deflection limits for glass components of deformation class to - SLS (serviceable limit state) (CEN/TS 19100-2, 2021)

(6) For deformation class 3 - ULS, the actual retained depth of the deformed glass pane inside the edge cover shall be verified accounting for the glass chord shortening due to its deflection and to the tolerances.

NOTE Recommended minimum nominal mechanical edge cover is given in Table 9.2 (NDP) unless the National Annex gives other values.

Table 9.2 (NDP) — Recommended minimum nominal mechanical edge cover s for glass components of deformation class 3-ULS[a]

Application	Further specification	Minimum nominal mechanical edge cover or edge support depth[b] s mm
Single glass component	Vertical	12
	Non-vertical	12
Floor		30
Balustrades	4 edges continuously supported	12
	1 edge continuously supported (clamped)	70
IGU	Vertical	12
	Non-vertical[c]	12

[a] This table is not exhaustive.
[b] See Figure 9.1.
[c] Accessible for maintenance only; otherwise see floors.

NOTE 2 The limit for the edge cover can depend on the application and on the expected service life of the glass component and sealants.

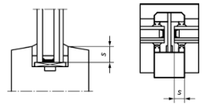

Key
1 pane

Table 11. Recommended minimum nominal mechanical edge cover S for glass components of deformation class 3-ULS (ultimate limit state) CEN/TS 19100-2 (2021).

During the construction of an IGU, two holes are drilled in the spacer. A tank filled with often argon gas is hooked into the spacer. The IGU is then filled up with argon, whereby the air escapes out of the second hole. The second hole is sealed, and often a small overpressure is pumped into the cavity.

This pressure varies because of temperature differences and atmospheric pressure. The gas expands with increased temperature, and contracts in colder situations. In the Netherlands, atmospheric pressure can be neglected.

In the Ansys model, a pressure of 1.03KPa is placed on the inner surfaces of the IGU, combined with a 1.0KPa pressure on the outer surfaces. The pressure inside the cavity will distribute a part the load on the first glass pane. Gas\s is compressible, but with the relatively small loads on the panel, the gas will not compress much, and distribute the load onto the second pane. To accurately mimic and predict this behaviour, fluid dynamic modelling can be used for modelling the pressurized cavity. This however is very complex to model and takes much computing power making out of scope for this research. It was chosen to work with a general rule of thumb, whereby 70% of the load is absorbed by the outer pane, and 30% is directed to the inner pane.

In table 13, wind pressure in the Netherlands is provided per region and by height. For this calculation, the maximum wind pressure is used: 2,07KPa. Although it must be stated that it is highly unlikely that a thin-glass building will be built in region 1 with a height of over 150 metres.

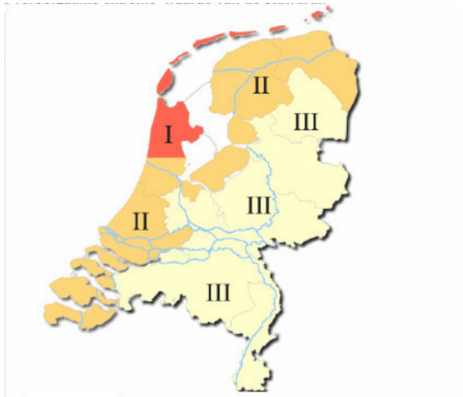

hoogte (m)	Windstuwdruk in kN/m²					
	gebied I		gebied II		gebied III	
	onbebouwd	bebouwd	onbebouwd	bebouwd	onbebouwd	bebouwd
≤ 2	0,64	0,64	0,54	0,54	0,46	0,46
3	0,70	0,64	0,54	0,54	0,46	0,46
4	0,78	0,64	0,62	0,54	0,49	0,46
5	0,84	0,64	0,68	0,54	0,55	0,46
6	0,90	0,64	0,73	0,54	0,59	0,46
7	0,95	0,64	0,78	0,54	0,63	0,46
8	0,99	0,64	0,81	0,54	0,67	0,46
9	1,02	0,64	0,85	0,54	0,70	0,46
10	1,06	0,70	0,88	0,59	0,73	0,50
11	1,09	0,76	0,91	0,64	0,76	0,54
12	1,12	0,81	0,94	0,68	0,78	0,58
13	1,14	0,86	0,96	0,72	0,80	0,61
14	1,17	0,90	0,99	0,76	0,82	0,64
15	1,19	0,94	1,01	0,79	0,84	0,67
16	1,21	0,98	1,03	0,82	0,86	0,70
17	1,23	1,02	1,05	0,85	0,88	0,72
18	1,25	1,05	1,07	0,88	0,90	0,75
19	1,27	1,08	1,09	0,90	0,91	0,77
20	1,29	1,11	1,10	0,93	0,93	0,79
25	1,37	1,23	1,18	1,03	1,00	0,88
30	1,43	1,34	1,24	1,12	1,06	0,95
35	1,49	1,43	1,30	1,20	1,11	1,02
40	1,54	1,50	1,35	1,26	1,15	1,07
45	1,58	1,57	1,39	1,32	1,19	1,12
50	1,62	1,62	1,43	1,37	1,23	1,16
55	1,66	1,66	1,46	1,42	1,26	1,20
60	1,69	1,69	1,50	1,46	1,29	1,24
65	1,73	1,73	1,53	1,50	1,32	1,27
70	1,76	1,76	1,56	1,54	1,34	1,31
75	1,78	1,78	1,58	1,57	1,37	1,33
80	1,81	1,81	1,61	1,60	1,39	1,36
85	1,83	1,83	1,63	1,63	1,41	1,39
90	1,86	1,86	1,65	1,65	1,43	1,41
95	1,88	1,88	1,68	1,68	1,45	1,44
100	1,90	1,90	1,70	1,70	1,47	1,46
110	1,94	1,94	1,74	1,74	1,51	1,50
120	1,98	1,98	1,77	1,77	1,54	1,54
130	2,01	2,01	1,80	1,80	1,57	1,57
140	2,04	2,04	1,83	1,83	1,60	1,60
150	2,07	2,07	1,86	1,86	1,62	1,62

Table 12. Wind pressure in the Netherlands sorted by region and building height (NEN 6703, 1990)

The wind load pressure is applied in 7 steps to ensure a stable model. Deflection and stress results can be observed in the figures and the table. The outer pane has a maximum deflection of 20,3 mm, and the inner pane has a maximum deflection of 3.8 mm. The eurocode limit of L/50 is 16mm in the case for this IGU. The deformation in the outer panel exceeds the limit of the eurocodes (16mm) by 4mm. This is not acceptable, but then, this is the wind load in zone 3 at 150 meters altitude, where wind loads are the highest. The deflection amount is related to the panel size and pane thickness. With larger panels, deflection will increase, so a maximum panel size or minimum thickness of a pane will have to be considered during the design stage of a project.

The stresses on the panel mostly concentrate around the edges, again showing the importance of edge finishing of these glass panes. The maximum princit- would be above the design stress for annealed and heat strengthened glass. However, 2KPa is the highest

step	time (s)	wind load	Wind load outer pane	Wind load inner pane	steps	Deflection outer pane	deflection inner pane	max principal stress (Pa
1	300	210	90	1	6,67E-03	1,75E-03	1,17E+07
				1,2	7,32E-03	1,90E-03	1,39E+07
				1,4	7,91E-03	2,04E-03	1,61E+07
				1,7	8,72E-03	2,22E-03	1,93E+07
2	600	420	180	2	9,46E-03	2,37E-03	2,23E+07
				2,2	9,93E-03	2,46E-03	2,43E+07
				2,4	1,04E-02	2,55E-03	2,64E+07
				2,7	1,10E-02	2,67E-03	2,92E+07
3	900	630	270	3	1,17E-02	2,79E-03	3,21E+07
				3,2	1,21E-02	2,86E-03	3,38E+07
				3,4	1,25E-02	2,92E-03	3,55E+07
				3,7	1,32E-02	3,02E-03	3,79E+07
4	1200	840	360	4	1,39E-02	3,11E-03	4,01E+07
				4,2	1,44E-02	3,17E-03	4,15E+07
				4,4	1,48E-02	3,22E-03	4,29E+07
				4,7	1,55E-02	3,30E-03	4,50E+07
5	1500	1050	450	5	1,62E-02	3,38E-03	4,72E+07
				5,2	1,68E-02	3,43E-03	4,90E+07
				5,4	1,74E-02	3,48E-03	5,09E+07
				5,7	1,82E-02	3,55E-03	5,37E+07
6	1800	1323	540	6	1,91E-02	3,62E-03	5,65E+07
				6,2	1,93E-02	3,66E-03	5,72E+07
				6,4	1,96E-02	3,69E-03	5,81E+07
				6,7	2,00E-02	3,75E-03	5,94E+07
7	2070	1449	621	7	2,03E-02	3,81E-03	6,07E+07
				7,2	2,03E-02	3,81E-03	6,06E+07
				7,4	2,03E-02	3,81E-03	6,06E+07
				7,7	2,03E-02	3,81E-03	6,06E+07
7	2070	1449	621	8	2,03E-02	3,81E-03	6,06E+07

Table 13. Deflection and stress results of flat panel (Own work)

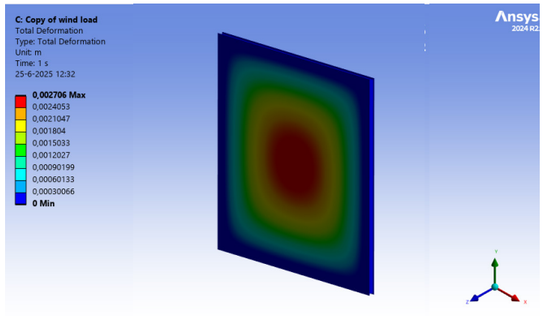

Figure 110. Maximum deflection of the entire panel (Own work)

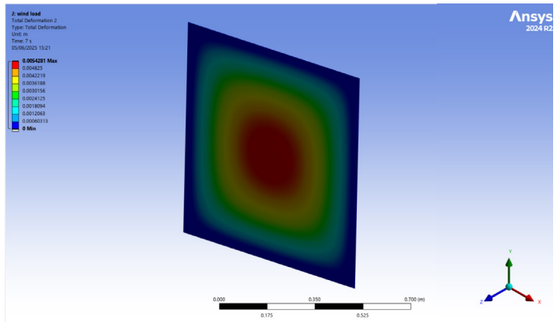

Figure 111. Maximum deflection of the inner pane of flat panel(Own work)

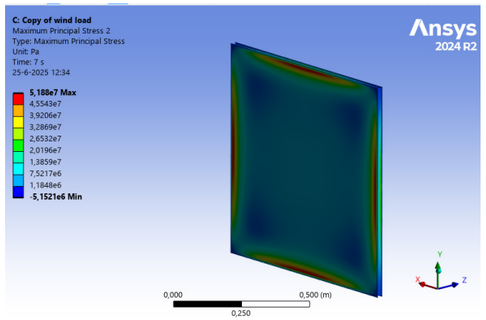

Figure 112. Maximum principal stress of flat panel (Own work)

possible wind pressure on 150metres and in zone one. Lower values for wind pressure are more realistic to include during the design phase. Still these values for maximum principle stress need to be considered in combination with the stress forming during the cold bending process itself.

Maximum deflection is reached at step 4.7. The corresponding wind load at step 4.7 is 1425. In the previously discussed table, it can be observed where this wind load takes place. It can be determined how high this glass can be used in each zone.

Zone 1
- Undeveloped area: 30 meters
- Developed area: 35 meters

Zone 2
- Undeveloped area: 50 meters high
- Developed area: 55 meters high

Zone 3
- Undeveloped area: 90 meters
- Developed area: 95 meters

This does limit the product to some amount. However, 50 meters is still a significant height. 95 meters alows for much flexibility and is a height not often reached in architecture in the netherlands.

For more resistance against wind, thicker glass panes will work, but will reduce the bending capacity. The single corner cold bent panel is also tested. The cold bending of the IGU creates more depth in the Z-direction. The panel should be able to withstand more wind loads as the force can be absorbed over more depth in the panel.

The single corner cold bent IGU shape is exported, and imported into the wind load model. The same properties and forces are given as to the flat panel.

The wind deflection is significantly less than simulated on the flat panel. The figures show that the panel gets divided along the clamped axis. The reduced effect from wind load is a promising result for this IGU as a viably product in the built environment. The deflection of the outer pane is 4 mm, which is wel below the 16 milimetres. from the eurocodes. The deflection of the innerpane gets reduced to 0.68 milimetres.

step time (s)	wind load	Wind load outer pane	Wind load inner pane	steps	Deflection outer pane	deflection inner pane	max principal stress (Pa)
0,2	0	0	0		8,75E-05	1,71E-05	8,99E+05
0,4					1,77E-04	3,44E-05	1,81E+06
0,6					2,69E-04	5,18E-05	2,74E+06
0,8					3,63E-04	6,94E-05	3,69E+06
1	300	210	90		4,59E-04	8,72E-05	4,65E+06
2	600	420	180		9,64E-04	1,74E-04	9,45E+06
3	900	630	270		1,53E-03	2,67E-04	1,47E+07
4	1200	840	360		2,13E-03	3,65E-04	2,01E+07
5	1500	1050	450		2,76E-03	4,69E-04	2,54E+07
6	1800	1323	540		3,61E-03	5,80E-04	3,31E+07
7	2100	1449	621		4,00E-03	6,79E-04	3,69E+07

Table 14. Deflection and stress results of corner bent IGU (Own work)

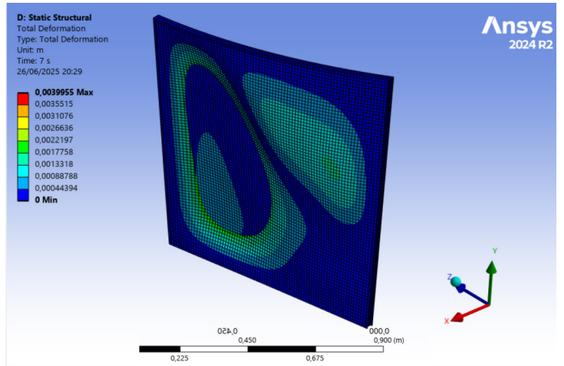

Figure 113. Total deformation of cold bent panel (Own work)

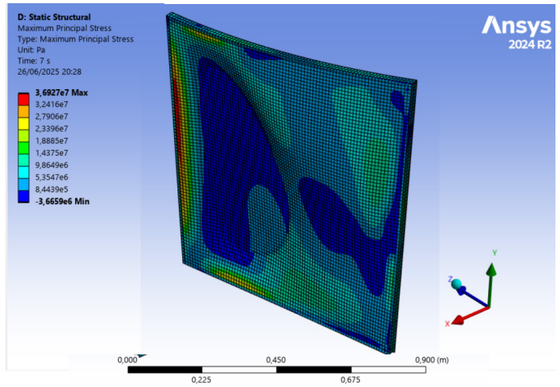

Figure 114. Maximum principal stress after wind loads (Own work)

9.2.2 Wind load deformation acceptance

In 2024, a study was conducted by (Hassen, M. Et. Al) on the user acceptability limits of glass deflection during a simulated wind load. This study was performed in order to explore the possibility of using thinner glass sheets which could increase carbon efficiëncy for façade panels. It was investigated if the current servicability limit for glazing (L/50) is too conservative. Three deflection situations where tested with a group of 38 people between the ages of 21 and 39. A double glazing unit with dimensions of 1467 by 972mm was inflated to simulate a wind load. Three deflections were tested.

- 10 mm (L/97) -> below serviceability limit
- 19 mm (L/50) -> **serviceability limit**
- 23 mm (~L/40)-> above serviceability limit.

The tests were performed both during day and night, with and without providing users background knowledge on glass safety and sustainability.

The panel was tested on movement, reflection, distortion and safety. The acceptance study on movement is relevant to this thin glass product. It was found that most participants noticed movement, whereby movement at night was perceived more than during the day. Simultaneously, acceptance of movement is higher during the day than during the night.

The designed flexible flat thin-glass IGU has a deformation at the centre of 20.3 millimetres. Which equals to L/39.4 and by the results of this research is acceptable during daytime, but is not acceptable during night time. The cold bent IGU has a centre deflection of 4.0 milimetres, which equals to L/200. As this value is far above the tested movements, this is likely acceptable during the day and night.

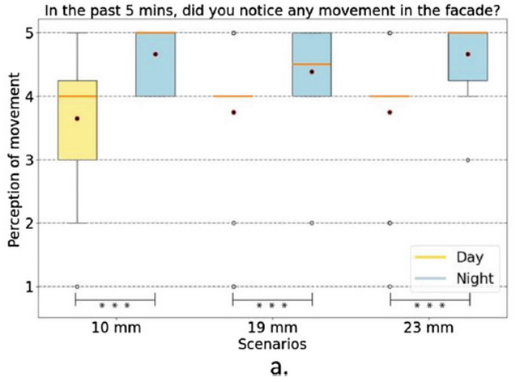

Figure 116. A Participant perception of movement from 5 (Strongly agree: Absolutely: there was a significant movement in the facade) to 1 (Strongly disagree: I didn't noticed anymovement of the façade), the "3" shows the neutral vote "I am unsure if there was any movement in the façade"

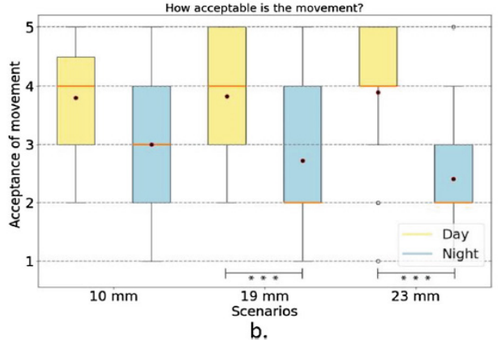

Figure 115. Participant acceptance of the movement:With a scale from 5 (Perfectly acceptable) to 1 (totally unacceptable), the "3" shows the neutral vote (Neither acceptable or not acceptable). The red dots shows the means while the orange lines the median. The levels of significance is shown as: "" p value < 0.05; "**" p value < 0.01; "***" p value < 0.001 (Hassen, M. Et al, 2024)*

9.3 Optical surface quality

As stated before, Datsiou. K (2014) has designed a flow chart for determining optical surface quality of monilithic glass panes during cold bending. For filling in this flowchart, specialized equipment is required, which unfortunately is of out scope for this research.

Therefore the optical quality of the surface of the glass during cold bending is tested with a visual reflection test using a zebra striped pattern.

A zebra pattern was printed on an A0 format (841X1159mm) this is the only printable size that is larger than the edges of the IGU. This is required because the reflection of the striped pattern has to cover the entire IGU. Using a striped pattern for optical quality is a common practice to test glass sheets coming out of the oven onto the rollers. One pane of the five thin glass IGU's has been painted black with a matte spray paint. The spray paint was chosen matte as it would not reflect itself, providing an honest reflection of just the thin glass. Ideally, the blackened pane is tested in both the convex and the concave side during cold bending. Unfortunately, only one IGU is made with a blackened pane. It is chosen to perform the optical test at the concave side of the pane during cold bending, as the buckling of the glass in its own plane could cause the biggest distortion during cold bending.

The black spray painted IGU was placed in the bending setup. The zebra pattern was placed both at the concave and convex side of the IGU. The entire bending process was recorded with camera's filming at 4k resolution. It proved to be a real challenge to construct an ideal setup, where the surface of the glass was completely covered by the zebra pattern. Lighting in the Stevin II lab was also not ideal. Therefore a construction lamp was used to illuminated the zebra pattern.

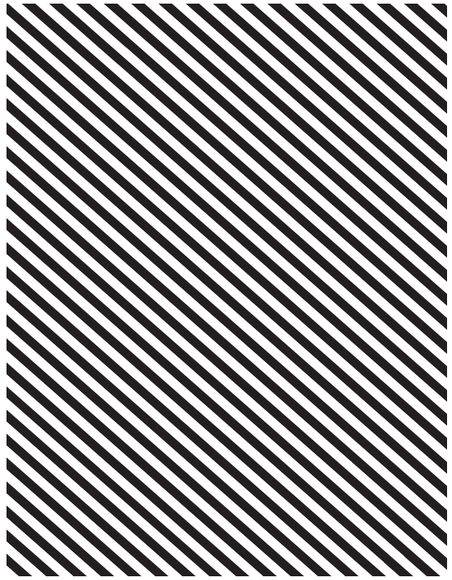

Figure 117. Zebra pattern used in optical quality tests (Own work)

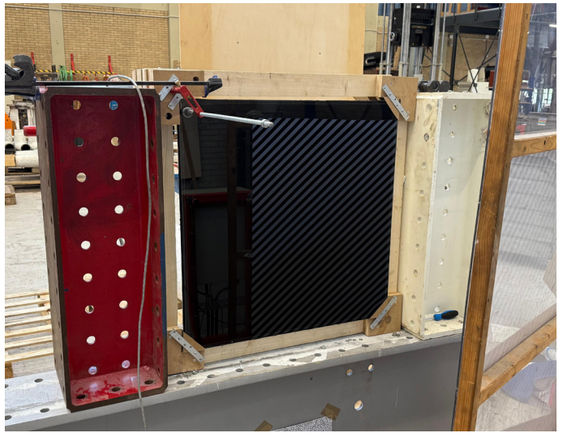

Figure 118. Zebra pattern used in optical quality tests (Own work)

Figure 119. Zebra pattern reflection before cold bending (Own work)

Figure 120. Zebra pattern after cold bending (Own work)

During the bending of the panel, it proved difficult to observe imperfections in the surface of the panel. The surface of the glass did not seem to show any large imperfections or ripples during far displacement. Small deviations from the straight lines can be observed near the edges of the panel.

The pictures above show the reflection of the zebra pattern during the cold bending. Both before and during/after the cold bending the lines on the zebra board do not show large surface ripples or distortions aside from the expected distortion as a result from the single corner cold bending. Where hot bending often leads to various ripples and imperfections on the surface of the glass, this is not observed during the cold bending of this thin glass. Therefore it performs excellently regarding optical quality.

Replacing hot bending with cold bending

Figure 121. Roof of Fenix Rotterdam made with hot bend panels (Picture taken by author, 2025)

Figure 122. VIsual study on the roof designed with cold bent panels, without hot bending distortion (Own work)

Replacing hot bending with cold bending

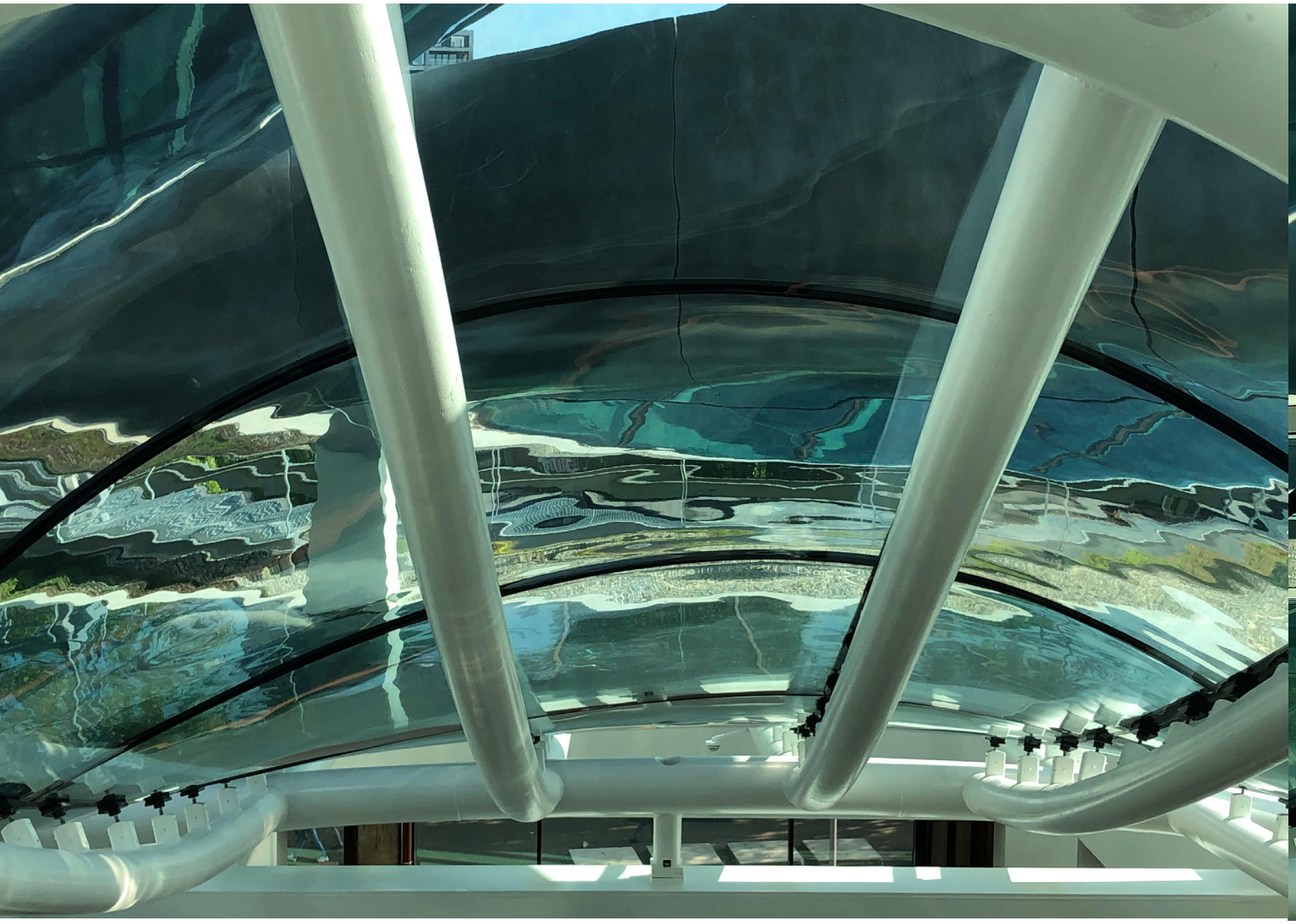

Figure 123. Roof of Fenix Rotterdam made with hot bend panels (Picture taken by author, 2025)

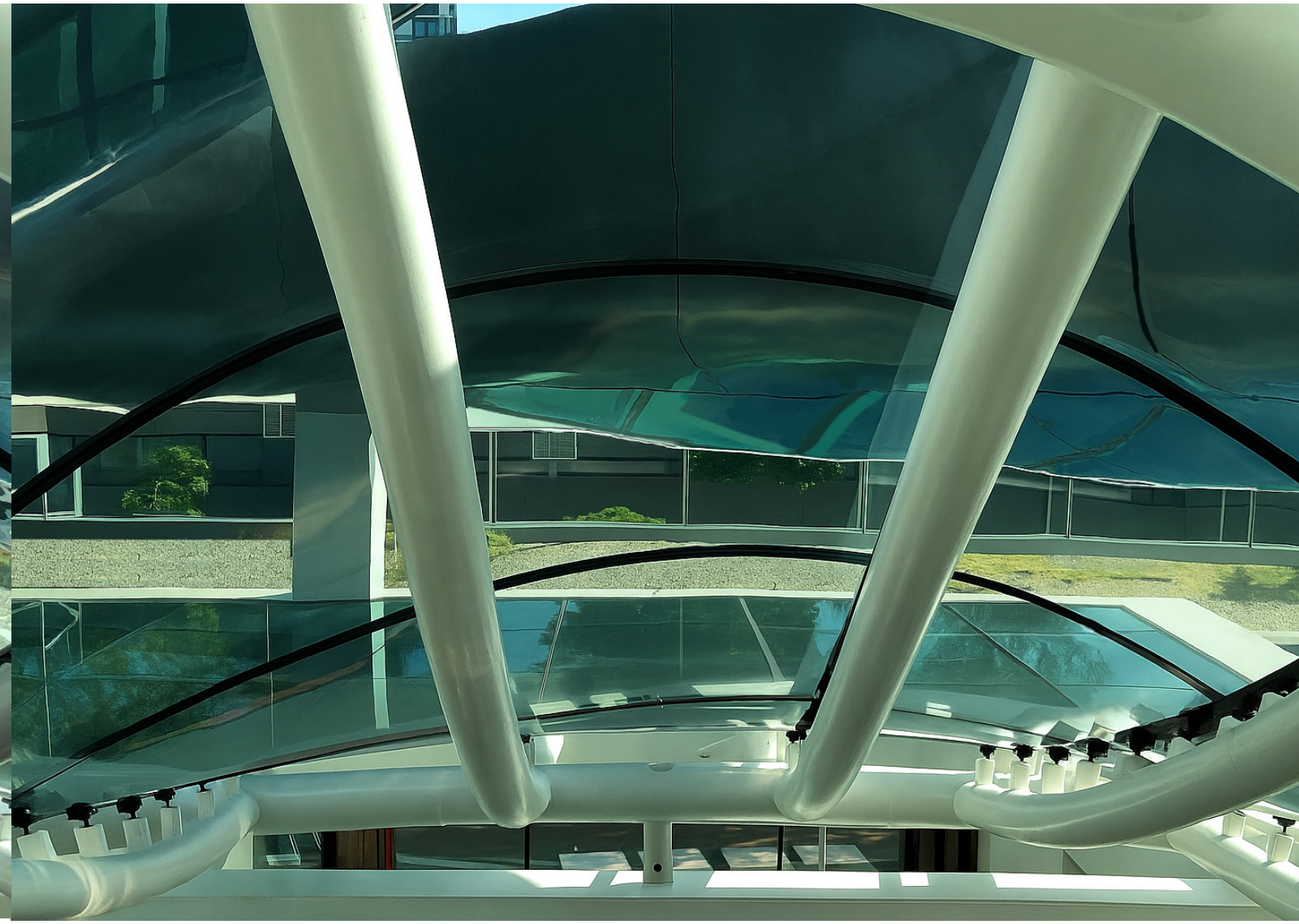

Figure 124. VIsual study on the roof designed with cold bent panels, without hot bending distortion (Own work)

9.4 IGU details

1. Tested and simulated IGU
The thin-glass IGU consists out of three components. The glass, the TriSeal spacer, and the Ködiglaze S sealant. The IGU tested in this thesis had a thickness of 20,2 millimetres and the glass had a thickness of 1,1 millimetres (Detail 1). The thickness' of these elements can be catered according to the size of the panels used in the façade. Different panel configurations are discussed below

2. Thin-spacer IGU
The thickness of the spacer has influence on the stiffness of the panel, and defines the shape the panel takes during cold bending. Implenting a thinner or thicker spacer can make the IGU more or less flexible. The 20.2 millimetres wide spacer used in these test IGU's is the widest spacer available from edgetech.

While the glass panes did not touch during the bending experiments, it was not measured how far they moved in (or out) of each other at the centre. The simulations also do not show the panes touching. Therefore it seems likely that using a thinner spacer would not result in contact between the two panes. Detail 2 shows a panel with a thinner spacer configuration

3. Triple glass IGU
For higher insulating values, a triple glass IGU could be constructed. Adding another pane of glass will have a significant influence on the stiffness of the panel and would therefore not be ideal for panels where a high curvature is required. It might be interesting to research an even thinner centerpane as it this panel does not serve any structural porpuse. Implementing a really thin centerpane could minimize the influence on the bending stiffness of the panel.

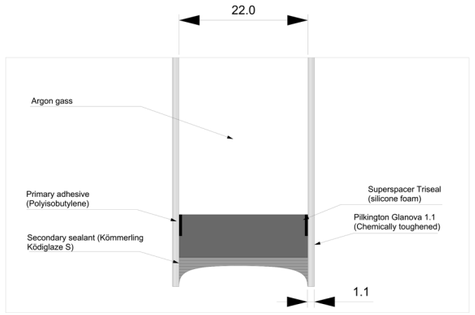

Figure 125. IGU configuration 1: Tested and simulated IGU

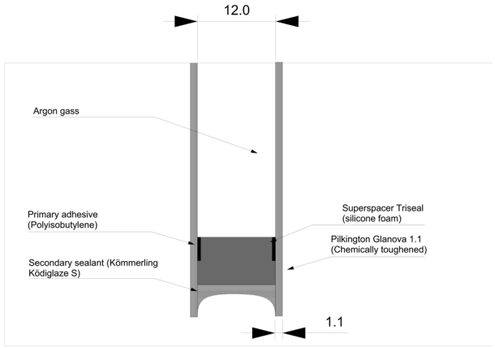

Figure 126. IGU configuration 2: Thin-spacer IGU

4 + 5. Laminated glass IGU
To increase safety, lamination of panels would make the glass panes stick to an adhesive after breakage. Lamination could be applied in both the inner and outer pane for optimal safety. Cold bending stresses rise nonlinearly with lamination. Panels with greater interlayer thickness show higher stress levels, indicating increased system stiffness due to the interlayer's rigidity(Zhang, X. 2021)

Furthermore, lamination could be the cause for multiple optical distortions

- 1. Lens Effect (Optical Distortion)
When two sheets of glass are laminated with a soft interlayer (like PVB), any non-uniform curvature or waviness creates a "lens" effect that distorts light. Cold bending induces uneven curvature, and the laminated layers don't always bend perfectly in sync, especially if spring-back or interlayer creep occurs. This could cause wavy reflections, ghosting, and blurred views in both transmission and reflection.

2. Iridescence and Color Fringe
iridiscence and colour fringe are Interference patterns (rainbow-like hues) caused by light interacting with thin layers or stress gradients.
Bending changes stress distribution across the panel, especially near edges, and the laminated construction can cause stress birefringence, producing iridescence in some lighting.

3. Intra-Ply Misalignment
During cold bending, if the layers shift slightly during lamination or spring-back differently, they may misalign microscopically. This results in edge distortion or "double vision" effects when viewed at an angle.

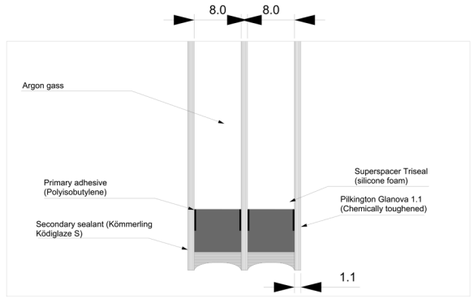

Figure 127. IGU configuration 3: Triple glass IGU

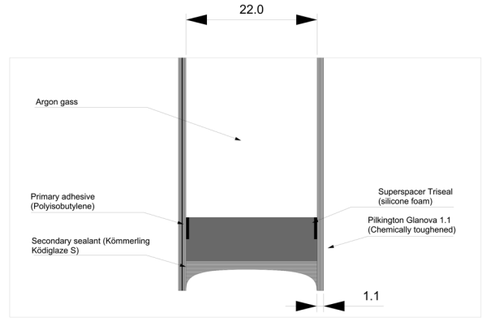

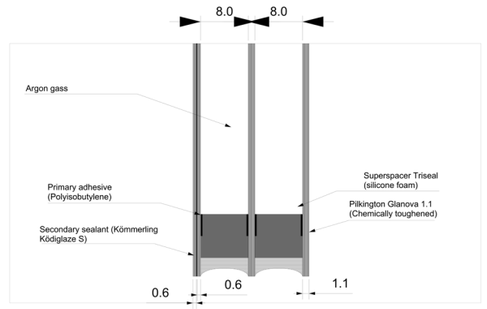

Figure 128. IGU configuration 4 + 5: double and triple laminated panes IGU

9.5 Panel installation

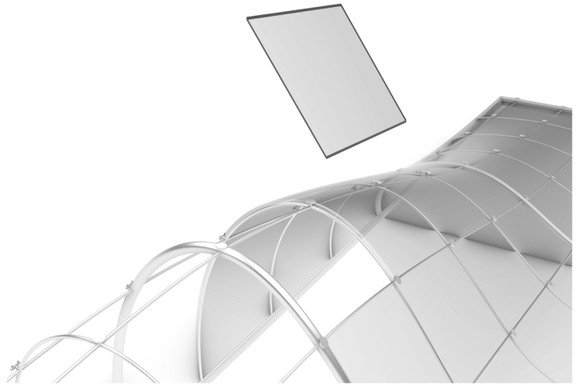

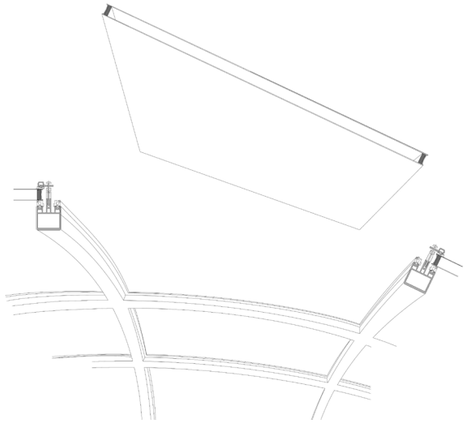

1. Flat IGU is brought onto site and lifted to position.

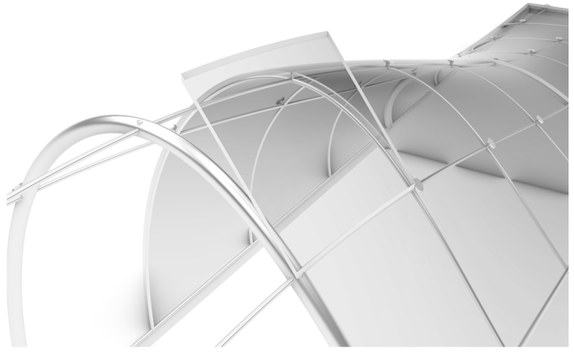

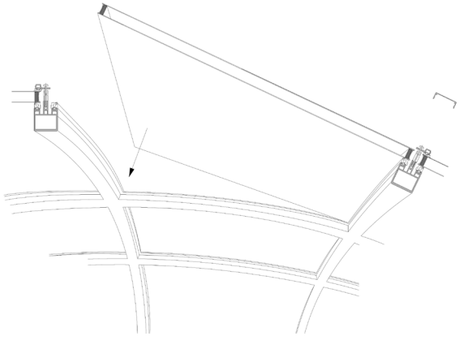

2. Connect first two corners along substructure and screw down the edges.

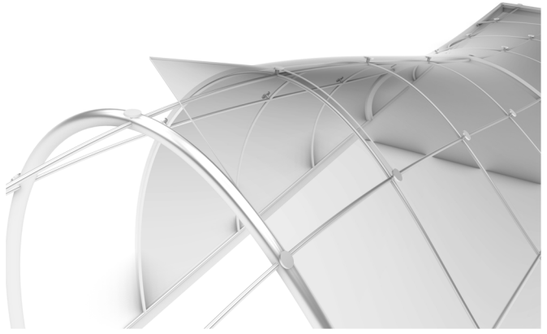

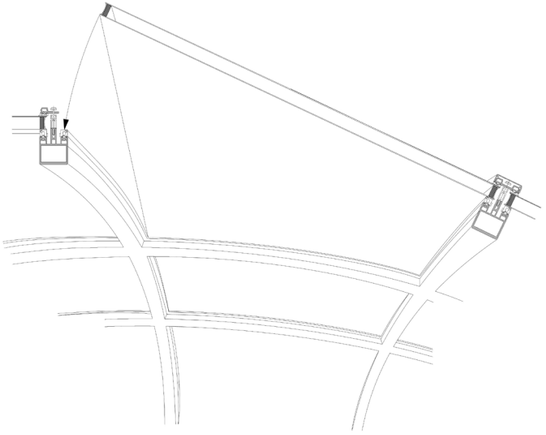

3. Press down second edge and third corner and screw down..

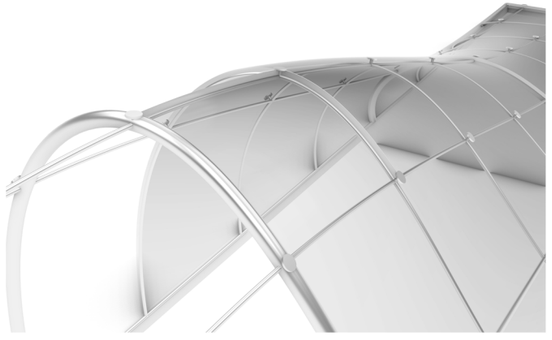

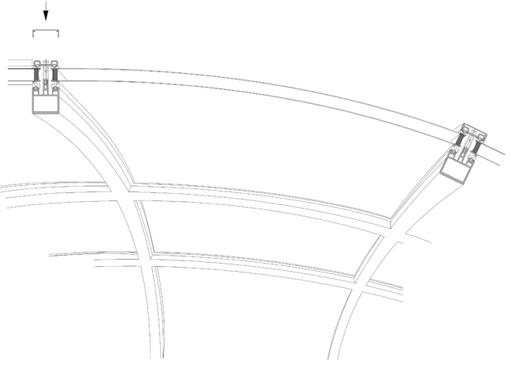

4. By pressing down the last corner, all the edges are bent into place. Screw down the last corner and cover the mechanism.

Figure 129. *Installation of flexible IGU panels (Own work)*

To cold bend the panels into the right shape on site, a cold bending mechanism has to be used. These systems consist out of a few pistons which are placed over the surface of the glass. The pistons can be pushed forwards essentially pushing the glass out of plane and thereby creating the desired shape of the panel. Since the thin-glass IGU's are flexible, relatively speaking, not much force has to be used to press the IGU into its desired shape.

Since the glass always wants to spring back to its original flat state, the glass has to be assembled to the substructure before releasing the cold bending mechanism from the panel. The IGU can be screwed onto the substructure. Then a cover cap can be clicked onto the profiles sealing of the exterior.

Alterntavely, it can be researched if the façade panels can be sealed onto the substructure for a cleaner detail. Though it needs to be researched if there are sealants which can withstand the high forces from the panel wanting to spring back to its original flat shape.

Figure 130. *Cold bending mechanical system (Octatube, 2021)*

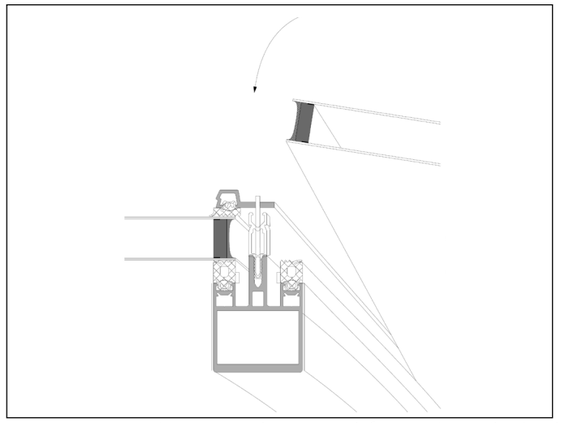

1. IGU corner is pressed onto subframe into desired position.

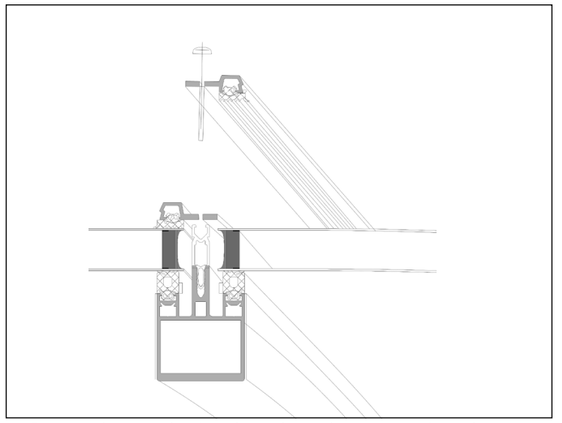

1. Press down glazing beads to keep IGU into bent position.

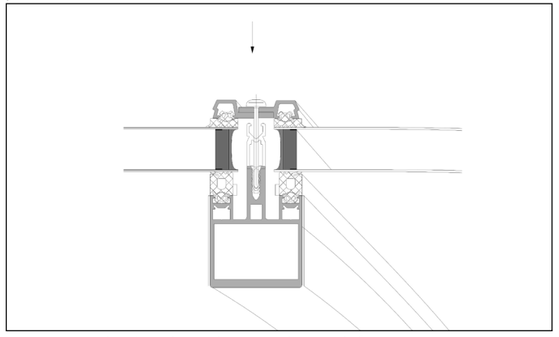

3 Screw glazing bead onto the subframe.

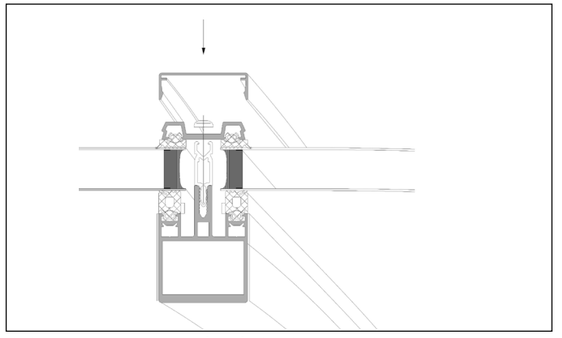

4. Install cover cap for finishing details.

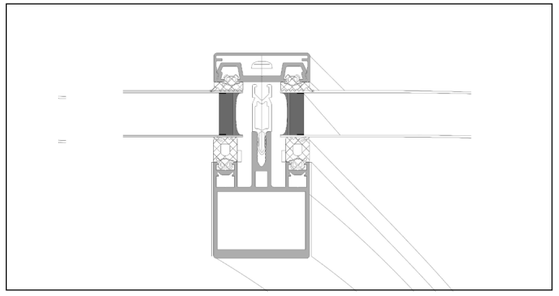

5. Finished Curved façade product, can be sealed off to make weather proof.

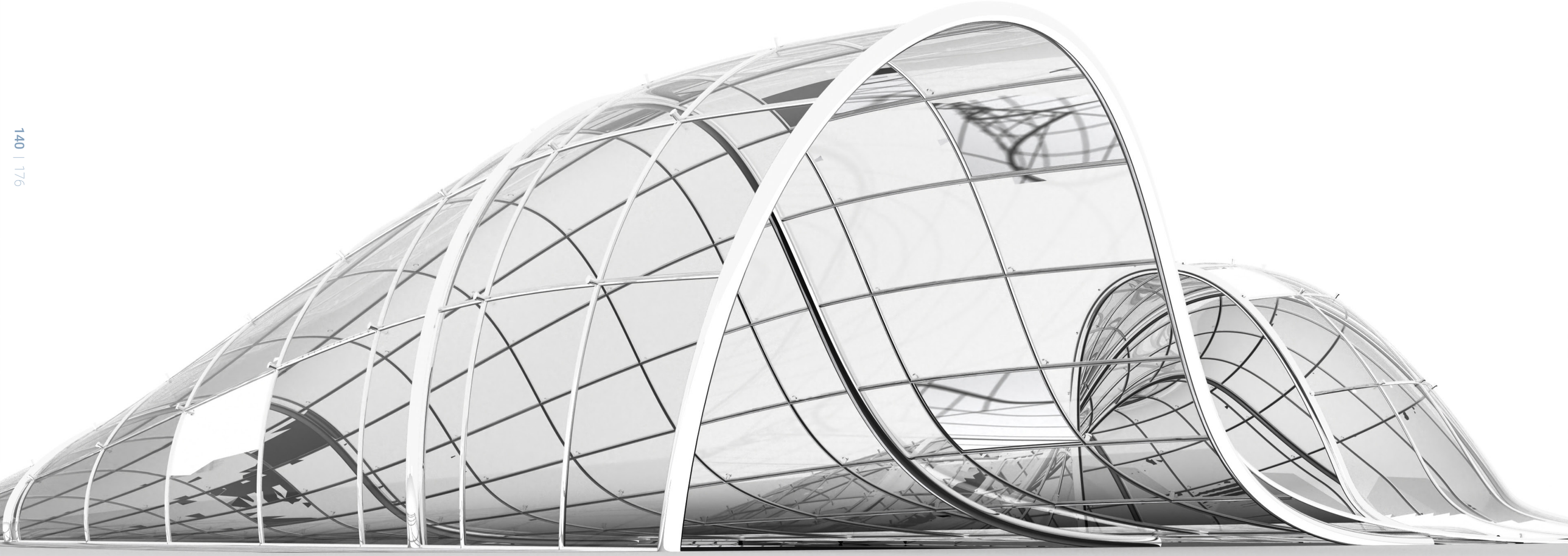

09

Conclusion

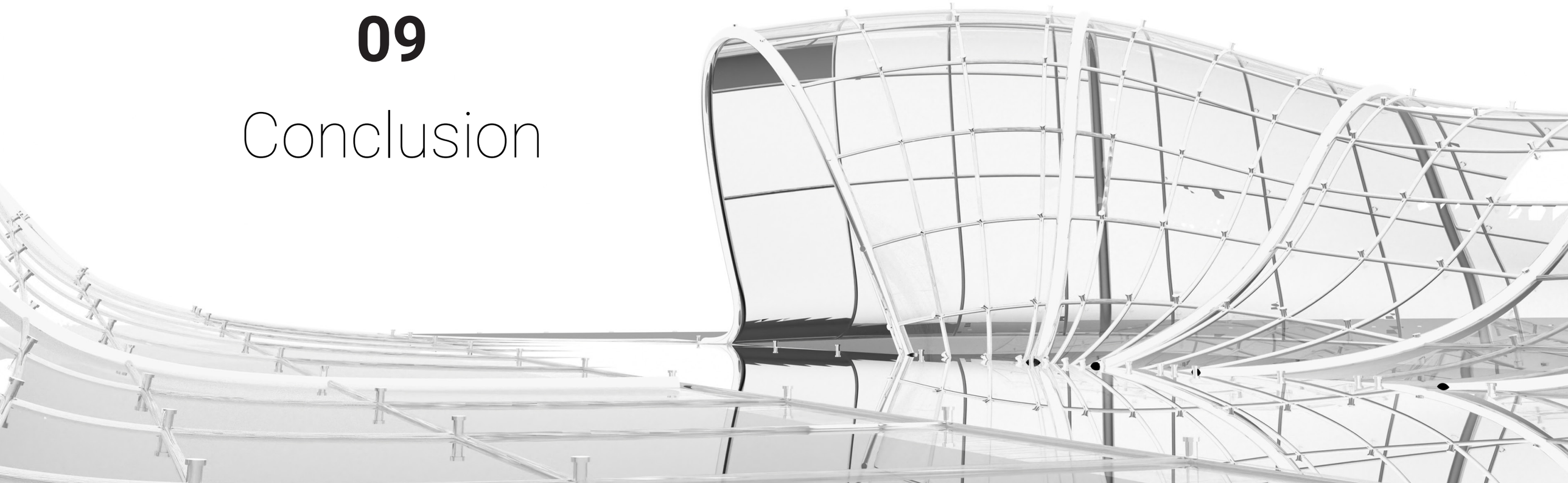

Conclusion

This master thesis is the final chapter of the master track "building technology" at the Delft University of Technology. This thesis explored the realm of both thin-glass and cold bending and conducted research through the steps as explained in the research methodology.

The following research question are answered in the next paragraphs by answering the sub questions first, which will result in the answer for the main research question.

Can a higher degree of curvature be achieved in cold bent insulated glass units by applying thin glass?

1. What dictates the maximum bending capacity of a cold bent glass panel

During the cold bending process, the maximum bending capacity is both dependant on the glass and the frame it is implemented in. In most cold bending applications, the glass is the first element of the panel that breaks. Glass thus dictates how far a panel can be cold bent, Since after breaking of the glass, the panel has exceeded its usable limit state.

In the realm of unitised façade panels, other difficulties arise during high curvature cold bending. Unitised glass panes will at a certain point (depending on many panel variables) fail to connect to each other and form a sealed bond. Solving these issues requires more research as its own project, and therefore this master thesis solely focusses on creating a flexible insulated glazing unit.

2. How can an IGU be designed to accommodate bending behaviour of thin glass?

As can be concluded from previous research, the way glass bends into shape during cold bending is highly dependant on the composition of the entire product. Single glass panes are able to cold bent without other limitations than the glass pane itself. It is concluded by Zhang, x. Et al (2021) that lamination has little effect to the cold bending capabilities of glass panes.

Further research conducted by Galuppi (2014) concluded that cold bending a monolithic glass pane into a hypar shape proved to by only possible at low displacement before the edges of the glass start buckling behaviour, and a shape more resembling of a single curved shape is achieved. The recommendation was made to enhance stiffness of the edges of the glass panes.

Young (2019) built further on this research and added GFRP profiles to a single glass pane and tried cold bending it into an anticlastic shape. van Driel (2021) added a second glass pane to the construction, thus creating an insulated glass unit. This IGU was tried to cold bent into anticlastic shape, and it was concluded that it was difficult or impossible to get close to a hypar.

The conclusions of this previous research proved that trying to cold bent glass into a hypar shape shows little promise for glass applications. Therefore, the anticlastic shape was discarded, and focus was put on free form glass curvatures, whereby the spacer does not necessarily require to stiffen the edges of the glass panes.

Research was conducted in finding the best fit for constructing a flexible insulated glazing unit. The conclusion of the research found that for flexible cold bending:

- Thinner glass sheets are a requirement to increase the maximum curvature allowed during the cold bending process.

- A warm edge spacer is flexible at room temperature and thus accommodates to the shape of the panel during cold bending. Warm edge spacers often include a primary adhesive in the product, making the requirement for another primary adhesive obsolete.

- To achieve maximum flexibility, a secondary sealant with highly flexible capabilities after hardening has to be applied

The required three main components were selected by reaching out suppliers and discussing what is available and achievable for this master thesis' research. The following materials were chosen

- 10 1.1mm Glanova Thin glass sheets - After consolidation with NSG/Pilkington.

- 99 metres of the Triseal spacer from Edgetech with dimensions of 20.2 by 7.3 millimetres. Included is a Polyisobutylene primary adhesive - after consolidation with Edgetech/superspacer.

- Kömmerling Ködiglaze S as a secondary sealant. Chosen because of its, and its required tools for application's availability at the faculty. It must be noted that while Ködiglaze S is not specifically made for cold bending, its material properties and its influence on the design allowed for this choice.

3. How can a setup be constructed for cold bending a thin glass IGU, and how can strain/stress data be accurately measured during the bending process?

A cold bending setup is constructed by creating a wooden frame with three clamped corners, and one deformation corner. The clamps are made by making one fixed supported side, and one "clampable" side. The clampable side is made out of a thin steel plate that can be tightened by screwing down two screws. Between the glass and the steel plate, a foam cushion is added to distribute large stress concentrations.

The deformation corner is constructed out of a screw-down bench clamp with an extended screw wire. The tip of this screw-wire has a ball-joint connection to a circular surface. This causes the pressure area to be aligned with the surface of the glass during the entire cold bending process, therefore minimizing high stress concentrations.

Strain gauges are applied to the surface of the panel where high strain level were expected to occur, to minimize noise and other external elements of influence.

A displacement gauge was positioned at the backside of the panel to accurately measure deformation at a fixed location, therefore offering comparable results between both multiple tests and the numerical model.

4. How accurate can a finite elements model be made to simulate cold bending of a thin glass IGU?

A finite elements model was constructed in Ansys FEM software. The boundary conditions of the model were influenced by the design of the test setup. Results of early iterations of the model simultaneously influenced further optimization in design of the test setup.

Modelling accurate behaviour of all the used materials required extensive research in the mechanical properties of said materials. Namely the mechanical properties of the spacer proved to be hard to determine, and was therefore tested in both a uni-axial tensile test, and a double lap shear test experiment. Data gathered from these tests was used as input for calibrating a hyper elastic model that could accurately describe the behaviour of the spacer during cold bending.

Accuracy of modelling the boundary conditions was largely dependant on the behaviour of the cushion foam. Material properties had to be estimated and "trial and error" fitted during this research. For further accuracy, a material with wider known material properties is advised to use.

It was found that a model can be simulated near decent accuracy. General behaviour of the strain probes from the model correspond with measurement of the strain gauges from the test setup. Exact values can differ for a number of reasons. Further improvement of the model could increase accuracy.

5. How does a thin glass IGU perform under a single corner deflection?

Three single corner cold bending tests have been performed on three separate thin-glass IGU's. All three of these panels were monitored with strain gauges, the first two with three strain gauges, and the third with one strain gauge. The last two tested panels performed very good whereby the panels could at least be bent until a corner displacement of 16,3 millimetres. Providing a deformation rate of at least d=0.20375. In every test, the back panel broke first, after which the test was finished. This is a large improvement from regular "thick" glass panels. Where these panels are expected

6. How does extreme cold bending affects the optical reflective quality of thin glass

Hot bending glass increases the chance for distortions on the surface to occur. The reflection experiment has shown that cold bending chemically strengthened thin glass panels does not cause extreme surface distortions. Distortions occurring onto the surface arise from the cold bending geometry itself, which warps the reflection, which is expected. Opposite to hot bent façades, cold bending could create beautiful glass façades without surface ripples or large distortions.

Can a higher degree of curvature be achieved in cold bent insulated glass units by applying thin glass?

Yes, using thinner panels achieves higher curvature for insulated glass units. The tests compared to numerical data prove that the thin-glass IGU bends:

- 5,25 times further than an annealed glass IGU with the same components
- 2,76 times further than heat strengthened glass IGU with the same components
- 2,2 times further than fully tempered glass IGU with the same components

Using thinner panels is currently avoided for either safety reasons, users preference and industrial availability. The chemical strengthening process hugely enhances the structural properties of the glass panes and therefore increases safety of the IGU's. For a viable product, lamination will have to be implemented to prohibit the glass from breaking into dangerous shards. Research about lamination impact and performance on highly curved cold bent panels should be researched further. In terms of wind loads and user acceptance, the tested panel performs fine for eurocode norms. For larger sized panels, glass pane thickness would have to grow accordingly to prohibit toolarge wind load related deflections.

Further research

While this thesis has demonstrated the feasibility and improved performance of cold bent insulated glass units (IGUs) using thin glass, several avenues remain open for future research. One critical area is the role of lamination in extreme cold bending conditions. Although lamination significantly enhances post-fracture safety and is common in architectural applications, its mechanical behavior under high deformations, especially in thin glass configurations, has not yet been thoroughly explored. Investigating how various interlayer materials affect flexibility, stress distribution, and long-term durability during severe cold bending would be valuable.

Another essential area for further investigation is the long-term behavior of adhesives and sealants used in the IGU assembly. Cold bending introduces sustained stresses in these materials, particularly at high curvatures. Research into how these sealants perform over time—including their resistance to creep, fatigue, environmental degradation, and potential delamination—would be crucial for real-world applications.

Finally, further research is recommended into the effect of panel shape and curvature geometry. This thesis focused primarily on single-corner cold bending, but different geometries—such as monoclastic shapes. Single corner cold bending with thin glass proved to produce an anticlastic shape at low deformations, and a synclastic shapes at higher deformations. The behaviour of anticlastic shapes has already been researched and seems currently not a viable option. Monoclastic shapes—could behave very differently under stress. Exploring how these shapes influence stress distribution, buckling behavior, and optical quality could broaden the application range of thin-glass IGUs in complex architectural façades.

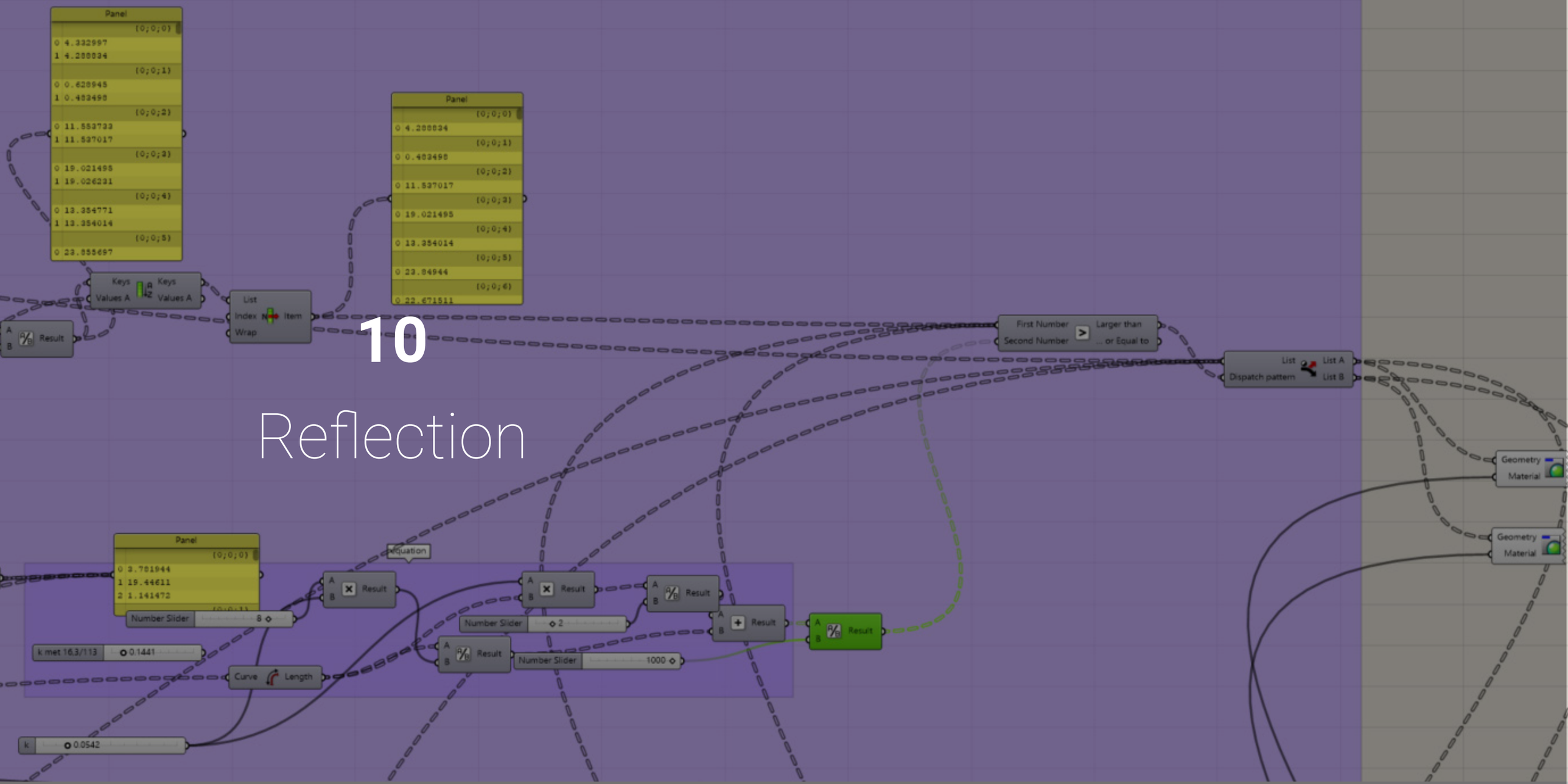
Panel
{0;0;0}
0 4.332997
1 4.288034
{0;0;1}
0 0.628945
1 0.483498
{0;0;2}
0 11.553733
1 11.537017
{0;0;3}
0 19.021495
1 19.026231
{0;0;4}
0 13.354771
1 13.354014
{0;0;5}
0 23.855697
Keys
Values A
Keys
Values A
List
Index
Item
Wrap
A
B
Result
Panel
{0;0;0}
0 4.288034
{0;0;1}
0 0.483498
{0;0;2}
0 11.537017
{0;0;3}
0 19.021495
{0;0;4}
0 13.354014
{0;0;5}
0 23.84944
{0;0;6}
0 22.671511
10
Reflection
First Number
Second Number
Larger than
... or Equal to
List
Dispatch pattern
List A
List B
Geometry
Material
Geometry
Material
Panel
{0;0;0}
0 3.781944
1 19.44611
2 1.141472
Equation
Number Slider
8
Result
Result
Number Slider
2
Result
Result
Number Slider
1000
Result
Result
k met 16.3/113
0.1441
Curve
Length
k
0.0542

1. What is the relation between your graduation project topic, your master track (A, U, BT, LA, MBE), and your master programme (MSc AUBS)?

Building technology to me is about bridging the perspective from the engineering mindset to the architectural mindset. In building technology i always tried to get a better understanding of all aspects of buildings, which can get very complex in all sorts of aspects. Myself I have taken an interest to the structural/facade design part during this master. Therefore i wanted to graduate in a subject that encompasses both subjects. Because by increasing my knowledge about structural engineering and applying this on a facade level, I can make better decisions during the design stage.

Still, when I thought of a project, I wanted to choose a subject that originated from the demands of an architect or designer. In this case that is more freedom in designing free-form glass façades, while simultaneously reducing the carbon footprint of the building.

2. How did your research influence your design?

During the research phase I found out about how cold bending is done currently. This includes how the materials of the facade panel or IGU affect the bending behaviour of the glass pane itself. Some research has been conducted on the cold bending of glass, and especially of cold bending glass in a hypar shape. A lot of valuable information was gathered to create a design that could increase the curvature of an insulated glazing unit. These are the reasons of for example the way of cold bending that has been chosen (single corner) and the type of spacer and sealant. Furthermore the design of the clamps were largely influenced by the preliminary numerical model.

3. How do you assess the value of your way of working (your approach, your used methods, used methodology)?

I think that the approach and methodology is valuable for this research. The choice was made to focus on both numerical research and physical testing.

The beginning of this research mostly consisted out of reading literature. This was an absolute requirement, because while we do learn about structural mechanics, and glass in particular, niche subjects like cold bending are uncharted territory. It was necessary to get a good understanding of the mechanical properties off glass, IGU's and behaviour of cold bending for this research. Other preliminary research includes getting hands on with finite elements modelling, which added another challenge for me as this software is untouched during previous education.

Numerical research required a lot of knowledge on materials, behaviour and some structural mechanics. This required and used a lot of theoretical knowledge i acquired during the bachelor and particularly the master. I learned many things from numerically modelling this particular setup. Making a numerical model is obviously very useful for accurate and extensive calculations.

The physical testing added another dimension to this research. Numerical research can only get you so far in trying to design and develop a new product (the flexible IGU). Physical testing was an absolute requirement for this research and it brought the numerical modelling to life. It is also very important, because some aspects can not be foreseen in numerical models, and have to be observed during real tests.

In conclusion, I think that these three methods combined offer a very complete research methodology which I hope will help me to become a better and complete future engineer.

4. How do you assess the academic and societal value, scope and implication of your graduation project, including ethical aspects?

• This research was focused on essentially cutting out an extra step out of the production of complex curved glass façades. Therefore

• reducing CO2 footprint by eliminating a secondary heating process.

• Reducing CO2 footprint by eliminating the required unique molds for unique hot bent glass panes.

• Increasing freedom for architects during the design stage.

• Decreasing construction time by eliminating an extra step during the production process.

Hopefully increasing re-usability of curved glass façades by designing a product that bends back to its original state after demontation. Further research will have to prove the serviceable time for these IGU's.

Trying to reduce CO2 footprint and construction time was the core drive behind the idea for a flexible IGU, and therefore i think it contributes on a societal level. In the case of ethical aspects. The safety of this product prototype is not assessed in this research further than the glass breaking. Therefore, should this product be used in future research or development, careful evaluation, and extensive testing is required.

5. How do you assess the value of the transferability of your project results?

This research conducted about this very specific thin-glass IGU. The research shows somewhat promising results, but for actual implementation of this prototype as a mock up, much more research has to be conducted. The transferability of the results are very specific about this IGU constructed out of these specific materials in use of this specific situation. The maximum bending values derived from the numerical model and the experiments are transferable for further research but have to be improved and expanded upon. Although multiple fabricants of materials have supported this research by supplying their products, there was no conflict of interest during this research.

6. How did unexpected events during the process of this thesis influence the methodology?

During this thesis I made my research dependant on a lot of factors for example: deliveries of products, availability of testing equipment an availability of computing power. These factors contributed to a lot of uncertainty, which made it hard for me to pin down a strategy that i could follow. The uncertainty if glass could be delivered on time, or even at all made me have to find a way to work with the possibility of testing without glass. This was decided to work around by designing, modelling and testing a plexiglass prototype. In hindsight this has been very helpful for this research, since plexiglass is much less brittle than glass. This way, the panel could be constructed and tested without

it breaking easily. This contributed to more physical tests being performed, which leads to more accurate, or at least more verifiable results. Still there are significant differences between glass and plexiglass which made it hard to gain accurate results from the numerical model, and physical tests.

The testing of the panels using strain gauges also caused for some delay in the process. It took me a long time to establish a connection to civil engineering where i could test with strain gauges. Another event caused for a two week delay during a critical time of my thesis. Should this not have happened, i would have had more time to create more accurate results in the numerical model. This learned me to take action much quicker regarding processes I do not have full control off.

6. Did you encompass both the structural design and façade product design graduation topics enough during this thesis.

I think both topics were of great influence during this research. The façade product design topic can be found in the selection of materials used for this insulated glazing unit. But also very practical knowledge that was obtained during for example the bucky-lab course was used in the design and construction for the cold bending rig.

Structural design relates more to material design in this case, calculating strain, stresses and material properties. Mostly this last subject, material properties, became very dominant during the numerical modelling phase. I had not foreseen that making an accurate numerical model relates this closely to accurately calculating the values for input parameters for these materials. Hyper-elastic modelling is something i had not heard of until this thesis, and i want to say even though i put a tremendous amount of time in this subject, i probably did not even scratch the surface. I underestimated the complexity of finite element modelling with this many materials and contact points.

I also included façade product design after the research on the panel itself was conducted. I made a possible construction manual detailing the connections between the IGU and the substructure. More time could have been helpful to further explore possibilities in construction details.

To conclude, while i do think my graduation project touched on both façade product design and structural design, although it leaned heavily to structural design.

References

Abbot, M., & Madocks, J. (2001). Roller wave distortion, causes and a novel approach to accurate, on-line measurement. Glass Processing Days Conference.

AGC. (n.d.). Flat glass manufacturing process. https://agc-electronics.com/en/specialty-glass/blog/detail/how-is-glass-made

Apple. (n.d.). Fifth Avenue - Apple Store - Apple. https://www.apple.com/retail/fifthavenue/

Arup, & Saint Gobain. (2022). Carbon footprint of façades: significance of glass. Findings from the life cycle assessment of 16 façade typologies & 18,000 design simulations. https://www.arup.com/perspectives/publications/research/section/carbon-footprint-of-facades-significance-of-glass

ASTM International. (2023). ASTM E1300-23: Standard practice for determining load resistance of glass in buildings. West Conshohocken, PA: ASTM International. https://www.astm.org/e1300

Baadmin. (2022, February 3). Laminated Glass vs Toughened Glass; what are the benefits of using Laminated Glass? - BA Systems. https://www.basystems.co.uk/blog/comparing-laminated-and-toughened-glass/

Beer, B. (2019). Options for Complex Geometry Façades – Single Corner vs. Free Form Cold-Bending. Glass Performance Days Proceedings.

Belis, J., Inghelbrecht, B., Van Impe, R., & Callewaert, D. (2007). Cold bending of laminated glass panels. Heron, 52(1–2), 123–146.

Bensend, A. (2018). The effects of cold warping on glass stiffness. Challenging Glass 6: Conference on Architectural and Structural Applications of Glass, May, 85–96. https://doi.org/10.7480/cgc.6.2119

Buddenber, S., et al. (2016). Climate loads in insulating glass units: comparison of theory and experimental results. Glass Structural Engineering, 1, 301–313. https://doi.org/10.1007/s40940-016-0028-z

Cornachio, J. (2021, May 27). Mind-Benders: 5 Unbelievable Curved Glass Façades. Journal. https://architizer.com/blog/inspiration/collections/curved-glass-facades/

Datsiou, K. C., & Overend, M. (2016). The mechanical response of cold bent monolithic glass plates during the bending process. Engineering Structures, 117, 575–590. https://doi.org/10.1016/j.engstruct.2016.03.019

Datsiou, K. G., & Overend, M. (2014, October). Behaviour of cold bent glass plates during the shaping process. In Engineered Transparency Conference (pp. 125–133).

Dow. (2022). Behavioral Data Sheet: DOWSILTM 795 Structural Glazing Sealant. The Dow Chemical Company.

Eclat Digital. (n.d.). Simulating tempering distortions. https://eclat-digital.com/simulating-tempering-distortions/

Emporia Shopping Mall. (2023, November 9). Fireshield Coatings. https://fireshieldcoatings.com/projects/emporia-shopping-mall/

European Committee for Standardization. (2019). EN 16612:2019 – Glass in building – Determination of the lateral load resistance of glass panes by calculation. Brussels, Belgium: CEN.

European Committee for Standardization. (2021). CEN/TS 19100-1:2021 – Design of glass structures – Part 1: Basis of design and materials. Brussels, Belgium: CEN.

European Committee for Standardization. (2021). CEN/TS 19100-2:2021 – Design of glass structures – Part 2: Design and verification. Brussels, Belgium: CEN.

European Committee for Standardization. (2021). CEN/TS 19100-3:2021 – Design of glass structures – Part 3: Assessment and evaluation. Brussels, Belgium: CEN.

Fedoseeva, Y. (2017). Cold bent GFRP-glass panels. University of Cambridge.

Fifth Avenue - Apple Store - Apple. (z.d.). Apple. https://www.apple.com/retail/fifthavenue/

Fireshield Coatings. (2023, November 9). Emporia Shopping Mall. https://fireshieldcoatings.com/projects/emporia-shopping-mall/

Flat glass manufacturing process. (z.d.). AGC. https://agc-electronics.com/en/specialty-glass/blog/detail/how-is-glass-made

Galuppi, L., Massimiani, S., & Royer-Carfagni, G. (2014). Buckling phenomena in double curved cold-bent glass. International Journal of Non-Linear Mechanics, 64, 70–84. https://doi.org/10.1016/j.ijnonlinmec.2014.03.015

Glass off the roll - Thin glass is revolutionising the performance spectrum of glass and glass panes. (2018, 23 januari). glassonweb.com. https://www.glassonweb.com/article/glass-roll-thin-glass-revolutionising-performance-spectrum-glass-and-glass-panes

glanova® - Ultra-thin glass for chemical strengthening | High-performance material - NSG GROUP. (z.d.). https://hpm.nsg.com/en/products/glanova/index.html

Glassonweb.com. (2018, January 23). Glass off the roll - Thin glass is revolutionising the performance spectrum of glass and glass panes. https://www.glassonweb.com/article/glass-roll-thin-glass-revolutionising-performance-spectrum-glass-and-glass-panes

Glassonweb.com. (2019, November 25). Quality Control and Specification for Distortions of Curved Glass. https://www.glassonweb.com/article/quality-control-and-specification-distortions-curved-glass

Glassonweb.com. (2019, November 12). Options for Complex Geometry Façades - Single Corner vs. Free Form Cold-Bending. https://www.glassonweb.com/article/options-complex-geometry-facades-single-corner-vs-free-form-cold-bending

Granta EduPack. (2022). Granta EduPack 2022 [Software]. Cambridge University Press. https://www.grantadesign.com/

Greco, R. (1978). Molecular weight dependence of stress relaxation of commercial polyisobutylene. European Polymer Journal.

Hassen, M., de la Barra, P., Oke, S., Overend, M., Bilow, M., & Luna-Navarro, A. (2024). Glass serviceability limits: New evidence from human-centred studies. Glass Structures & Engineering. https://doi.org/10.1007/s40940-024-00280-1

History of Glass. (n.d.). The History of Glass - Glass Facts. https://www.historyofglass.com/

iGuzzini. (n.d.). Our project Gallery. https://www.iguzzini.com/projects/project-gallery/evolution-tower,-a-distinctively-luminous-landmark-on-the-moscow-night-skyline/

Innovationzentrum Spartherm. (n.d.). https://www.octatube.nl/project-item/projectitem/219-innovationzentrum-spartherm.html

Love, A. (1888). XVI. The Small Free Vibrations and Deformation of a Thin Elastic Shell. Philosophical Transactions of the Royal Society of London, 179, 491–546.

Muis, R. (n.d.). MAD Architects toont nieuwe beelden Fenix II in Rotterdam. Architectenweb. https://architectenweb.nl/nieuws/artikel.aspx?id=48472#photoid=377266

Meechoowas, E., et al. (2013). Alternative soda-lime glass batch to reduce energy consumption. Key Engineering Materials.

Norfinch Glass & Mirrors Mfg. Ltd. (2024, July 31). Insulated Seal Units. https://norfinchglass.ca/product/insulated-seal-units/

NSG GROUP. (n.d.). glanova® - Ultra-thin glass for chemical strengthening | High-performance material. https://hpm.nsg.com/en/products/glanova/index.html

NSG GROUP. (n.d.). UFF® - Ultra-thin soda-lime glass | High-performance material. https://hpm.nsg.com/en/products/uff/index.html

Overend, M. (2022). Lecture 6 – Structural Glass Design, 1–21.

Rahimzadeh, K., et al. (2022). Extreme Cold-bending: geometric considerations and shape prediction with machine learning. Challenging Glass Conference Proceedings - Volume 8. Ghent University, Belgium.

Staaks, D. (2003). Koud torderen van glaspanelen in blobs (unpublished master's thesis). Delft University of Technology, Delft, The Netherlands.

"TGB 1990 - Belastingen en vervormingen - Grondslagen voor het ontwerp en berekening van gebouwen en civieltechnische werken"
(Translation: "TGB 1990 - Loads and deformations - Principles for the design and calculation of buildings and civil engineering works.")

The History of Glass - Glass Facts. (n.d.). https://www.historyofglass.com/

Timoshenko, S., & Woinowsky-Krieger, S. (1959). Theory of plates and shells (2nd ed.). McGraw-Hill.

UFF® - Ultra-thin soda-lime glass | High-performance material - NSG GROUP. (z.d.). https://hpm.nsg.com/en/products/uff/index.html

Vanceva. (n.d.). Emporia Shopping. Architonic. https://www.architonic.com/en/project/vanceva-emporia-shopping/20033453

Appendix A: ansys plexiglass results

SITUATION	Corner A Y side		Corner B Nothing just clamped			Corner C X side	
	X-Component	0	X-Component	free		X-Component	free
	Y-Component	free	Y-Component	free		Y-Component	0
	Z-Component	free	Z-Component	free		Z-Component	free
	X-Rotation	free	X-Rotation	free		X-Rotation	free
	Y-Rotation	free	Y-Rotation	free		Y-Rotation	free
	Z-Rotation	free	Z-Rotation	free		Z-Rotation	free
1	**Expanded Polyethylene foam (Closed cell)**						
	Density	30 kg m3	**kg/m3**				
	iotropic elasticity						
	YOUNG'S MODULUS	10	MPa				
	Poisson's Ratio	0,3					
	bulk modulus	4,167*10^6	Pa				
	shear modulus	1,93*10^6	Pa				
2	**Ködiglaze S**			1. increase stiffness of the support blocks			
	Density	1370	**kg/m3**	**2. Make pressure point a softer material**			
	Arruda Boyce						
	Initial Shear Modulus Mu	0,7066	MPa				
	Limiting Network Stretch	2,9^10					
	Incompressibility Parameter D1	0,2143	Mpa^-1				
	Tensile Yield strength	2,1^6	Pa				
3	**PMMA PLANE**						
	Density	1,19 g/cm3	**g/cm3**				
	iotropic elasticity						
	Coefficient of thermal exp	0,0001207	C^-1				
	YOUNG'S MODULUS	2,798	Gpa				
	Poisson's Ratio	0,37					
	bulk modulus	3,5872*10^9	Pa				
	shear modulus	1,0212*10^9	Pa				
	Tensile Yield strength		MPa				
	Compressive yield strength		MPa				
4	**Triseal Spacer (silicone foam)**						
	Density	700	**kg/m3**				
	YEOH 1st order						
	Initial Shear Modulus Mu	0,28	MPa				
	incompressibitlity Parameter	10	Mpa^-1				
	from tabular tensile test data						
	bulk modulus						
	shear modulus						
3	**Structural steel (Support block)**						
contacts	**frictional**						
PMMA foam	0,6	assymetric					
PMMA foam	0,6	assymetric					
PMMA foam	0,6	assymetric					
PMMA foam	0,6	assymetric					
PMMA foam	0,6	assymetric					
PMMA foam	0,6	assymetric					

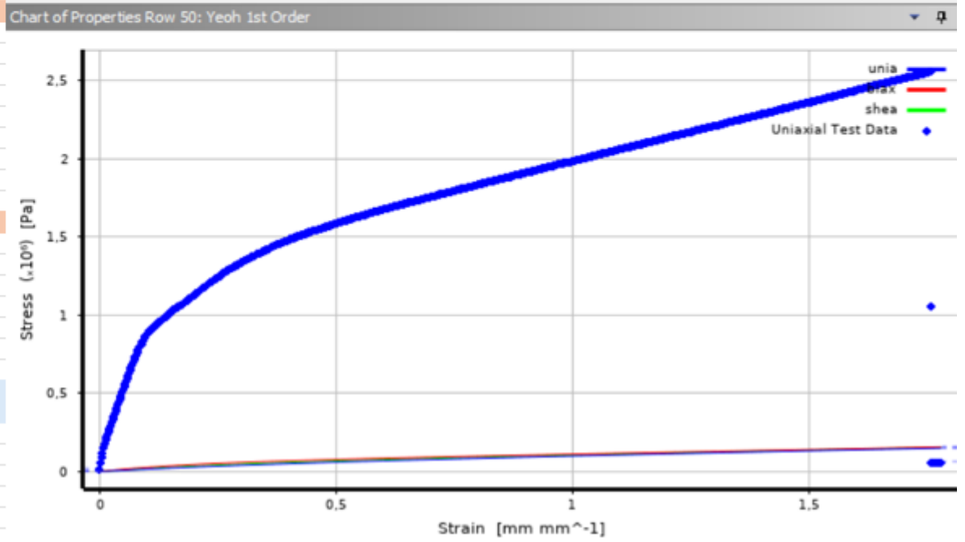

MESH	0,02m							at 3x3cm from support block	3x3
SIM 10	1.1mm	Step Time (S)	Deformation (m)	Deformation meter	deformation	data for measurement	strain gauge 1 Y direction	strain gauge 2 X-direction	Strain gauge 3 X direction
		1	1,00E-02	-7,81E-03	7,8139		5,69E-05	-2,14E-05	6,34E-0
		1,1	1,10E-02	-8,56E-03	8,5626		6,40E-05	-2,40E-05	7,13E-0
		1,15	1,15E-02	-8,94E-03	8,9352		6,74E-05	-2,54E-05	7,53E-0
		1,2	1,20E-02	-9,31E-03	9,3066		7,09E-05	-2,67E-05	7,92E-0
		1,275	1,28E-02	-9,86E-03	9,8615		7,61E-05	-2,88E-05	8,50E-0
		1,3313	1,33E-02	-1,03E-02	10,276		7,99E-05	-3,03E-05	8,94E-0
		1,3875	1,39E-02	-1,07E-02	10,689		8,37E-05	-3,19E-05	9,37E-0
		1,4719	1,47E-02	-1,13E-02	11,307		8,94E-05	-3,43E-05	1,00E-0
		1,5384	1,60E-02	-1,22E-02	12,228		9,77E-05	-3,79E-05	1,10E-0
		1,725	1,73E-02	-1,31E-02	13,145		1,06E-04	-4,16E-05	1,19E-0
		1,9148	1,91E-02	-1,45E-02	14,512		1,18E-04	-4,73E-05	1,33E-0
		2	2,00E-02	-1,51E-02	15,124		1,23E-04	-4,98E-05	1,39E-0
		2,2	2,20E-02	-1,66E-02	16,556		1,34E-04	-5,59E-05	1,53E-0
		2,4	2,40E-02	-1,80E-02	17,986		1,46E-04	-6,21E-05	1,66E-0
		2,7	2,70E-02	-2,01E-02	20,127		1,62E-04	-7,14E-05	1,86E-0
		3	3,00E-02	-2,23E-02	22,266		1,78E-04	-8,09E-05	2,05E-0
		3,2	3,20E-02	-2,37E-02	23,692		1,89E-04	-8,73E-05	2,18E-0
		3,4	3,40E-02	-2,51E-02	25,117		1,99E-04	-9,37E-05	2,30E-0
		3,7	3,70E-02	-2,73E-02	27,253		2,14E-04	-1,03E-04	2,48E-0
		4	4,00E-02	-2,94E-02	29,388		2,29E-04	-1,13E-04	2,66E-0
		4,2	4,20E-02	-3,08E-02	30,812		2,38E-04	-1,20E-04	2,77E-0
		4,4	4,40E-02	-3,22E-02	32,234		2,48E-04	-1,26E-04	2,89E-0
		4,7	4,70E-02	-3,44E-02	34,368		2,62E-04	-1,36E-04	3,05E-0
		5	5,00E-02	-3,65E-02	36,501		2,75E-04	-1,46E-04	3,21E-0
		5,2	5,21E-02	-3,79E-02	37,923		2,84E-04	-1,52E-04	3,32E-0
		5,4	5,41E-02	-3,93E-02	39,345		2,93E-04	-1,59E-04	3,42E-0
		5,7	5,71E-02	-4,15E-02	41,479		3,06E-04	-1,68E-04	3,57E-0
		6	6,01E-02	-4,36E-02	43,612		3,19E-04	-1,78E-04	3,72E-0
		6,2	6,21E-02	-4,50E-02	45,035		3,27E-04	-1,84E-04	3,82E-0
		6,4	6,41E-02	-4,65E-02	46,458		3,36E-04	-1,90E-04	3,91E-0
		6,7	6,71E-02	-4,86E-02	48,592		3,48E-04	-2,00E-04	4,06E-0
		7	7,02E-02	-5,07E-02	50,728		3,60E-04	-2,10E-04	4,19E-0
		7,2	7,22E-02	-5,22E-02	52,153		3,68E-04	-2,15E-04	4,28E-0
		7,4	7,42E-02	-5,36E-02	53,577		3,76E-04	-2,22E-04	4,37E-0
		7,7	7,72E-02	-5,57E-02	55,715		3,87E-04	-2,31E-04	4,50E-0
		8	8,02E-02	-5,79E-02	57,854		3,98E-04	-2,41E-04	4,63E-0
		8,2	8,23E-02	-5,93E-02	59,281		4,05E-04	-2,47E-04	4,72E-0
		8,4	8,43E-02	-6,07E-02	60,708		4,12E-04	-2,53E-04	4,80E-0
		8,7	8,73E-02	-6,29E-02	62,851		4,23E-04	-2,62E-04	4,92E-0
		9	9,04E-02	-6,50E-02	64,994		4,33E-04	-2,71E-04	5,04E-0
		9,2	9,24E-02	-6,64E-02	66,424		4,40E-04	-2,77E-04	5,12E-0
		9,4	9,44E-02	-6,79E-02	67,855		4,46E-04	-2,83E-04	5,20E-0
		9,7	9,75E-02	-7,00E-02	70,002		4,56E-04	-2,92E-04	5,32E-0
		9,85	9,90E-02	-7,11E-02	71,077		4,61E-04	-2,96E-04	5,38E-0
		10	0,1005	-7,22E-02	72,152		4,66E-04	-3,00E-04	5,43E-0
		10,2	0,10253	-7,36E-02	73,586		4,72E-04	-3,06E-04	5,51E-0
		10,4	0,10457	-7,50E-02	75,02		4,78E-04	-3,11E-04	5,58E-0
		10,7	0,10762	-7,72E-02	77,175		4,88E-04	-3,19E-04	5,68E-0
		11	0,11068	-7,93E-02	7,93E+01		4,97E-04	-3,27E-04	5,79E-0

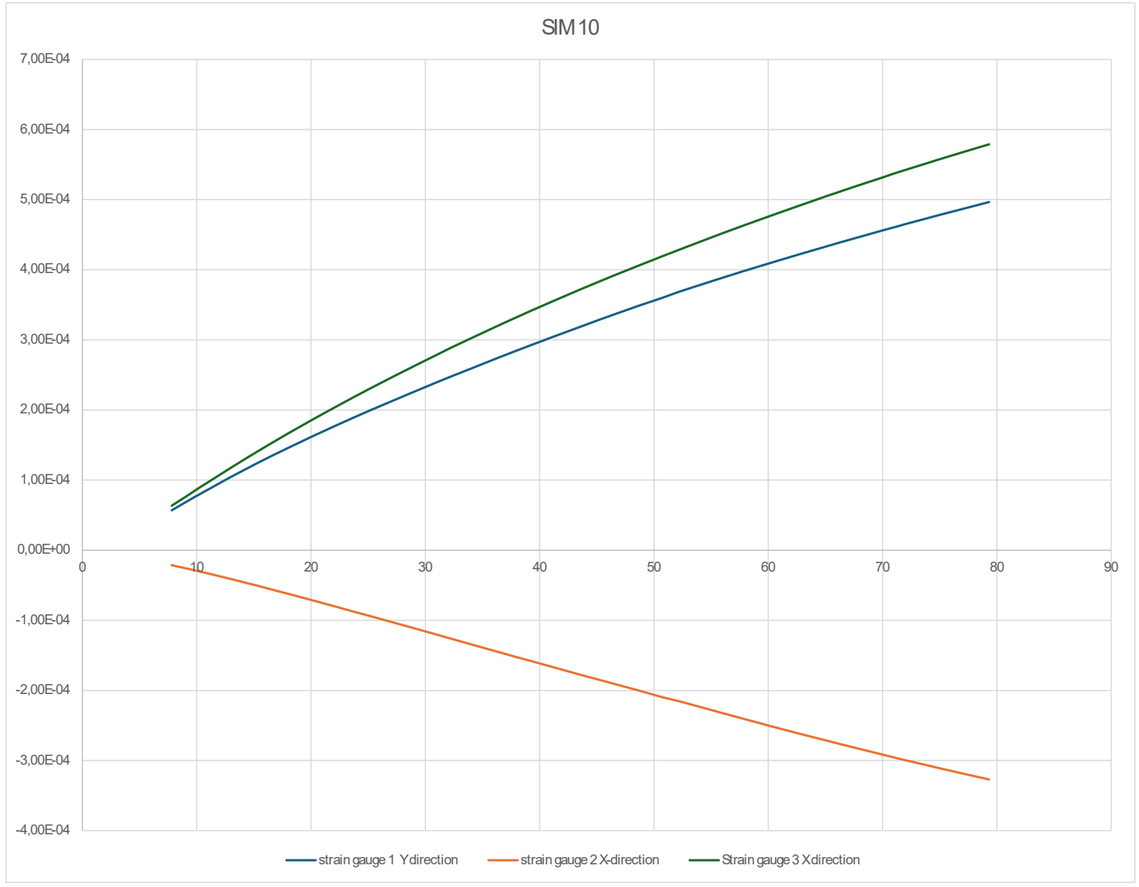
SIM 10
7,00E-04
6,00E-04
5,00E-04
4,00E-04
3,00E-04
2,00E-04
1,00E-04
0,00E+00
-1,00E-04
-2,00E-04
-3,00E-04
-4,00E-04
0
10
20
30
40
50
60
70
80
90
strain gauge 1 Y direction
strain gauge 2 X-direction
Strain gauge 3 X direction

Appendix B: ansys thin-glass results

1	**Expanded Polyethylene foam (Closed cell)**			
	Density	30 kg m3	**kg/m3**	
	iotropic elasticity			
	YOUNG'S MODULUS	40	MPa	
	Poisson's Ratio	0,3		
	bulk modulus	4,167 *10^6	Pa	
	shear modulus	1,93 *10^6	Pa	
2	**Ködiglaze S**			1. increase stiffness of the support blocks
	Density	1370	**kg/m3**	**2. Make pressure point a softer material**
	Arruda Boyce			
	Initial Shear Modulus Mu	0,7066	MPa	
	Limiting Network Stretch	2,9 ^10		
	Incompressibility Paramet	0,2143	Mpa ^-1	
	Tensile Yield strength	2,1 ^6	Pa	
3	**NSG Glanova Thin glass**			
	Density	1,19 g/cm3	**g/cm3**	
	iotropic elasticity			
	Coefficient of therm	0,0001207	C^-1	
	YOUNG'S MODULUS	2,798	Gpa	
	Poisson's Ratio	0,37		
	bulk modulus	3,5872 *10^9	Pa	
	shear modulus	1,0212*10^9	Pa	
	Tensile Yield strength		MPa	
	Compressive yield strength		MPa	
4	**Triseal Spacer (silicone foam)**			
	Density	700	**kg/m3**	
	neo Hookean			
	Initial Shear Modulus Mu	0,27	MPa	
	incompressibitlity Param	10	Mpa^-1	
	from tabular tensile test data			
	curve fitted to shear test data			
3	**Structural steel (Support block)**			
contacts	**frictional**			
PMMA foam	0,6	assymetric		
PMMA foam	0,6	assymetric		
PMMA foam	0,6	assymetric		
PMMA foam	0,6	assymetric		
PMMA foam	0,6	assymetric		
PMMA foam	0,6	assymetric		

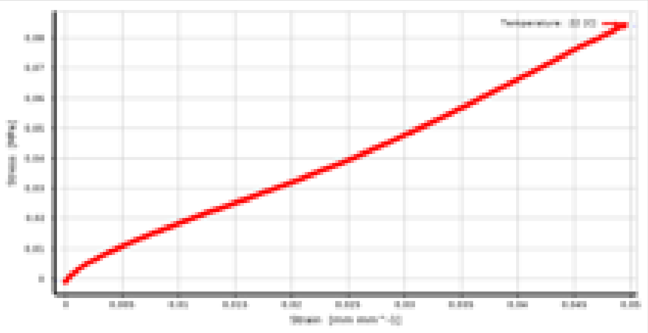

strain probes at measurable locations

MESH	0,02m							at 3x3cm from suppo	3x3			
SIM 11	1.1mm	Step Time (S)	Deformation (m)	Deformation meter	deformation	data for measurement	strain gauge 1 Y	strain gauge 2 X-dir	Strain gauge 3 X direction			max principal stress
		1	1,00E-02	-7,67E-03	-7,67E+00		1,16E-06	-4,47E-07	1,17E-06			9,28E+06
		1,2	1,20E-02	-9,13E-03	-9,13E+00		1,46E-06	-6,18E-07	1,46E-06			1,29E+07
		1,4	1,40E-02	-1,06E-02	-1,06E+01		1,81E-06	-8,23E-07	1,82E-06			1,85E+07
		1,475	1,48E-02	-1,11E-02	-1,11E+01		1,94E-06	-9,06E-07	1,95E-06			2,06E+07
		1,55	1,55E-02	-1,16E-02	-1,16E+01		2,07E-06	-9,92E-07	2,07E-06			2,28E+07
		1,6625	1,66E-02	-1,24E-02	-1,24E+01		2,25E-06	-1,12E-06	2,26E-06			2,61E+07
		1,8312	1,83E-02	-1,36E-02	-1,36E+01		2,51E-06	-1,33E-06	2,53E-06			3,10E+07
		2	2,00E-02	-1,48E-02	-1,48E+01		2,75E-06	-1,55E-06	2,77E-06			3,60E+07
		2,2	2,20E-02	-1,62E-02	-1,62E+01		3,01E-06	-1,82E-06	3,03E-06			4,19E+07
		2,4	2,40E-02	-1,76E-02	-1,76E+01		3,24E-06	-2,09E-06	3,25E-06			4,79E+07
		2,7	2,70E-02	-1,98E-02	-1,98E+01		3,50E-06	-2,51E-06	3,49E-06			5,68E+07
		3	3,00E-02	-2,19E-02	-2,19E+01		3,67E-06	-2,94E-06	3,62E-06			6,57E+07
		3,2	3,20E-02	-2,33E-02	-2,33E+01		3,72E-06	-3,22E-06	3,64E-06			7,17E+07
		3,4	3,40E-02	-2,47E-02	-2,47E+01		3,72E-06	-3,50E-06	3,60E-06			7,76E+07
		3,7	3,70E-02	-2,68E-02	-2,68E+01		3,63E-06	-3,91E-06	3,41E-06			8,65E+07
		3,85	3,85E-02	-2,79E-02	-2,79E+01		3,54E-06	-4,12E-06	3,29E-06			9,10E+07
		4	4,00E-02	-2,89E-02	-2,89E+01		3,43E-06	-4,32E-06	3,11E-06			9,57E+07
		4,2	4,20E-02	-3,03E-02	-3,03E+01		3,25E-06	-4,59E-06	2,85E-06			1,02E+08
		4,4	4,40E-02	-3,17E-02	-3,17E+01		3,00E-06	-4,84E-06	2,51E-06			1,08E+08
		4,6	4,60E-02	-3,31E-02	-3,31E+01		2,74E-06	-5,10E-06	2,17E-06			1,14E+08
		4,8	4,80E-02	-3,46E-02	-3,46E+01		2,43E-06	-5,34E-06	1,79E-06			1,21E+08
		5	5,00E-02	-3,60E-02	-3,60E+01		2,02E-06	-5,58E-06	1,25E-06			1,27E+08
		5,2	5,20E-02	-3,74E-02	-3,74E+01		1,57E-06	-5,80E-06	6,97E-07			1,33E+08
		5,4	5,40E-02	-3,88E-02	-3,88E+01		1,11E-06	-6,03E-06	4,94E-08			1,39E+08
		5,7	5,71E-02	-4,09E-02	-4,09E+01		3,13E-07	-6,35E-06	-9,68E-07			1,48E+08
		6	6,01E-02	-4,30E-02	-4,30E+01		-5,90E-07	-6,64E-06	-2,14E-06			1,57E+08
		6,2	6,21E-02	-4,44E-02	-4,44E+01		-1,23E-06	-6,83E-06	-2,96E-06			1,63E+08
		6,4	6,41E-02	-4,58E-02	-4,58E+01		-1,94E-06	-7,01E-06	-3,87E-06			1,69E+08
		6,7	6,71E-02	-4,79E-02	-4,79E+01		-3,05E-06	-7,26E-06	-5,31E-06			1,78E+08
		7	7,01E-02	-5,01E-02	-5,01E+01		-4,26E-06	-7,49E-06	-6,86E-06			1,87E+08
		7,2	7,21E-02	-5,15E-02	-5,15E+01		-5,09E-06	-7,64E-06	-7,90E-06			1,93E+08
		7,4	7,41E-02	-5,29E-02	-5,29E+01		-6,00E-06	-7,76E-06	-9,05E-06			1,99E+08
		7,7	7,72E-02	-5,50E-02	-5,50E+01		-7,39E-06	-7,94E-06	-1,08E-05			2,08E+08
		8	8,02E-02	-5,71E-02	-5,71E+01		-8,86E-06	-8,10E-06	-1,27E-05			2,17E+08
		8,2	8,22E-02	-5,86E-02	-5,86E+01		-9,87E-06	-8,20E-06	-1,40E-05			2,23E+08
		8,4	8,42E-02	-6,00E-02	-6,00E+01		-1,09E-05	-8,28E-06	-1,53E-05			2,28E+08
		8,7	8,73E-02	-6,21E-02	-6,21E+01		-1,25E-05	-8,38E-06	-1,74E-05			2,37E+08
		9	9,03E-02	-6,42E-02	-6,42E+01		-1,42E-05	-8,47E-06	-1,96E-05			2,46E+08
		9,2	9,23E-02	-6,57E-02	-6,57E+01		-1,54E-05	-8,53E-06	-2,11E-05			2,52E+08
		9,4	9,43E-02	-6,71E-02	-6,71E+01		-1,66E-05	-8,55E-06	-2,27E-05			2,58E+08
		9,6	9,64E-02	-6,85E-02	-6,85E+01		-1,78E-05	-8,58E-06	-2,42E-05			2,64E+08
		9,9	9,94E-02	-7,06E-02	-7,06E+01		-1,96E-05	-8,60E-06	-2,66E-05			2,73E+
		10	0,10041	-7,14E-02	-7,14E+01		-2,03E-05	-8,59E-06	-2,75E-05			2,76E+
		10,2	0,10244	-7,28E-02	-7,28E+01		-2,15E-05	-8,59E-06	-2,91E-05			2,82E+
		10,4	0,10447	-7,42E-02	-7,42E+01		-2,28E-05	-8,58E-06	-3,08E-05			2,88E+
		10,7	0,10752	-7,64E-02	-7,64E+01		-2,48E-05	-8,53E-06	-3,34E-05			2,97E+
		11	0,11057	-7,85E-02	-7,85E+01		-2,67E-05	-8,48E-06	-3,63E-05			3,06E+
		11,2	0,1126	-8,00E-02	-8,00E+01		-2,80E-05	-8,43E-06	-3,81E-05			3,12E+
		11,4	0,11464	-8,14E-02	-8,14E+01		-2,94E-05	-8,36E-06	-3,99E-05			3,18E+
		11,7	0,1177	-8,35E-02	-8,35E+01		-3,14E-05	-8,25E-06	-4,27E-05			3,27E+
		12	0,12076	-8,57E-02	-8,57E+01		-3,35E-05	-8,11E-06	-4,57E-05			3,36E+
		12,2	0,12281	-8,71E-02	-8,71E+01		-3,49E-05	-8,02E-06	-4,76E-05			3,42E+
		12,4	0,12486	-8,86E-02	-8,86E+01		-3,63E-05	-7,91E-06	-4,95E-05			3,48E+
		12,7	0,12793	-9,07E-02	-9,07E+01		-3,85E-05	-7,72E-06	-5,24E-05			3,57E+
		13	0,131	-9,29E-02	-9,29E+01		-4,06E-05	-7,52E-06	-5,54E-05			3,66E+
		13,2	0,13306	-9,43E-02	-9,43E+01		-4,21E-05	-7,38E-06	-5,73E-05			3,72E+
		13,4	0,13511	-9,58E-02	-9,58E+01		-4,36E-05	-7,23E-06	-5,93E-05			3,78E+

		13,4	0,13511	-9,58E-02	-9,58E+01		-4,36E-05	-7,23E-06	-5,93E-05		3,78E+
		13,7	0,1382	-9,79E-02	-9,79E+01		-4,58E-05	-7,00E-06	-6,23E-05		3,87E+
		14	0,14129	-0,10011	-1,00E+02		-4,80E-05	-6,73E-06	-6,52E-05		3,96E+
		14,2	0,14335	-0,10156	-1,02E+02		-4,96E-05	-6,56E-06	-6,72E-05		4,02E+
		14,4	0,14542	-0,10301	-1,03E+02		-5,11E-05	-6,38E-06	-6,93E-05		4,09E+
		14,505	0,1465	-0,10377	-1,04E+02		-5,19E-05	-6,28E-06	-7,02E-05		4,12E+
		14,61	0,14759	-0,1045	-1,05E+02		-5,27E-05	-6,17E-06	-7,14E-05		4,15E+
		14,665	0,14816	-0,1049	-1,05E+02		-5,31E-05	-6,12E-06	-7,19E-05		4,17E+
		14,72	0,14873	-0,1053	-1,05E+02		-5,35E-05	-6,06E-06	-7,25E-05		4,18E+
		14,803	0,14959	-0,1059	-1,06E+02		-5,41E-05	-5,97E-06	-7,33E-05		4,21E+
		14,927	0,15087	-0,1068	-1,07E+02		-5,51E-05	-5,84E-06	-7,46E-05		4,25E+
		15	0,15163	-0,10733	-1,07E+02		-5,56E-05	-5,76E-06	-7,54E-05		4,27E+
		15,2	0,1537	-0,1088	-1,09E+02		-5,71E-05	-5,56E-06	-7,74E-05		4,33E+
		15,4	0,15578	-0,11025	-1,10E+02		-5,86E-05	-5,33E-06	-7,96E-05		4,39E+
		15,7	0,15889	-0,11243	-1,12E+02		-6,10E-05	-4,97E-06	-8,26E-05		4,49E+
		16	0,16202	-0,11462	-1,15E+02		-6,33E-05	-4,60E-06	-8,57E-05		4,58E+

Appendix C: ansys material engineering data

Properties of Outline Row 8: Kodiglaze Kömmerling S

	A	B	C	D	E
1	Property	Value	Unit		
2	Material Field Variables	Table			
3	Density	1370	kg m^-3		
4	Arruda-Boyce				
5	Initial Shear Modulus Mu	0,7066	MPa		
6	Limiting Network Stretch	2,9E+11			
7	Incompressibility Parameter D1	0,2143	MPa^-1		
8	Tensile Yield Strength	2,1E+06	Pa		

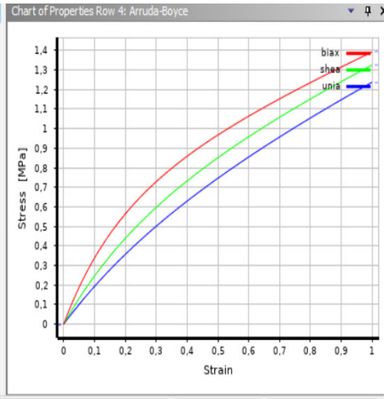

Properties of Outline Row 6: Expanded Polyethylene foam (Closed cell)

	A	B	C	D	E
1	Property	Value	Unit		
2	Material Field Variables	Table			
3	Density	30	kg m^-3		
4	Isotropic Elasticity				
5	Derive from	Young's Modulus and ...			
6	Young's Modulus	40	MPa		
7	Poisson's Ratio	0,3			
8	Bulk Modulus	3,3333E+07	Pa		
9	Shear Modulus	1,5385E+07	Pa		

Properties of Outline Row 10: Triseal spacer

	A	B	C	D	E
1	Property	Value	Unit		
2	Shear Test Data	Tabular			
3	Has Lateral Strain	No			
4	Scale	1			
5	Offset	0	MPa		
6	Neo-Hookean				
7	Initial Shear Modulus Mu	0,27308	MPa		
8	Incompressibility Parameter D1	10	MPa^-1		

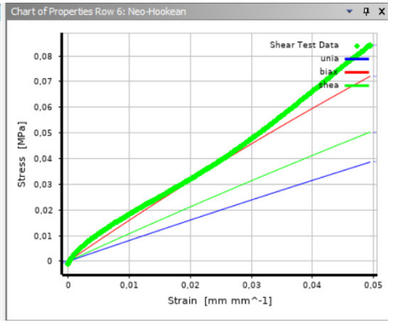

Properties of Outline Row 14: Plastic, PMMA (cast sheet)

	A	B	C	D	E
1	Property	Value	Unit		
2	Material Field Variables	Table			
3	Density	1,19	g cm^-3		
4	Isotropic Secant Coefficient of Thermal Expansion				
6	Isotropic Elasticity				
7	Derive from	Young's Modulus and ...			
8	Young's Modulus	2,798E+09	Pa		
9	Poisson's Ratio	0,37			
10	Bulk Modulus	3,5872E+09	Pa		
11	Shear Modulus	1,0212E+09	Pa		
12	Tensile Yield Strength	Tabular			
13	Tensile Ultimate Strength	Tabular			

	A	B	C	D	E
1	Property	Value	Unit		
2	Material Field Variables	Table			
3	Density	2,48	g cm^-3		
4	Isotropic Elasticity				
5	Derive from	Young's Modulus and ...			
6	Young's Modulus	75,4	GPa		
7	Poisson's Ratio	0,24			
8	Bulk Modulus	4,8333E+10	Pa		
9	Shear Modulus	3,0403E+10	Pa		
10	Tensile Yield Strength	260	MPa		
11	Compressive Yield Strength	700	MPa		

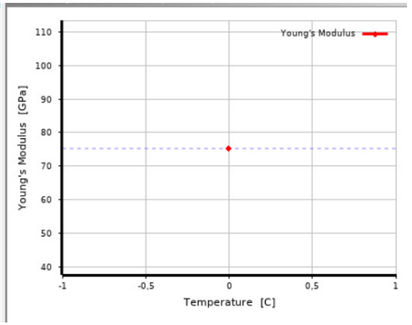

	A	B	C	D	E
1	Property	Value	Unit		
2	Material Field Variables	Table			
3	Density	7850	kg m^-3		
4	Isotropic Secant Coefficient of Thermal Expansion				
6	Isotropic Elasticity				
7	Derive from	Young's Modulus and ...			
8	Young's Modulus	2E+11	Pa		
9	Poisson's Ratio	0,3			
10	Bulk Modulus	1,6667E+11	Pa		
11	Shear Modulus	7,6923E+10	Pa		
12	Strain-Life Parameters				
20	S-N Curve	Tabular			
24	Tensile Yield Strength	2,5E+08	Pa		
25	Compressive Yield Strength	2,5E+08	Pa		
26	Tensile Ultimate Strength	4,6E+08	Pa		
27	Compressive Ultimate Strength	0	Pa		

	A	B	C	D	E
1	Property	Value	Unit		
2	Material Field Variables	Table			
3	Density	1090	kg m^-3		
4	Neo-Hookean				
5	Initial Shear Modulus Mu	0,24	MPa		
6	Incompressibility Parameter D1	0,0001	Pa^-1		

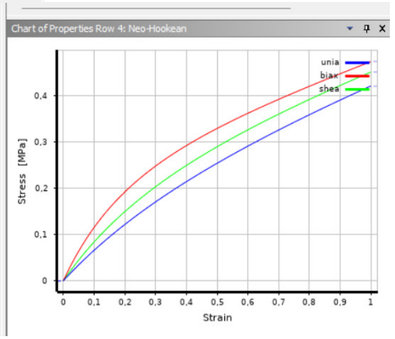

Appendix F: Stevin lab Plexiglass test data

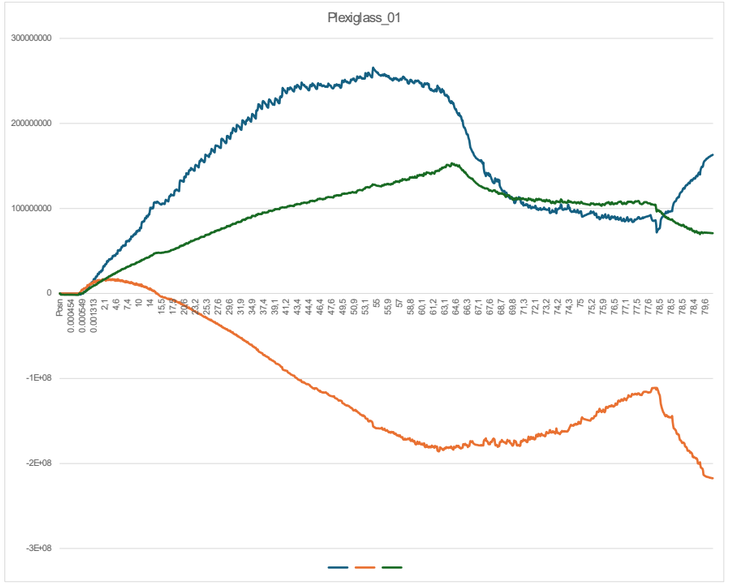

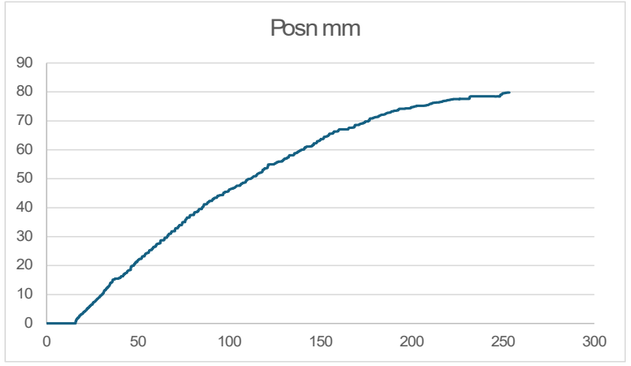

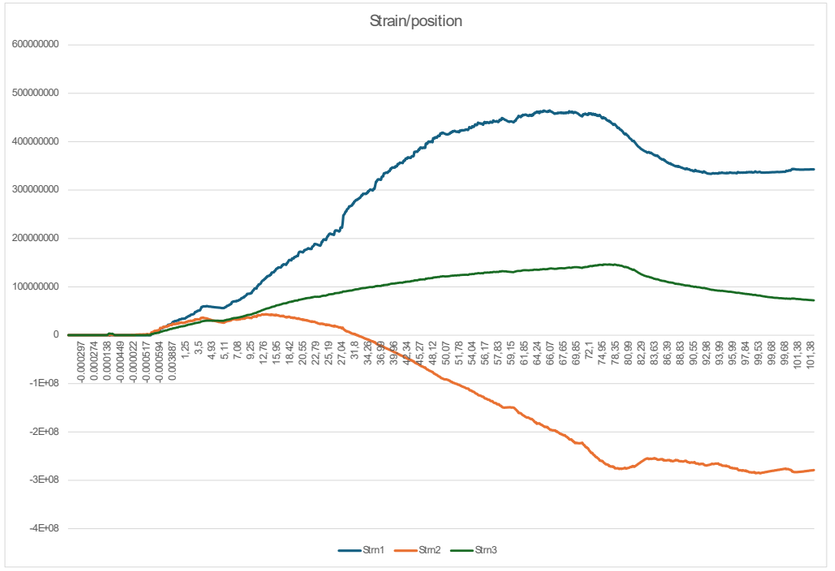

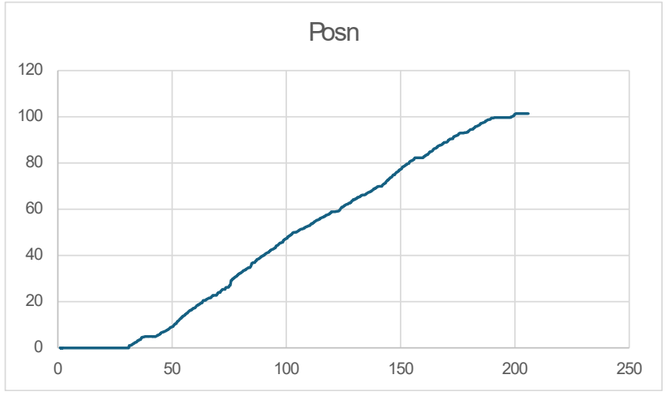

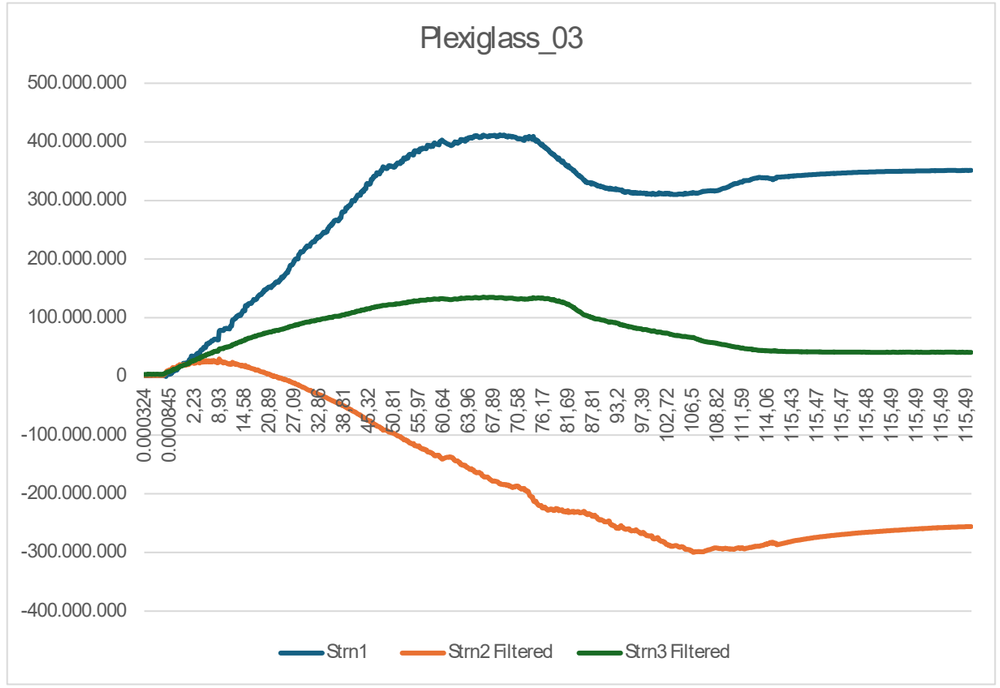
Plexiglass_03
500.000.000
400.000.000
300.000.000
200.000.000
100.000.000
0
-100.000.000
-200.000.000
-300.000.000
-400.000.000
0.000324
0.000845
2,23
8,93
14,58
20,89
27,09
32,86
38,81
45,32
50,81
55,97
60,64
63,96
67,89
70,58
76,17
81,69
87,81
93,2
97,39
102,72
106,5
108,82
111,59
114,06
115,43
115,47
115,47
115,48
115,49
115,49
115,49
115,49
Strn1
Strn2 Filtered
Strn3 Filtered

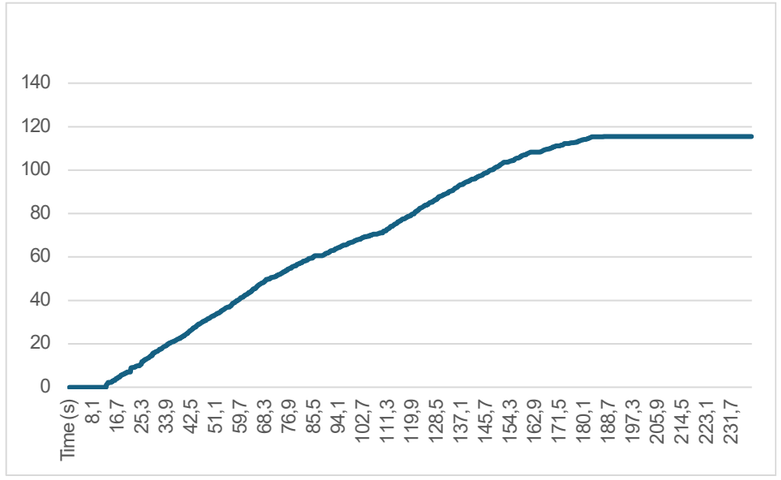
140
120
100
80
60
40
20
0
Time (s)
8,1
16,7
25,3
33,9
42,5
51,1
59,7
68,3
76,9
85,5
94,1
102,7
111,3
119,9
128,5
137,1
145,7
154,3
162,9
171,5
180,1
188,7
197,3
205,9
214,5
223,1
231,7

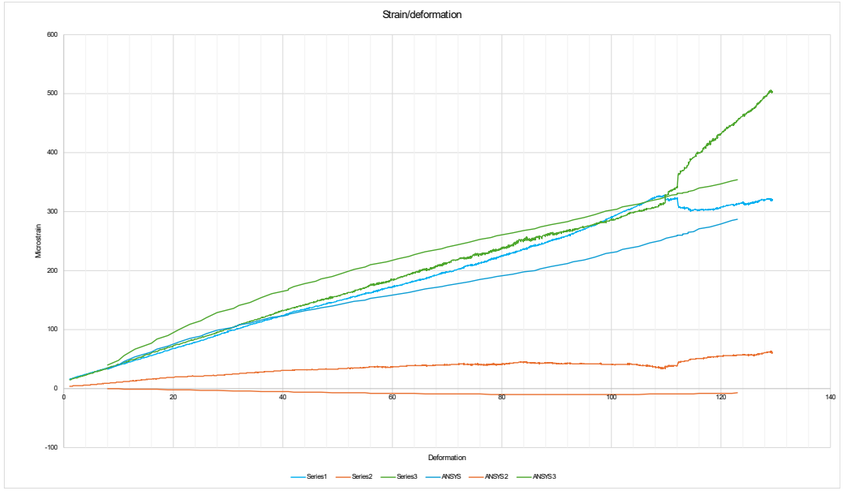

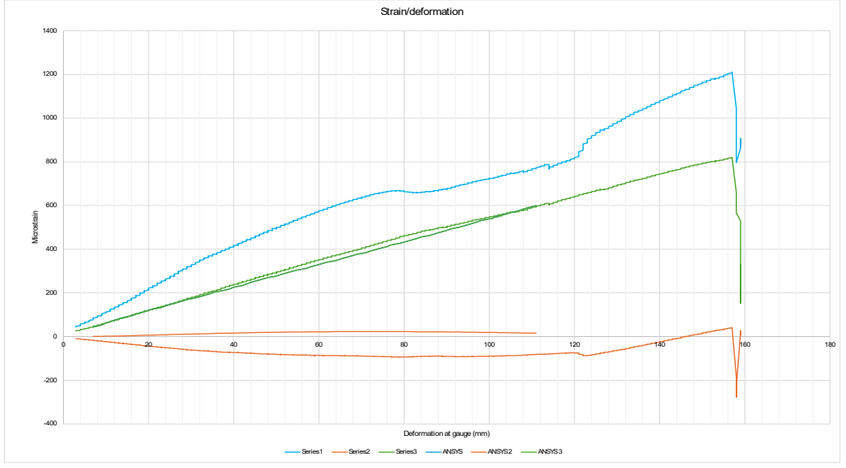

Appendix E: double-lap shear test data

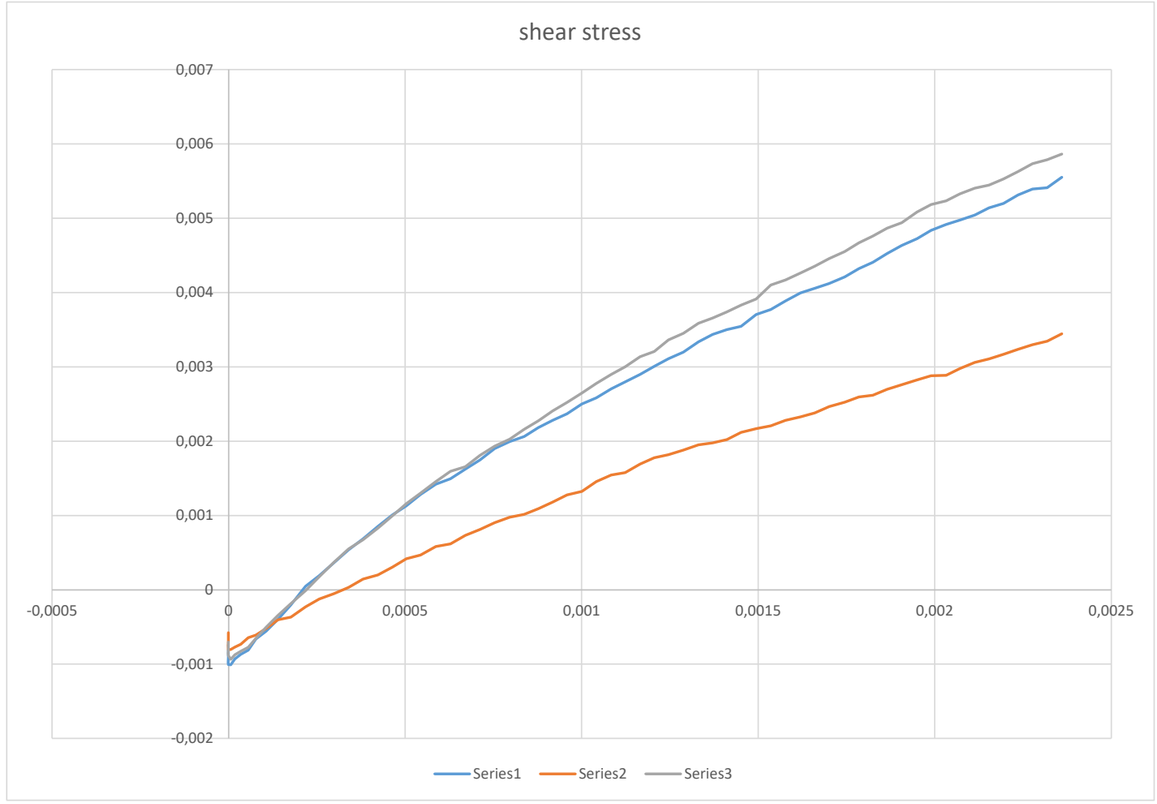

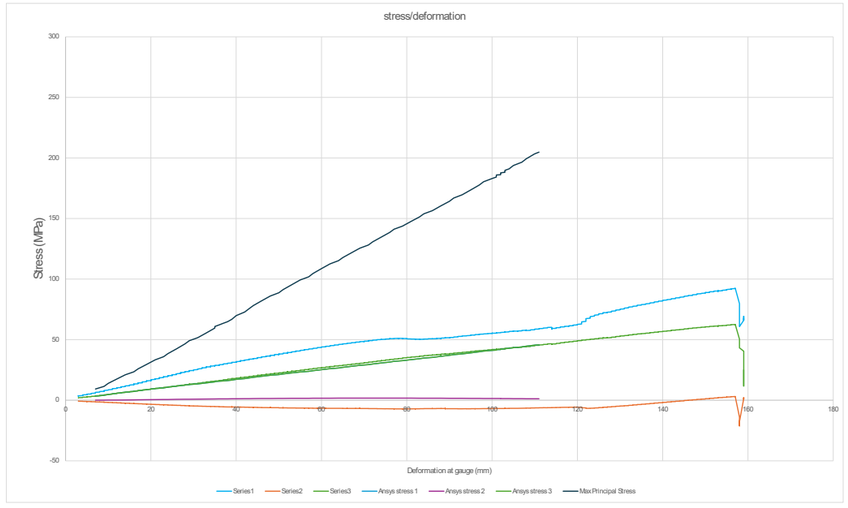
stress/deformation
Stress (MPa)
Deformation at gauge (mm)
Series1
Series2
Series3
Ansys stress 1
Ansys stress 2
Ansys stress 3
Max Principal Stress

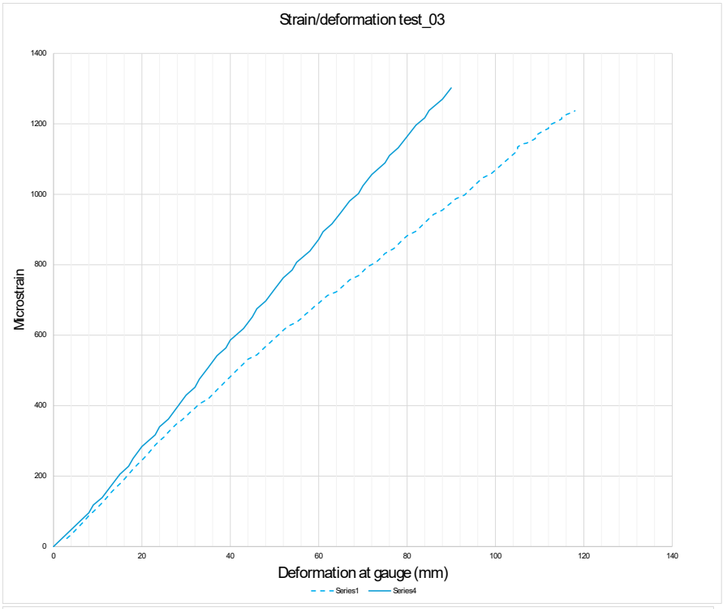
Strain/deformation test_03
Microstrain
Deformation at gauge (mm)
Series1
Series4

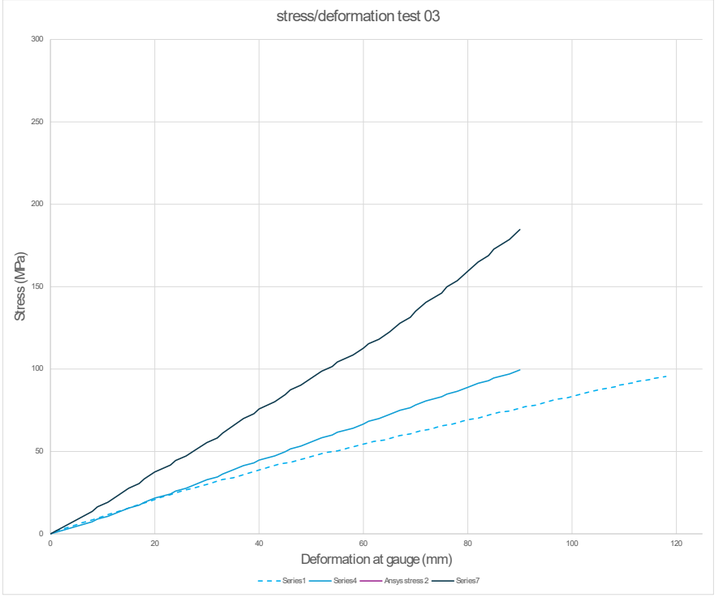
stress/deformation test 03
Stress (MPa)
Deformation at gauge (mm)
Series1
Series4
Ansys stress 2
Series7

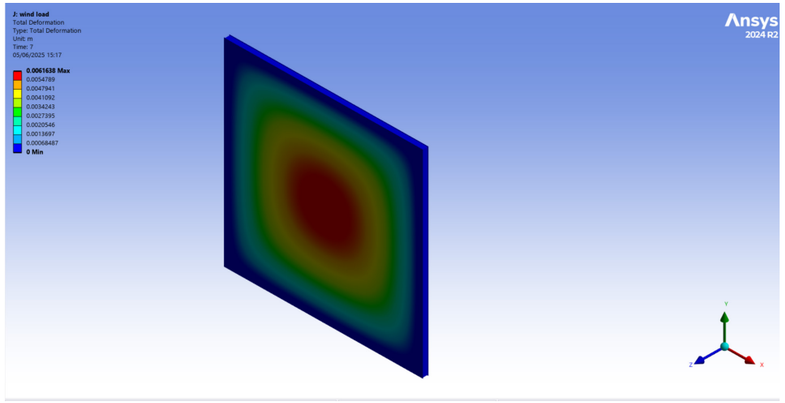
J: wind load
Total Deformation
Type: Total Deformation
Unit: m
Time: 7
05/06/2025 15:17
0,0061638 Max
0,0054789
0,0047941
0,0041092
0,0034243
0,0027395
0,0020546
0,0013697
0,00068487
0 Min
Ansys
2024 R2

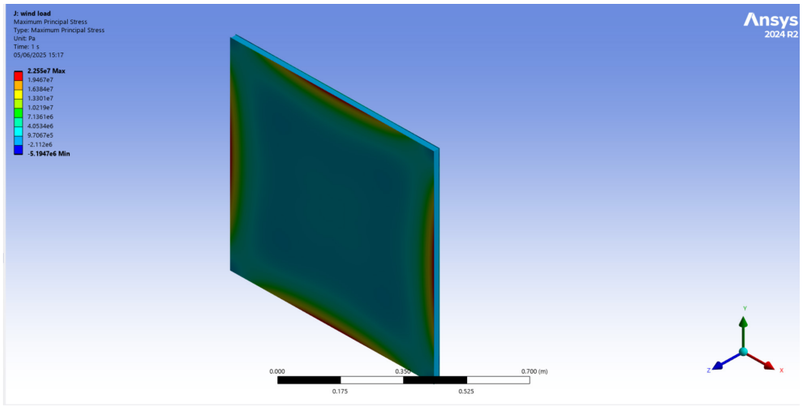
J: wind load
Maximum Principal Stress
Type: Maximum Principal Stress
Unit: Pa
Time: 1 s
05/06/2025 15:17
2,255e7 Max
1,9467e7
1,6384e7
1,3301e7
1,0219e7
7,1361e6
4,0534e6
9,7067e5
-2,112e6
-5,1947e6 Min
Ansys
2024 R2
0,000
0,350
0,700 (m)
0,175
0,525

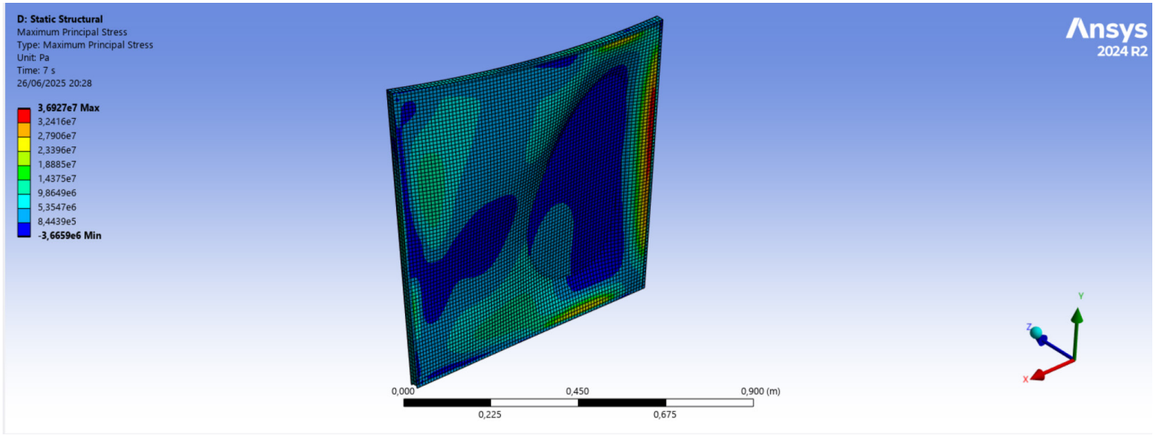
D: Static Structural
Maximum Principal Stress
Type: Maximum Principal Stress
Unit: Pa
Time: 7 s
26/06/2025 20:28
3,6927e7 Max
3,2416e7
2,7906e7
2,3396e7
1,8885e7
1,4375e7
9,8649e6
5,3547e6
8,4439e5
-3,6659e6 Min
Ansys
2024 R2
0,000
0,450
0,900 (m)
0,225
0,675

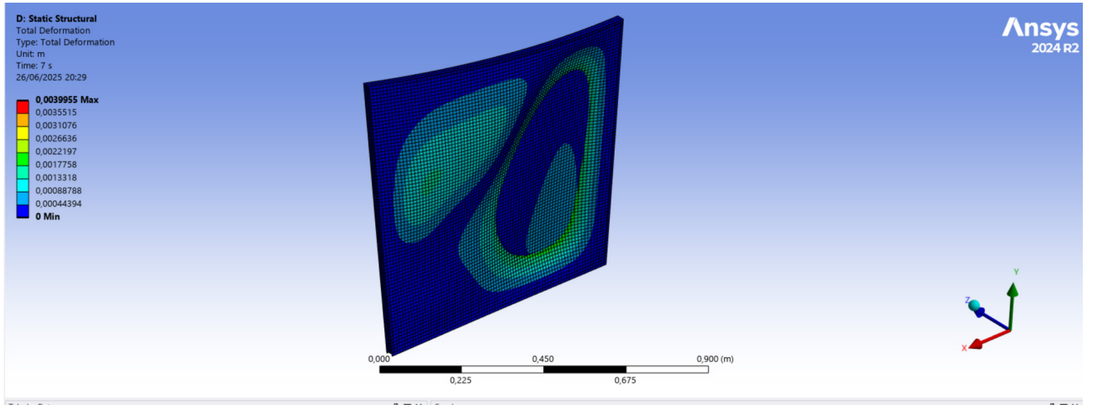
D: Static Structural
Total Deformation
Type: Total Deformation
Unit: m
Time: 7 s
26/06/2025 20:29
0,0039955 Max
0,0035515
0,0031076
0,0026636
0,0022197
0,0017758
0,0013318
0,00088788
0,00044394
0 Min
Ansys
2024 R2
0,000
0,450
0,900 (m)
0,225
0,675